LINKING ENDOSOMAL TRAFFIC AND PAMP-TRIGGERED IMMUNITY IN PLANTS

Inaugural-Dissertation
zur
Erlangung des Doktorgrades
der Mathematisch-Naturwissenschaftlichen Fakultät
der Universität zu Köln
vorgelegt von
Susanne Anna Salomon
aus Bonn

Köln, April 2009

Die vorliegende Arbeit wurde am Max-Planck-Institut für Züchtungsforschung in Köln in der Abteilung für Molekulare Phytopathologie (Direktor: Prof. Dr. P. Schulze-Lefert) angefertigt.

Berichterstatter:	Prof. Dr. Paul Schulze-Lefert
	Prof. Dr. Ulf-Ingo Flügge
	Prof. Dr. Sacco de Vries
Prüfungsvorsitzender:	Prof. Dr. Martin Hülskamp
Tag der Disputation:	29. Juni 2009

TABLE OF CONTENTS

ABBREVIATIONS

% (v/v)	volume percent
% (w/v)	weight/volume percent
3’	downstream region (of a gene or sequence)
5’	upstream region (of a gene or sequence)
µ	micro
A	alanine
aa	amino acid
AP	adaptor protein
APS	ammonium persulfate
ATP	adenosine trisphosphate
At*, A.th., A. thaliana*	*Arabidopsis thaliana*
Arabidopsis	*Arabidopsis thaliana*
°C	degrees Celsius
Ca^{2+}	calcium ions
cDNA	copy DNA
Ce, C. elegans	*Caenorhabditis elegans*
CEBiP	chitin oligosaccharide elicitor-binding protein
Col-0	*Arabidopsis thaliana* ecotype Columbia-0
Cr	*Catharanthus roseus*
CSP	cold shock protein
C-terminus	carboxy terminus
D	aspartate
dH_2O	de-ionized water
Dm	*Drosophila melanogaster*
DMSO	dimethyl sulfoxide
DNA	desoxy ribonucleic acid
dNTPs	desoxyribonucleotides
DRP	dynamin-related protein
DTT	dithiothreitol
E	glutamate
E.coli	*Escherichia coli*
EDTA	ethylene diamine tetra-acetate

EFR	EF-Tu receptor
EIX	ethylene-induced xylanase
EMS	ethyl methane sulfonate, or methane sulfonic acid ethyl ester
ER	endoplasmic reticulum
ET	ethylene
ETI	effector-triggered immunity
F_1	first filial generation after crossing two different parental lines
F_2	second filial generation after crossing two different parental lines
FLS2	flagellin sensing receptor 2
g	gram
G	glycine
GBP	ß-glucan binding protein
GFP	green fluorescent protein
GTP	guanidine trisphosphate
h	hour
H	histidine
H.a.	*Hyaloperonospora arabidopsis*
his	histidine
HG	heptaglucan
hpi	hours post inoculation
HR	hypersensitive response
HRP	horse radish peroxidase
Hrs	hepatocyte growth factor-regulated tyrosine kinase substrate
I	isoleucine
i.e.	id est
JA	jasmonic acid
K	kilo
kb	kilo base
kD	kilo Dalton
l	liter
L	leucine
Le	*Lycopersicum esculentum*
leu	leucine
LPS	lipo-polysaccaride

lys	lysine
m	milli
M	molar (mol/l)
M_1	first filial generation after mutagenesis
M_2	second filial generation after mutagenesis
M_3	third filial generation after mutagenesis
MAP4	mammalian microtubule-associated protein 4
MAPK	mitogen activated protein kinase
mbd	microtubule binding domain
MeOH	methanol
min	minutes
mRNA	messenger RNA
mYFP	monomeric yellow fluorescent protein fluorescent protein
n	nano
NASC	Nottingham *Arabidopsis* Stock Centre
Nb	*Nicotiana benthamiana*
nm	nano meter
Nt	*Nicotiana tabacum*
N-terminus	amino terminus
OD	optical density
Os	*Oryza sativa*
P	probability value
p35S	promoter of Cauliflower mosaic virus promoter 35S
PAGE	polyacrylamide gel electrophoresis
PAMP	pathogen-associated molecular pattern
PAT	phosphinothricin-acetyltransferase
PCR	polymerase chain reaction
PGN	peptidoglycan
pH	negative logarithm of proton concentration
PRR	Pattern-recognition receptor
Pfu	*Pyrococcus furiosus*
PM	plasma membrane
PTI	PAMP-triggered immunity
pv.	pathovar

RLK	receptor-like kinase
RLP	receptor-like protein
RME	receptor-mediated endocytosis
RNA	ribonucleic acid
rpm	rounds per minute
RT	room temperature
s	seconds
S	serine
SD	standard deviation
SDS	sodium dodecyl sulphate
SEM	standard error of the mean
SNARE	soluble N-ethylmaleimide-sensitive factor adaptor protein receptor
SSLP	simple sequence length polymorphism
SYP	syntaxin of plants
T	tryptophane
T_1	first filial generation after transformation
T_2	second filial generation after transformation
T_3	third filial generation after transformation
Taq	*Thermophilus aquaticus*
TBS	tris buffered saline
TBS-T	TBS with 0,5% Tween-20
TEMED	N,N,N',N'-Tetramethylethylenediamine
TGN	trans-Golgi-network
TLR	Toll-like receptor
trp	tryptophane
TUA	α-tubulin
TUB	β-tubulin
u	(enzymatic) unit
U	uracile
V	valine
V	volt
v	volume
w	weight
WT	wild-type

X

PUBLICATIONS

Salomon, S. and Robatzek, S. (2008). Natural variation of the FLS2 mediated flagellin response. Paper 49 in: Biology of Plant-Microbe Interactions, Volume 6. M. Lorito, S. L. Woo, and F. Scala, eds. International Society for Molecular Plant-Microbe Interactions, St. Paul, MN.

Mersmann, S., **Salomon, S.**, Vetter, M. and Robatzek, S. (2008). Selbst oder Nicht-Selbst - Pflanzliche Immunrezeptoren. BIOspektrum 14, 6: 593-596.

Salomon, S., and Robatzek, S. (2006). Induced Endocytosis of the Receptor Kinase FLS2. Plant Signaling & Behavior 1, 6: 293-295.

SUMMARY

One of the first layers of active defense in plant-microbe interactions is based upon the recognition of pathogen associated molecular patterns (PAMPs). Although biochemically well studied, components of PAMP signaling await to be identified. Furthermore, emerging data point to a function of endocytosis in signaling (Chinchilla et al., 2007a; Geldner et al., 2007). Here, we conducted reverse and forward genetic approaches to identify components and to elucidate the role of endocytosis in PAMP signaling.

Previous successful forward genetic approaches were refined to identify additional components in PAMP signaling (Gomez-Gomez and Boller, 2000). The sensitivity of the response to flg22 by seedling growth inhibition was enhanced by UV-B treatment (Logemann and Hahlbrock, 2002), and by employing a modified seedling growth inhibition assay on plates with reduced flagellin dosis. *Arabidopsis thaliana* ecotypes were inspected and most insensitive accessions were mutated in *FLS2* alleles. Furthermore, screening a γ-irradiation population revealed several *fli* mutants (for flagellin-insensitive). Notably, only late PAMP responses such as callose deposition, seedling growth arrest and resistance to PtoDC3000 infection were impaired. The tested *fli1-8* mutants were not allelic to *FLS2* or *BAK1*, which suggests that yet unknown components of flg22 signaling are affected. While *fli* mutants were more susceptible to bacterial infection they appear more resistant to the oomycete *Hyaloperonospora arabidopsis* cv. Cala2. Taken together, potentially novel components involved in late PAMP responses were identified.

FLS2 endocytosis is one of the flg22 responses and appears to contribute to flg22 signaling. We therefore tested several knock-out mutants in known endocytosis components for their response to flg22 and bacterial infection. While most mutants displayed wild-type-like flg22 responses, *vps28-2*, *vps37-1*, *vps28-1 elch*, and *gnl1-1* exhibited enhanced susceptibility to PtoDC3000 infection. VPS28-2, VPS37-1, and VPS28-1 ELCH are components of the ESCRT I system responsible for sorting ubiquitinated proteins. GNL1 is an ARF GEF regulating vesicle trafficking at the Golgi and PM. To further delineate the role of endocytosis in plant immunity, a genetic screen for novel endocytosis mutants was established. Applying quantitative confocal microscopy 12 *fel* mutants (for FYVE-GFP endosome levels) with altered endosomal numbers in cotyledons were identified. Two selected mutants, *fel4* with an increased

endosome number and a few enlarged endosomes and *fel5* with a reduced endosome number, were characterized in more detail. Both *fel* mutants displayed minor developmental defects, which did not co-segregate with the endosomal phenotype, and revealed unaltered endosomal levels in roots.

In total, these approaches allowed us to isolate novel components involved in PTI and components regulating endocytosis in *Arabidopsis*. Map-based cloning will unravel the genetic identity of these mutants and elucidate how endocytosis contributes to immunity.

ZUSAMMENFASSUNG

Eine der ersten Abwehrmechanismen in der Pflanzen-Pathogen-Interaktion basiert auf der Erkennung von Pathogen-assoziierten molekularen Mustern (so genannte PAMPs). Obwohl biochemisch gründlich untersucht, sind viele Komponenten der PAMP Signaltransduktion unbekannt. Zudem deuten vermehrt Studien auf eine Rolle der Endozytose in der Signaltransduktion hin (Chinchilla et al., 2007a; Geldner et al., 2007). In dieser Arbeit wurden reverse und vorwärtsgerichtete genetische Ansätze zur Identifizierung von neuen Komponenten und zur Aufklärung der Rolle der Endozytose in der Signaltransduktion angewandt.

Bereits etablierte vorwärtsgerichtete genetische Ansätze wurden verfeinert, um zusätzliche Komponenten in der PAMP Signaltransduktion zu identifizieren (Gomez-Gomez and Boller, 2000). Dabei wurde die Empfindlichkeit der Keimlinge gegenüber der durch flg22 ausgelösten Inhibierung des Keimlingswachstums auf zwei unterschiedliche Weisen erhöht: (i) durch UV-B Behandlung (Logemann and Hahlbrock, 2002) und (ii) durch Durchführung des Tests auf Platte in Gegenwart geringere Flagellinkonzentration. *Arabidopsis thaliana* Ökotypen wurden durchgemustert und die meisten insensitiven Ökotypen stellten sich als *FLS2* Allele heraus. Weiterhin ergab die Durchmusterung von einer mit gamma-Strahlen mutagenisierten Population mehrere *fli* Mutanten (für flagellin-insensitiv). Interessanterweise waren nur die späten PAMP Antworten wie die Callose Deposition, die Keimlingswachstumsinhibierung und die Anfälligkeit gegenüber PtoDC3000 beeinträchtigt. Die Mutanten *fli1-8* wiesen keine Unterschiede zur Wild-typ Sequenz von *FLS2* oder *BAK1* auf. Dies deutet darauf hin, dass bisher unbekannte Komponenten der flg22 Signalweiterleitung betroffen sein könnten. Während die *fli* Mutanten erhöhte Anfälligkeit gegenüber bakterieller Infektion aufwiesen, schienen sie resistenter gegenüber einer Infektion mit dem Oomyceten *Hyaloperonospora arabidopsis* cv. Cala2 zu sein.

FLS2 Endozytose stellt nicht nur eine der flg22 Antworten dar, sondern scheint auch an der flg22 Signalweiterleitung beteiligt zu sein. Daher wurden verschiedene knock-out Mutanten in bekannten Endozytose Komponenten auf ihre flg22 Antworten und auf ihre Anfälligkeit gegenüber Bakteriern untersucht. Die meisten Mutanten zeigten Wildtyp-ähnliche flg22 Antworten, während *vps28-1*, *vps37-1*, *vps28-1 elch* und *gnl1-1* eine erhöhte Anfälligkeit gegenüber PtoDC3000 Infektion zeigten. VPS28-1, VPS37-1, und

VPS28-1 ELCH sind Komponenten des ESCRT I Systems, welches für den Transport von mit Ubiquitin markierten Proteinen verantwortlich ist. GNL1 ist ein ARF GEF, der Vesikeltransport am Golgi und der Plasmamembran reguliert.

Um die Rolle der Endozytose in der pflanzlichen Immunabwehr weiter aufzuklären, wurde ein genetisches Durchmusterungsverfahren für neue Endozytosemutanten etabliert. Durch die Anwendung quantitativer konfokaler Mikroskopie konnten 12 *fel* Mutanten (für FYVE-GFP endosome levels) mit veränderten Endosomenzahlen in Kotelydonen identifiziert werden. Zwei dieser Mutanten, *fel4* mit erhöhter Anzahl und teilweise vergrößerten Endosomen sowie *fel5* mit reduzierter Anzahl an Endosomen, wurden näher charakterisiert. Beide *fel* Mutanten zeigten leichte Defekte in ihrer Entwicklung, die nicht mit dem Endosomen Phänotyp ko-segregierten, und Wildtyp-ähnliche Anzahl an Endosomen in den Wurzeln.

Zusammenfassend erlaubten uns diese Ansätze neue Komponenten in der PAMP-vermittelten Immunabwehr sowie Komponenten der Endozytoseregulation in *Arabidopsis* zu identifizieren. Die Kartierung der Mutanten sollte ihre genetische Identifizierung und neue Einblicke in die Rolle der Endozytose in der Immunabwehr ermöglichen.

1 INTRODUCTION

1.1 THE PLANT IMMUNE SYSTEM

Plants solely depend on their innate immune system to recognize and protect themselves against potentially harmful microbes. Devoid of an acquired immune system based on antigen presentation, plants posses a large repertoire of innate immune receptors, which mediate a multi-layered immune response (Chisholm et al., 2006). In a first line of active defense conserved pathogen-associated molecular patterns (PAMPs) are recognized by cell-surface receptors, so called pattern-recognition receptors (PRRs), thus restricting pathogen growth. However, successful pathogens have evolved effector molecules to overcome PAMP-triggered immunity (PTI). Effectors manipulate the host to create a suitable niche for pathogen survival and proliferation, thereby promoting virulence. Best studied are effectors which are secreted via a type III secretion system (TTSS). As a second surveillance layer plants express mostly intracellular localized immune receptors, which specifically recognize pathogen-derived effector molecules in a plant-cultivar and strain-specific manner, thus initiating effector-triggered immunity (ETI) (Chisholm et al., 2006; Jones and Dangl, 2006). A hallmark of PTI is that responses occur rapidly and transiently without harm to the cell, while ETI typically triggers a hypersensitive response (HR), a form of programmed cell death. Moreover, upon local infection plants can mount a systemic response to prevent secondary infection in adjacent or distant tissues. Recently, membrane compartmentalization and trafficking has emerged to play a role in the plant immune system.

1.2 THE FIRST LINE OF ACTIVE DEFENSE

Receptor-like kinases (RLKs) represent one of the largest protein families identified in *Arabidopsis thaliana*, with about ~610 members (Shiu et al., 2004). RLKs consist of an extracellular, a transmembrane and a cytoplasmic serine/threonine kinase domain. A major subgroup comprises RLKs carrying leucine-rich repeats (LRRs) in their extracellular domains. Only few LRR-RLKs have been functionally characterized e.g. CLAVATA1 (CLV1) involved in meristem development (Clark et al., 1996) or Brassinosteroid Insensitive 1 (BRI1) and BRI1-associated kinase 1 (BAK1), which mediate perception of the plant hormone brassinosteroid (Russinova et al., 2004). Two

well characterized LRR-RLKs exhibit roles as PRRs and are implicated in plant immunity by mediating perception of bacterial PAMPs (Fig. 1). To date the best characterized PRR in plants is the *Arabidopsis* flagellin sensing receptor kinase FLS2 recognizing bacterial flagellin (flg22) (Gomez-Gomez and Boller, 2000; Zipfel et al., 2004; Chinchilla et al., 2006). The biological significance of the FLS2/flg22 pathway in plant immunity was shown by Zipfel et al. (2004) and further characterized by Melotto et al. (2006). *fls2* mutants are more susceptible than wild-type plants when phytopathogenic bacteria were sprayed onto the leaf surface (Zipfel et al., 2004). Perception of flg22 induced closure of stomata, the entry sites for infections, providing pre-invasive immunity (Melotto et al., 2006).

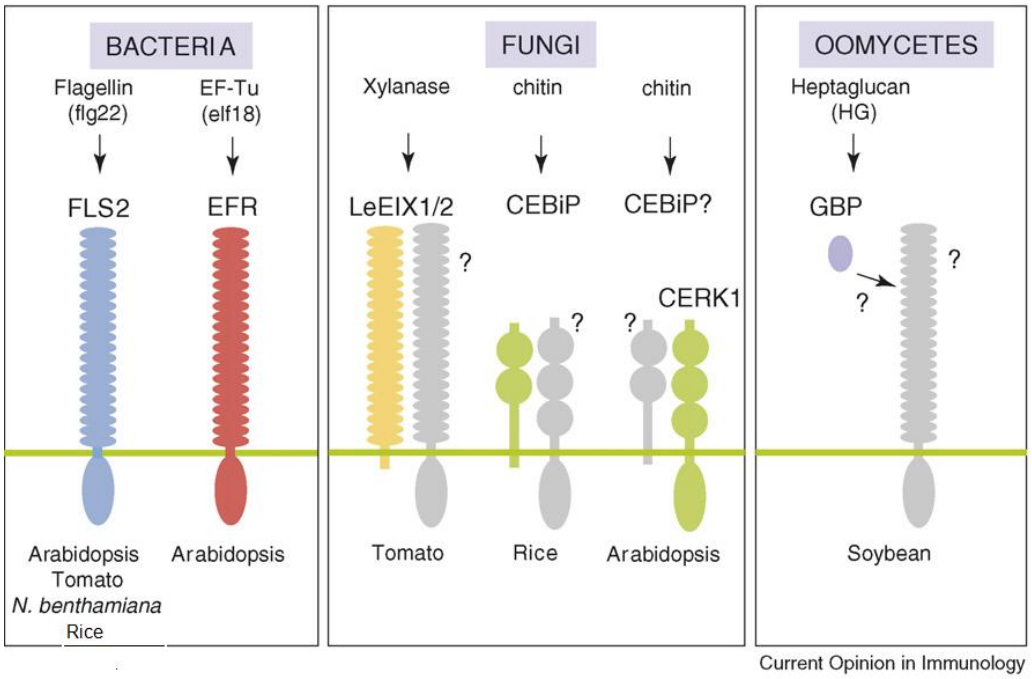

Fig. 1: Known PRRs in Plants. Bacterial flagellin (flg22) and EF-Tu (elf18) are recognized by the LRR-RLKs FLS2 and EFR, respectively. Both PRRs require BAK1 for signaling. FLS2 orthologues are present in tomato, *N. benthamiana* and rice. Oomycete heptaglucan is recognized by soluble GBP. Fungal xylanase is perceived by LeEIX1/2 in tomato. Fungal chitin is recognized by CEBiP in rice and chitin responses are mediated by CERK1 in *Arabidopsis*. Image modified from (Zipfel, 2008).

The other well characterized LRR-RLK is EFR, which is responsible for recognizing the bacterial elongation factor EF-Tu (elf18) (Zipfel et al., 2006). EFR groups into the same LRR-RLK subfamily XII than FLS2 and is therefore highly related (Shiu and Bleecker, 2001). Interestingly, the ligands flg22 and elf18 trigger an almost identical set of defense responses which suggests that both receptor pathways use common

components. Moreover, transcripts of approximately 50 *Arabidopsis* LRR-RLK genes accumulated upon treatment with various PAMPs, which implies that additional members of this large protein family play a role in plant immunity (Zipfel et al., 2004; Nürnberger and Kemmerling, 2006).

Other known plant PRRs perceive fungal or oomycete PAMPs (Fig. 1). In tomato, ethylene-induced xylanase (EIX) is sensed by two receptor-like proteins (RLP) LeEIX1 and LeEIX2 (Ron and Avni, 2004). However, only LeEIX2 confers signaling when expressed heterologously in tobacco. Surprisingly, the PRR LeEIX2 triggers HR, which does not confirm the current understanding of PTI. Chitin, a ß-1,4-linked polymer of N-acetylglucosamine, characteristic for fungal cell walls, is perceived in rice by the chitin oligosaccharide elicitor-binding protein (CEBiP) containing two extracellular LysM domains (Kaku et al., 2006). In *Arabidopsis*, a RLK with three extracellular LysM domains, CERK1, is required for chitin response (Miya et al., 2007). To date, physical binding of chitin to CERK1 remains to be shown. In legumes, a ß-glucan binding protein (GBP) recognizes 1,6-ß-linked and 1,3-ß-branched heptaglucan, which is present in the cell wall of oomycetes (Umemoto et al., 1997). Interestingly, GBP contains an intrinsic endo-1,3-ß-glucanase activity, thus potentially releasing and binding ligands concomitantly (Fliegmann et al., 2004).

Although some plant PRRs have been isolated recently, there are additional PAMPs known to be perceived by animal PRRs that are also recognized in plants such as peptidoglycans, lipo-polysaccharides or bacterial cold shock protein (Felix and Boller, 2003; Gust et al., 2007; Silipo et al., 2008); however, the corresponding PRRs in plants remain to be isolated.

1.3 RECOGNITION OF BACTERIAL FLAGELLIN

Flagellin perception is a widespread mechanism contributing to PTI in many plant species. In *Arabidopsis*, the receptor kinase FLS2 (AtFLS2) was identified in a screen for mutant plants that were insensitive to bacterial flagellin (Gomez-Gomez and Boller, 2000). Chinchilla et al. demonstrated physical interaction between FLS2 and flg22, the elicitor active epitope corresponding to the most conserved domain of flagellin (Chinchilla et al., 2006). Moreover, it could be shown that FLS2 is not only present in

Arabidopsis and other *Brassicaceae* species but orthologues are also present in tomato (LeFLS2) (Felix et al., 1999; Robatzek et al., 2007), tobacco (NbFLS2) (Hann and Rathjen, 2007) and rice (OsFLS2) (Takai et al., 2008). Interestingly, species-specific differences for flagellin perception were found in plants (Bauer et al., 2001; Chinchilla et al., 2006). LeFLS2 and AtFLS2 recognize different flagellin epitopes. Moreover, flagellin signaling differs to some extent between AtFLS2 and NbFLS2. In tobacco, flagellin perception not only triggers PAMP responses but also induces HR. To circumvent host flagellin perception, some bacteria such as *Agrobacterium*, *Rhizobium*, *Ralstonia*, and *Xanthomonas* produce flagellins with a different sequence, which are not recognized by FLS2 (Felix et al., 1999; Pfund et al., 2004; Sun et al., 2006). As a counter defense strategy also plants adapt to these changes by a variation of FLS2 sequences (e.g. within *Brassicaceae* species) (Dunning et al., 2007). Interestingly, some FLS2 alleles contain premature stop codons (e.g. Ws-0). Future studies will help to elucidate which selection forces drive evolution of PRRs such as FLS2 into different directions.

In mammals, well-studied PRRs that recognize PAMPs are the Toll-like receptors (TLRs), which are important for innate and adaptive immunity (Hayashi et al., 2001). TLR5 mediates perception of bacterial flagellin through direct binding of monomeric flagellin (Smith et al., 2003). Interestingly, TLR5 recognizes a conserved site on flagellin that is structurally distinct from the site recognized by FLS2 (Felix et al., 1999; Smith et al., 2003). This finding suggests that recognition of bacterial flagellin evolved independently in plants and mammals. In addition to the surface localized TLR5, mammals also possess a cytosolic flagellin receptor, IPAF (pro-caspase-1-activating protein), which belongs to the class of Nod-like receptors (Franchi et al., 2006; Miao et al., 2006). Whether or not plants also contain a cytosolic recognition system for intracellular flagellin remains open.

1.4 RECEPTOR ACTIVATION AND SIGNALING

Based on flagellin perception in tomato cells, the address-message-concept has been proposed as molecular mechanism for receptor activation (Meindl et al., 2000). In this model, the ligand binds to the receptor in a first step, which triggers phosphorylation and/or conformational changes of the respective PRR. In a second step, the PRR is able

to bind to other signaling molecules (e.g. heterodimerize with a co-receptor) thereby transducing the signal. Immediate early responses occur within minutes of receptor activation and include the activation of reactive oxygen species (ROS), medium alkalinisation, Ca^{2+} fluxes, the activation of mitogen activated protein (MAP) kinase cascades, transcriptional reprogramming, salicylic acid accumulation and ethylene production (Felix et al., 1999; Nühse et al., 2000; Bauer et al., 2001; Asai et al., 2002; Kunze et al., 2004; Navarro et al., 2004; Zipfel et al., 2004; Mishina and Zeier, 2007). Typical late responses, which develop over one to several days, comprise accumulation of antimicrobial metabolites, callose deposition into the cell wall and inhibition of seedling growth (Gomez-Gomez et al., 1999; Kunze et al., 2004; Zipfel et al., 2006). The plethora of responses then restrict pathogen growth (Zipfel et al., 2004; Zipfel et al., 2006). To date, the contribution of individual defense responses for establishment of disease resistance is largely unknown.

The address-message-concept for FLS2 activation is supported by the recent finding that FLS2 and the receptor kinase BAK1 (also called SERK3 for somatic embryo receptor kinase 3) form a complex *in vivo* in a flg22-dependent manner (Chinchilla et al., 2007a). Moreover, *bak1* mutants are not impaired in flg22 binding but in all other flg22 responses (Chinchilla et al., 2007a). Another study indicates that FLS2 does not form homodimers in the absence or presence of flg22 (Ali et al., 2007). However, it demonstrates that 75 % of FLS2 in the plasma membrane (PM) moves rapidly and that FLS2 is less mobile in the presence of flg22, suggesting its ligand-dependent confinement to microdomains or transient interaction with less mobile membrane proteins (Ali et al., 2007). Together these results indicate that the activation of the PRR FLS2 involves hetero- but not homodimerization at least in the *Arabidopsis* protoplast system.

Other models for PRR activation in plants have been discussed that are derived from ligand-mediated receptor internalization of the epidermal growth factor receptor (EGFR) in mammals. Activation of EGFR by ligand binding accelerates EGFR endocytosis, sorting to endosomal compartments, and subsequent degradation in lysosomes and signal attenuation (Sorkin and Goh, 2009). Notably, EGFR complexes remain active in endosomes and continue to signal after internalization (von Zastrow and Sorkin, 2007). Similarly, this model could apply for FLS2, which was shown to re-localize to endosomes in a flg22-dependent manner (Robatzek et al., 2006).

1.5 RECEPTOR TRAFFICKING AND ENDOCYTOSIS IN PLANTS

Receptor-mediated endocytosis (RME) in plants is a newly emerging field involving LRR-RLKs, which mediate plant growth, development and immunity. In plants, endocytosis has been best studied in tip-growing root hairs and pollen tubes. In root cells, polar identity resulting from an auxin gradient based on asymmetric localization of PINFORMED (PIN) auxin transporters is mainly generated by clathrin-dependent endocytosis (Dhonukshe et al., 2007), and recycling involving GNOM, an ADP-ribosylation factor GTPase guanine-nucleotide exchange factor (ARF GEF) (Geldner et al., 2003; Kleine-Vehn et al., 2008). This endocytic recycling is crucial for regulating auxin efflux activity at the cell surface (Paciorek et al., 2005) and allows rapid relocation of PIN proteins upon developmental and environmental cues (Friml et al., 2002).

The first report on ligand-dependent RME in plant immunity was provided by Robatzek et al. demonstrating that a functional fusion of FLS2 to the green fluorescent protein (GFP) strictly localizes to cell membranes and rapidly and specifically internalizes into mobile vesicles upon addition of flg22 (Robatzek et al., 2006). Prolonged flg22 incubation resulted in a loss of FLS2-GFP signal indicating lysosomal and/or proteasomal degradation (Robatzek et al., 2006). Treatment with cytoskeleton inhibitors revealed a strongly reduced formation of flg22-induced FLS2-GFP vesicles (Robatzek et al., 2006). Furthermore, brefeldin A (BFA) known to affect post-Golgi derived vesicles (Geldner et al., 2003), did not inhibit flg22-triggered FLS2 internalization (Robatzek et al., 2006). Wortmannin, however, competent to inhibit the formation of multivesicular bodies (MVBs) in *Nicotiana tabacum* BY-2 cells (Tse et al., 2004) abolished flg22-triggered FLS2 internalization, which provides evidence for an endocytic process (Robatzek et al., 2006). It is worth to note that wortmannin caused a significant reduction in flg22-triggered MAP kinase activation (Chinchilla et al., 2007a), suggesting a link between FLS2 endocytosis and flg22 signaling.

A key observation of Robatzek et al. was that flg22-induced FLS2-GFP internalization is blocked in the presence of kinase inhibitors (Robatzek et al., 2006). Following up the role of phosphorylation in FLS2 endocytosis, site-directed mutagenesis revealed a

threonine residue within the juxta membrane region of FLS2 (T867) that when mutated rendered FLS2 impaired in internalization. In addition, flg22 responses were affected, which further supports a link between endocytosis and signaling. Robatzek et al. (2006) also showed that a mutation within a PEST-like motif, which is implicated in ubiquitin-triggered receptor endocytosis in yeast and animals (Haglund and Dikic, 2005), abolished FLS2 endocytosis and downstream flg22 signaling. Interestingly, unlike the $FLS2^{T867V}$ variant, $FLS2^{P1076A}$ was still able to mediate flg22-triggered oxidative burst (Salomon and Robatzek, 2006). In line with these findings, chemical interference revealed two compounds (Triclosan and Fluazinam) that impair FLS2 endocytosis and also affect flg22 responses (Serrano et al., 2007).

Recent examples demonstrate that LRR-RLKs can enter the endocytic route either constitutively or transiently upon ligand-binding (Fig. 2). Prime models are BRI1 and BAK1, which constitutively recycle between plasma membrane and endosomes (Russinova et al., 2004). Like FLS2, BRI1 physically interacts with its ligand and resides in cell membranes. Moreover, BRI1 was found to constitutively localize to endosomes, likely driven by endogenously present brassinosteroids. However, BRI1 endocytosis could not be further stimulated by exogenous applied brassinosteroid. BAK1 and BRI1 form heterodimers upon brassinosteroid perception (Russinova et al., 2004). Furthermore, BRI1 endocytosis appeared to be accelerated in the presence of BAK1 (Russinova et al., 2004). In contrast, membrane-resident FLS2 only relocalizes to intracellular dynamic vesicles upon ligand-binding (Robatzek et al., 2006). It could be shown that FLS2 endocytosis is abolished in *bak1* mutants, suggesting that the co-receptor BAK1 is required (Chinchilla et al., 2007b). Besides ligand-induced endocytosis, it is likely that non-flg22-triggered FLS2 also undergoes constitutive endocytosis at the PM (Robatzek et al., 2006). Notably, current data provide evidence that both BRI1 and FLS2 signal from endosomes (Robatzek et al., 2006; Chinchilla et al., 2007a; Geldner et al., 2007; Serrano et al., 2007).

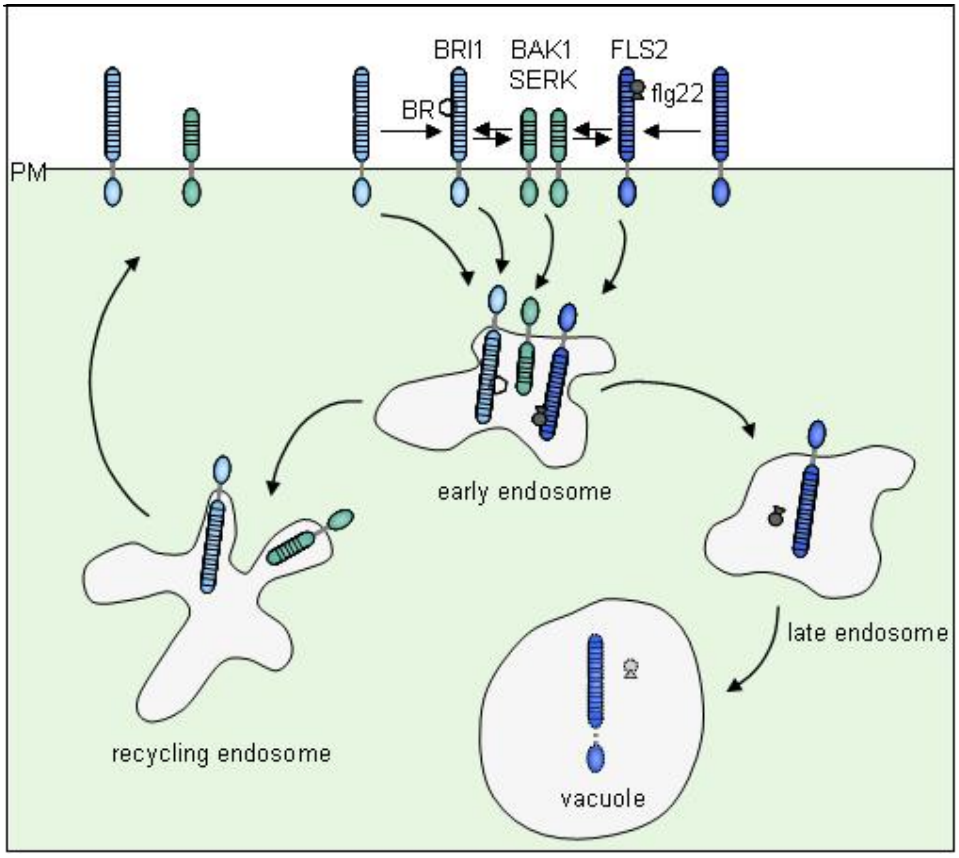

Fig. 2: Model of RME Subcellular Trafficking in Plants According to the Prime Examples BRI1, BAK1, and FLS2 (graphic taken from (Geldner and Robatzek, 2008). BRI1 and BAK1 constitutively localize to PM and endosomes. FLS2 resides in the PM and only re-localizes to endosomes upon flg22 binding. The co-receptor BAK1 is also required for FLS2 internalization. Current data provide evidence that both BRI1 and FLS2 signal from endosomes.

Similar to FLS2, ligand-dependent endocytosis was demonstrated for TLR4 upon perception of bacterial lipopolysaccharides (LPS) in mammals (Husebye et al., 2006). Husebye *et al.* detected elevated LPS signaling when TLR4 endocytosis was impaired, and observed LPS-triggered TLR4 ubiquitination (Husebye et al., 2006). Therefore, TLR4 endocytosis seemed to be involved in attenuation of LPS signaling. The authors discuss that several tyrosine-based tretrapeptide YxxΦ (Y = Tyr, x = any amino acid, ϕ = hydrophobic residue) motifs, that have been shown to function as endocytic signature, could mediate TLR4 endocytosis by (mono)-ubiquitination. Other TLRs that are localized on endosomes, recognize different nucleic acids (Chi and Flavell, 2008).

The LRR-RLK EFR does not contain a PEST-like motif like FLS2 but a tyrosine-based endocytic motif YxxΦ suggesting that EFR is also endocytosed. Functional relevance of the YxxΦ motif in plants was shown by Ron and Avni, who identified the xylanase receptor LeEIX (Ron and Avni, 2004). Mutation of the YxxΦ motif rendered LeEIX non-functional, which suggests an involvement of LeEIX endocytosis in xylanase signaling (Ron and Avni, 2004).

Other examples for endocytosed RLKs include SERK1, which plays a role in somatic embryogenesis, or ARABIDOPSIS CRINKLY4 (ACR4), which is required for L1 cell layer organization. SERK1 is only endocytosed in the presence of the kinase-associated protein phosphatase (KAPP) (Shah et al., 2002). ACR4 showed a rapid turnover and endocytosis, which was dependent on its ß-propeller-forming extracellular domain (Gifford et al., 2005). Although receptor activation as well as down regulation of PRRs is poorly understood, one key component, KAPP, was reported to interact with FLS2 and other RLKs (BRI1, BAK1, SERK1, CLV1 and SRK), thus interfering with signal activation (Trotochaud et al., 1999; Gomez-Gomez et al., 2001; Shah et al., 2002; Ding et al., 2007).

1.6 KNOWN COMPONENTS OF ENDOCYTOSIS IN PLANTS

In mammals, different mechanisms of endocytosis are described: (1) clathrin-dependent, (2) caveolae-dependent, (3) clathrin- and caveolae-independent endocytosis, (4) macropinocytosis, and (5) phagocytosis (Johannes and Lamaze, 2002; Conner and Schmid, 2003). Recently, evidence for clathrin-dependent endocytosis of PIN auxin efflux transporters in plants was obtained (Dhonukshe et al., 2007). Detailed electron micrographs of several plant species revealed the presence of clathrin-coated structures at the PM (Van Der Valk and Fowke, 1981; Emons and Traas, 1986; Derksen et al., 1995; Robinson, 1996; Fowke et al., 1999; Dhonukshe et al., 2007). Moreover, endocytosis motifs identified from mammalian proteins such as the tetrapeptide Yxxϕ or the di-Leu (D,E)xxxL(I,L) motif are present in most plant cell surface receptors (Geldner and Robatzek, 2008). Whether FLS2 internalization is also mediated by clathrin-dependent endocytosis, however, remains to be identified.

Different protein classes are likely involved in RME in plants. Adaptor proteins (AP) e.g. *Arabidopsis* AP180, which functions as a clathrin assembly protein, are important for initial vesicle formation (Barth and Holstein, 2004). All components required for clathrin-dependent endocytosis and homologs of adaptor proteins have been identified in *Arabidopsis* (Holstein, 2002). Moreover, dynamins are essential for pinching off vesicles from membranes. In *Arabidopsis*, 6 Dynamin-Related Protein (DRP) subfamilies were identified (Rojo et al., 2003). Recently, a study demonstrated that *drp1a* null mutants exhibit reduced endocytic uptake of the marker FM4-64 (Collings et al., 2008). Moreover, DRP1C-GFP was shown to colocalize with a clathrin light chain fluorescent fusion protein, suggesting that DRP1C may participate in clathrin-mediated membrane dynamics (Konopka et al., 2008).

Other important players are the endosomal sorting complex required for transport (ESCRT) machinery (Hurley, 2008; Hurley et al., 2009), which targets transmembrane proteins marked with a single ubiquitin to multi-vesicular bodies (MVBs), a membrane compartment with key sorting function (Fig. 3). MVBs consist of clusters of internal vesicles that were formed by invagination from the PM. From the MVB cargo is either recycled back to the PM, entered into the retrograde trafficking to the trans-Golgi network (TGN), or targeted for degradation in the lytic vacuole. *In silico* analysis revealed that homologs of the ESCRT I, II, and III complexes are present in the *Arabidopsis* genome (Spitzer et al., 2006; Winter and Hauser, 2006). To date, only one ESCRT I component, ELCH, has been functionally characterized and revealed a role in cytokinesis (Spitzer et al., 2006). The final invagination of endosomal membrane is then mediated by the AAA ATPase SKD1 (suppressor of K^+ transport growth defect1) and at least one positive regulator LIP5 (lyst-interacting protein5), presumably by releasing the ESCRT complex (Haas et al., 2007).

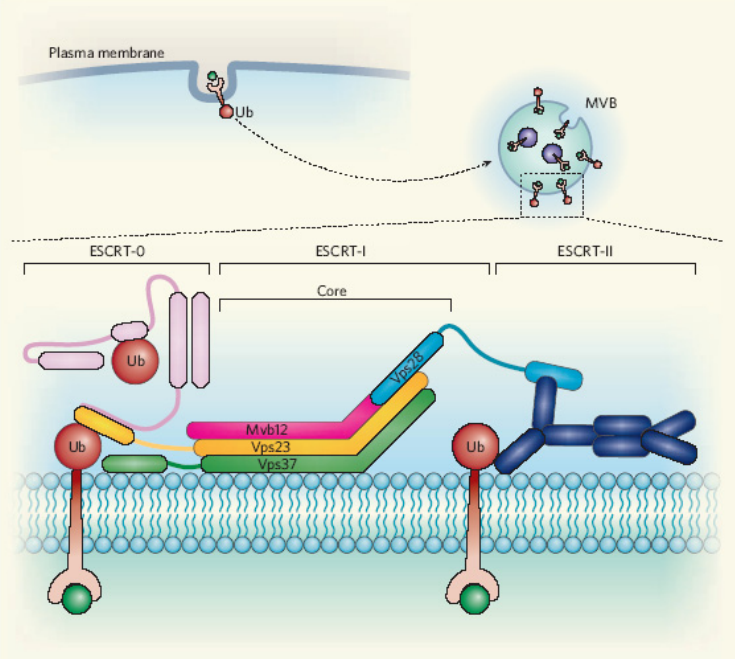

Fig. 3: Schematic Representation of the Localization and Structure of the ESCRT Complex. After internalization, transmembrane proteins tagged with ubiquitin (Ub) enter specialized vesicles called MVBs. The sorting of these proteins to vesicles in MVBs — and their subsequent degradation in lysosomes — is mediated by ESCRT complexes. (Taken from Alam and Sundquist, 2007).

Another important step, the fusion of endosomes to target membranes, is mediated by soluble N-ethylmaleimide-sensitive factor adaptor protein receptor (SNARE) components (Lipka et al., 2007). Several studies implicate SNARE components in diverse biological functions such as cytokinesis, gravitropism and plant defense (Lipka et al., 2007). An intact cytoskeleton is also crucial for endocytic processes. Not surprisingly, depolymerising drugs affecting actin stability like cytochalasin D and lactrunculin B inhibit endocytosis (Baluska et al., 2002; Aniento and Robinson, 2005). Numerous other proteins also contribute to RME in plants e.g. Rab and ARF GTPases and GEFs, cytoskeleton interactors, or sterols (Grebe et al., 2003; Bloch et al., 2005; Nielsen et al., 2008; Pan et al., 2009).

For cell biological studies, several MVB marker lines are available e.g. fluorescently-tagged Rab GTPases (Ara6, Ara7, and Rha1) that are commonly used (Ueda et al., 2001; Sohn et al., 2003; Ueda et al., 2004). Rab GTPases cycle between an inactive cytosolic GDP-bound form and an active GTP-bound form that associates with specific membranes. Hence, Rab GTPases are important determinants of membrane identity and

membrane targeting (Woollard and Moore, 2008). In addition, lipophylic dyes such as FM4-64 are used to stain endosomal compartments (Bolte et al., 2004; Griffing, 2008). Moreover, lipids were successfully used as endosomal markers of MVBs (Voigt et al., 2005). For example, proteins containing a FYVE domain specifically bind to phosphoinositol 3-phosphate (Gaullier et al., 1998), which is known to accumulate in endosomal membranes (Gillooly et al., 2001). Interestingly, the *Arabidopsis* genome contains 16 proteins with a predicted FYVE domain (van Leeuwen et al., 2004). To date, functional characterization of FYVE domain containing proteins is missing. Increased numbers of markers for specific endosomal compartments in plants will enhance the understanding of the function of individual compartments and help to elucidate similarities and differences to endocytic routes in mammals.

1.7 AIM OF THE THESIS

PTI constitutes the first line of active defense in plants. Although biochemically well studied, components of PAMP signaling remain to be identified, of which one could be endocytosis. To test the hypothesis that endocytosis is involved in PTI, two strategies were followed: (1) to monitor PAMP responses, and (2) to better understand endocytosis in *Arabidopsis*. Previous successful forward genetic screening was refined (Gomez-Gomez and Boller, 2000), e.g. by enhancing the sensitivity of the response to flg22 by seedling growth, through crosstalk between flg22 and UV-B (Logemann and Hahlbrock, 2002), and by modifying the seedling growth inhibition assay. Different *A. thaliana* populations were inspected to search for mutants with altered flg22 responses. To link endocytosis and PTI, we pursued a combinatorial approach analyzing T-DNA insertion lines with known implication in endocytosis for defects in flg22 signaling, and developing a high-throughput fluorescence imaging-based forward genetic screen, which monitors quantitative differences in endosome numbers of a chemically mutagenized endosomal marker line (FYVE-GFP). To gain knowledge on the overall contribution of the identified mutants to plant immunity, we planned to test their response to different pathogens. Together, these approaches should allow us to isolate novel components involved in PTI. Characterization of the identified mutants should shed more light on the importance of membrane trafficking to plant immunity. In short, we addressed the following questions in this study: What is the contribution of endocytosis to PAMP signaling? What are the components of PAMP signaling?

2 MATERIAL AND METHODS

The Material and Methods section is subdivided into two parts. In the first part (2.1) Materials used throughout this study, including plant lines, pathogens, chemicals, enzymes, media, buffers and solutions are listed. Methods applied in this work are described in the second part (2.2).

2.1 MATERIALS

2.1.1 Plant materials

Arabidopsis wild-type and mutant lines used in this study are listed in Table 1 and Table 2, respectively. The 18 *Arabidopsis* endocytosis mutant lines used in the reverse genetics approach are listed in Table 3. The 180 *Arabidopsis* accessions (Nordborg and Koornneef collection) tested in the flg22/UV-B screen are listed in Suppl. Table 1 (page 40) and were kindly provided by Matthieu Reymond (MPIZ).

Table 1: Wild-type *Arabidopsis* Accessions Used in this Study

Accession	Abbreviation	Original source
Columbia	Col-0	J. Dangl[a]
Landsberg erecta	La-er	NASC[b]
Wassilewskija	Ws-0	K. Feldmann[c]

[a]University of North Carolina, Chapel Hill, NC, USA; [b]Nottingham *Arabidopsis* Stock Centre; [c]University of Arizona, Tucson, AZ, USA

Table 2: Mutant and Transgenic *Arabidopsis* Lines Used in this Study

Gene/construct	Accession	Description	Reference/Source
fls2	Col-0	T-DNA	(Zipfel et al., 2004)
fls2-17	La-er	EMS	(Gomez-Gomez and Boller, 2000)
bak1-4	Col-0	T-DNA	(Chinchilla et al., 2007b)
efr	Col-0	T-DNA	(Zipfel et al., 2006)
eds1-2	La-er	FN	(Vreugdenhil et al., 2004)
pFLS2*::*FLS2-GFP	Ws-0	T-DNA	(Robatzek et al., 2006)
p35S::GFP-2xFYVE	La-er/Col-0	T-DNA	(Voigt et al., 2005; Vermeer et al., 2006)
p35S::GFP-MAP4mbd	Col-0	T-DNA	(Marc et al., 1998)

EMS: ethylmethane sulfonate; FN: fast neutron; T-DNA: transfer-DNA

Table 3: Mutant Alleles of Endocytosis Regulator Genes Used in this Study

Biological process	Gene	Mutant allele	Function	AGI code	Line designation	Comment	Accession	Source
Regulation of endocytosis	*ELC*	*elch*	ESCRT I	At3g12400	INRA	T-DNA	Ws-2	Spitzer et al., 2006
	VPS28-1	*vps28-1*	ESCRT I	At4g21560	SAIL_690_E05	T-DNA	Col-0	provided by S. Schellmann, University of Cologne
	VPS28-2	*vps28-2*	ESCRT I	At4g05000	SALK_040274	T-DNA	Col-0	provided by S. Schellmann, University of Cologne
	VPS37-1	*vps37-1*	ESCRT I	At3g53120	SAIL_97_H04	T-DNA	Col-0	provided by S. Schellmann, University of Cologne
	VPS37-2	*vps37-2*	ESCRT I	At2g36680	GABI_281A06	T-DNA	Col-0	provided by S. Schellmann, University of Cologne
		vps28-1 vps37-1	ESCRT I			T-DNA	Col-0	provided by S. Schellmann, University of Cologne
		vps28-2 vps37-1	ESCRT I			T-DNA	Col-0	provided by S. Schellmann, University of Cologne
		vps28-1 elch	ESCRT I			T-DNA	Col-0/Ws-2	provided by S. Schellmann, University of Cologne
		vps28-2 elch	ESCRT I			T-DNA	Col-0/Ws-2	provided by S. Schellmann, University of Cologne
		vps37-1 elch	ESCRT I			T-DNA	Col-0/Ws-2	provided by S. Schellmann, University of Cologne
		vps37-2 elch	ESCRT I			T-DNA	Col-0/Ws-2	provided by S. Schellmann, University of Cologne
		elch vps28-2 vps37-1	ESCRT I			T-DNA	Col-0/Ws-2	provided by S. Schellmann, University of Cologne
	ARA6/RABF1	*ara6*	RabGTPase	At3g54840	SAIL_880_C07	T-DNA	Col-0	Ueda et al., 2001
	ARA7/RABF2b	*ara7*	RabGTPase	At4g19640	WiscDsLox355B06	T-DNA	Col-0	Ueda et al., 2004
	RHA1/RABF2a	*rha1*	RabGTPase	At5g45130	SAIL_596_A03	T-DNA	Col-0	Ueda et al., 2004
	LIP5	*lip5*	SKD1 interactor	At4g26750	SAIL_854_F08	T-DNA	Col-0	Haas et al., 2007
	GNL1	*gnl1-1*	ARF GEF	At5g39500	NM_123312	T-DNA	Col-0	Richter et al., 2007
	VPS9a-2	*vps9a-2*	Rab5 GEF	At3g19770	GABI_557C02	T-DNA	Col-0	Goh et al., 2007

2.1.2 Pathogens

2.1.2.1 Pseudomonas syringae pv. tomato DC3000

Pseudomonas syringae pv. *tomato* (Pto) strain DC3000 (Rif_{50}) and PtoDC3000 ΔAvrPto/AvrPtoB (Rif_{50}, Kan_{50}) lacking two effector proteins were used throughout this study (Rosebrock et al., 2007).

2.1.2.2 Hyaloperonospora arabidopsis pv. Cala2

Hyaloperonospora arabidopsis (former *H. parasitica*) (*H.a.*) isolate Cala2 was initially obtained from oospore infection of a single seedling (Holub et al., 1994). *H. a.* cv. Cala2 was maintained as mass conidiosporangia culture on leaves of their genetically susceptible *Arabidopsis* ecotype (La-er) over a 7 d cycle. *H.a*. cv. Cala2 inoculations were done on 2-week-old plants by spray-inoculation with *H. a.* conidiospores (4×10^4 spores/ml) as previously described (Vreugdenhil et al., 2004).

2.1.3 Oligonucleotides

Listed below are oligonucleotides used in this study that were synthesized by Invitrogen (Karlsruhe, Germany) or Operon Biotechnologies (Cologne, Germany). Table 4 provides information on primers used for map based cloning. Table 5 lists all other primers used in this study. Lyophilised primers were re-suspended in nuclease-free water to a final concentration of 100 pmol/µl (= 100 µM). Working stocks were diluted to 10 pmol/µl (=10 µM).

Table 4: Sequences of Primers Used for Rough Mapping Analysis

chromosome	primer name	forward sequence	reverse sequence
1	F21M12	GGCTTTCTCGAAATCTGTCC	TTACTTTTTGCCTCTTGTCATTG
1	MSAT 1.3	GGAACTGTTGTCTGGGTAAG	CGATTGCACTAAAAGCTCTC
1	ciw1	ACATTTTCTCAATCCTTACTC	GAGAGCTTCTTTATTTGTGAT
1	nga280	CTGATCTCACGGACAATAGTGC	GGCTCCATAAAAAGTGCACC
1	nga111	TGTTTTTTAGGACAAATGGCG	CTCCAGTTGGAAGCTAAAGGG
2	NGA1139	TAGCCGGATGAGTTGGTACC	TTTTTCCTTGTGTTGCATTCC
2	MSAT 2.28	AATAGAAATGGAGTTCGACG	TGAACTTGTTGTGAGCTTTG
2	MSAT 2.21	ATTTTTAGCCCAATCACGTTT	AGGTCAAGTGAAAGGGTAAGG
2	MSAT 2.9	TAAAAGAGTCCCTCGTAAAG	GTTGTTGTTGTGGCATT
2	MSAT 2.4	TGGGTTTTTGTGGGTC	GTATTATTGTGCTGCCTTTT

3	nga162	CATGCAATTTGCATCTGAGG	CTCTGTCACTCTTTTCCTCTGG
3	ciw11	CCCCGAGTTGAGGTATT	GAAGAAATTCCTAAAGCATTC
3	ciw4	GTTCATTAAACTTGCGTGTGT	TACGGTCAGATTGAGTGATTC
3	nga6	TGGATTTCTTCCTCTCTTCAC	TGGATTTCTTCCTCTCTTCAC
4	ciw5	GGTTAAAAATTAGGGTTACGA	AGATTTACGTGGAAGCAAT
4	ciw6	CTCGTAGTGCACTTTCATCA	CACATGGTTAGGGAAACAATA
4	NGA1139	TAGCCGGATGAGTTGGTACC	TTTTTCCTTGTGTTGCATTCC
4	nga1107	GCGAAAAAACAAAAAAATCCA	CGACGAATCGACAGAATTAGG
5	CTR1	CCACTTGTTTCTCTCTCTAG	TATCAACAGAAACGCACCGAG
5	ciw8	TAGTGAAACCTTTCTCAGAT	TTATGTTTTCTTCAATCAGTT
5	PHYC	CTCAGAGAATTCCCAGAAAAATCT	AAACTCGAGAGTTTTGTCTAGATC
5	ciw9	CAGACGTATCAAATGACAAATG	GACTACTGCTCAAACTATTCGG
5	ciw10	CCACATTTTCCTTCTTTCATA	CAACATTAGCAAATCAAC

Table 5: Sequences of Primers Used for Standard PCR and RT-PCR Analysis

primer	forward sequence	reverse sequence
WRKY 22	AAAGTGTGCCATGTAGCAGCAG	TAATCATATTCCTCCGGTGGTA
WRKY 29	ATCCAACGGATCAAGAGCTG	GCGTCCGACAACAGATTCTC
FRK1	AACTTTGAGAGAGTTATTGGCA	ACGATTCCTCTAATGTCTCCGT
Actin	GGTAACATTGTGCTCAGTGGTGG	AACGACCTTAATCTTCATGCTGC
BAK1- # 167	TGGGTGGTAGCTTAATCGAAG	
BAK1- # 104	ATGAGGGATAGTTCTAGGGTTTG	
BAK1- # 105	TTCCAAACTTGCAGTACTTGTAAG	
BAK1- # 108	TTTTGGTTGTTCTCGTGTGTC	
BAK1- # 110	TTCACTTTTCACTCCAATCAGG	
BAK1- # 111	TAAAAGAGGAGCGCACCCAAGGTGG	
BAK1- # 114	TGATGATGTCATGTTACTAGACTGG	
BAK1- # 121		GTGACACACGAGAACAACCAA
BAK1- # 122		AACTGCAGTTCGCCACCTTGGG
BAK1- # 123		TGTGAATCAAGTGCGCAACA
FLS2-for	TTCAACTCTTCTAAAGTCTAAACCATGAAGTTAC	
FLS2-for3	CTCTGGTTCGATTCCTTCTGGAATC	
FLS2-for2	ATGATATCTTCAACTGTTCA	
FLS2-rev3		CGGTGCAGTTACTTATGCTGGAAGG
FLS2-rev2		TCTCGAGGAATCGGTCCAGTGAGAGAGTTATATG
FLS2-eco2	CAGATTCATTCAACAGTGCCAACATCATTGGC	
FLS2-eco1		AGCTTCTGTGTAGAACCACTTGTCTGATTCTG
FLS2-spe		CTAAACTTCTCGATCCTCGTTACGATC

pmr4-1	CAAGGACGGCATTCATAGGT	CCGTCTCGCCTCTAGATTCA
TUA4-1for	AAAATCAGATCTAGATTCAG	
TUA4-2for	CATACCTGTTTAGATCTGAG	
TUA4-3for	TAACAATTTCGCCCGTGGTC	
TUA4-4for	TTGTAGCCAGCCTCAACCAG	
TUA4-5for	CGCACTATTCAGTTTGTTGACTG	
TUA4-6rev		GGCAGAAACGATTTAACACACA
TUA6-1for	CACCTTCCTCATAACCTAGAAATC	
TUA6-2for	GGACTGGTACTTACCGTCAGC	
TUA6-3for	ATGTCTCCATCCTCCTCGAC	
TUA6-4for	GCTGTTTGATGTACCGTGGTG	
TUA6-5for	AGAGGTCGGTGCTGAAGGTG	
TUA6-6rev		CCATGTTCAAGACAGTAAAGCTC
TUA6-7rev		TTCGAGCCCCCATTCATCACAA

2.1.4 Enzymes

Restriction enzymes were bought from New England Biolabs (Frankfurt, Germany) or Roche (Mannheim, Germany) and were used according to the manufacturer's reaction conditions in the provided reaction buffers. Other enzymes used were *Taq*-Polymerase purchased from Ambion (Copenhagen, Denmark), SuperScriptII-Reverse Transcriptase and DNAse both from Invitrogen (Karlsruhe, Germany).

2.1.5 Chemicals

Laboratory grade chemicals and reagents were purchased from Sigma-Aldrich (Deisenhofen, Germany), Roth (Karlsruhe, Germany), Merck (Darmstadt, Germany), Invitrogen (Karlsruhe, Germany), and Serva (Heidelberg, Germany) unless otherwise stated.

2.1.6 Peptides

Peptides were synthesized by EZBiolab Inc. (Westfield IN, USA) with following sequences and 80 % purity:

flg22 – QRL STG SRI NSA KDD AAG LQI A

Tyr-flg22 – Y QRL STG SRI NSA KDD AAG LQI A

elf18 – SKE KFE RTK PHV NVG TIG

Tyr-flg22 was labelled with [^{125}I] iodine at the tyrosine residue to yield ^{125}I-Tyr-flg22 with specific radioactivity of 12 µCi/ml by Biotrend Chemikalien GmbH (Cologne, Germany). For the binding assay 10 µl (0.1 µCi or 400-500 kBq) were used per sample.

2.1.7 Antibiotics

Kanamycin (Kan)	50 mg/ml in dH_2O
Ampicillin (Amp)	100 mg/ml in dH_2O
Rifampicin (Rif)	100 mg/ml in DMSO

Stock solutions (1000x) were stored at -20° C. Aqueous solutions were sterile filtrated.

2.1.8 Media

Media were sterilised by autoclaving at 121° C for 20 min. For the addition of antibiotics and other heat labile compounds the solution or media were cooled down to 55° C. Heat labile compounds were sterilised using filter sterilisation units prior to addition.

Pseudomonas syringae media

NYGA broth

Bactopepton	5.0	g/l
Yeast extract	3.0	g/l
Glycerol	20.0	ml/l

pH 7.0

For NYGA agar plates 1.5 % (w/v) bacto agar (Becton, Dickinson and Company, LePont de Claix, France) was added to the above broth.

Arabidopsis thaliana media

MS (Murashige and Skoog) medium

MS powder including vitamins	4.4	g/l
Sucrose	10.0	g/l

pH 5.8

For MS plates 0.8 % (w/v) bacto agar (Becton, Dickinson and Company, LePont de Claix, France) was added. For the growth inhibition screen on plates and for microscopy seeds were sown on MS plates supplied with Nitch vitamins. MS powder including vitamins or nitch vitamins were purchased from Duchefa (Haarlem, Netherlands).

2.1.9 Antibodies

Listed below are primary and secondary antibodies used for western blot analysis.

Primary antibodies

Antibody	Source	Dilution	Reference
α-FLS2	rabbit polyclonal	1:5 000	V. Göhre[a]
α-BAK1	rabbit polyclonal	1:300	D. Chinchilla[b]

[a]Max Planck Institute for Plant Breeding Research, Carl-von-Linné-Weg 10, 50829 Cologne, Germany; synthesized by Eurogentec (Seraing, Belgium)
[b]University Basel, Hebelstr. 1, Basel 4056, Switzerland

Secondary antibodies

Antibody	Feature	Dilution	Source
goat anti-rabbit IgG-AP	alkaline phosphatase conjugated	1:30 000	Sigma Aldrich, Deisenhofen, Germany

2.1.10 Buffers and Solutions

Buffers and solutions used in this study are described below each method. If not otherwise stated, buffers were prepared in dH_2O and aqueous solutions were sterilised by autoclaving at 121°C for 20 min.

2.2 METHODS

2.2.1 Maintenance and cultivation of *Arabidopsis*

A. thaliana seeds were sown onto moist turf substrate (Stender, Schermbeck, Germany) containing 10 mg/l Confidor® WG 70 pesticide (Bayer, Leverkusen, Germany) or for pathogen assays on jiffy pellets (Jiffy Products International AS, Kristiansand, Norway), containing sphagnum peat. Before sowing the jiffy pellets were moistened in H_2O supplied with 1 ml/l Wuxal (Stender, Schermbeck, Germany) fertilizer. Seeds were stratified for two to three days at 4°C in darkness. Germination was induced by transferring the pots to a controlled environment growth chamber under short day conditions (10 h photoperiod, light intensity of approximately 200 µE/m^2s, 22°C during light period and 20°C during darkness, and 60 % humidity). For pathogen treatment plants were transferred to growth chambers designated for the respective pathogen (10 h photoperiod, 22°C and 65 % humidity). *A. thaliana* seeds used for the Opera Screen

were transferred to a Vötsch growth chamber with a 12 h light period and 60 % humidity. If required for setting seed, plants were transferred to long day conditions (16 h photoperiod) to allow early bolting and setting of seed. To collect seed, aerial tissue was enveloped with a paper bag and sealed with tape at its base until siliques shattered.

2.2.2 Generation of *Arabidopsis* F_1 and F_2 progeny

Fine tweezers and a magnifying-glass were used to emasculate an individual flower. To prevent self-pollination, only flowers that had a well-developed stigma but immature stamen were used for crossing. Fresh pollen from three to four independent donor stamens was dabbed onto each single stigma. Mature siliques containing F_1 seed were harvested and allowed to dry. Approximately ten F_1 seeds per cross were grown as described above and allowed to self pollinate. Produced F_2 seeds were collected and stored.

2.2.3 EMS mutagenesis of *Arabidopsis*

10 000 seeds were imbibed in a humid chamber and left at 4°C for 4 days. A 50 ml Falcon tube was filled with 50 ml deionised water and 0.15 ml of 0.3 % (v/v) aqueous methanesulfonic acid ethyl ester (EMS) solution was added and shaken until it was homogenous. Subsequently, the seeds were added and incubated for 10 h on a shaker. After mutagenesis the EMS solution was carefully decanted and the seeds were washed four times with 45 ml water. After transferring the seeds to a new Falcon tube, they were washed again ten times. For planting the seeds were transferred to 2 l of 0.1 % agarose solution and 10 ml were pipetted per TEKU soil pot (approximately 50 seeds per TEKU). M_2 seeds were harvested in two bags per TEKU soil pot.

For the endocytosis genetic screen the line La/FYVE-GFP was mutagenized with EMS. The efficiency of EMS treatment was estimated according to frequency of albino mutants impaired in pigment biosynthesis. 10,700 M_2 plants of 35 M_2 families were scored for an albino phenotype. Mutation frequencies for well mutagenized M_2 populations should be in the range of 2-10 % (Martinez-Zapater and Salinas, 1998). Here, a frequency of 2.7 % was observed, suggesting an optimal and sufficient mutagenesis rate.

Decontamination solution: 160 g NaOH in 4 l H_2O + 50 ml Thioglycolic acid

2.2.4 *Arabidopsis* seed sterilization

Small quantities of *A. thaliana* seeds were sterilized by ethanol treatment. Seeds were placed in columns (from DNA purification Kits, Qiagen, Hilden, Germany) and incubated in 70 % ethanol for 1 min. After centrifugation for 1 min at max. speed, the flow-through was discarded. The seeds were washed a second time in 70 % ethanol for 1 min, centrifugated for 1 min and the flow-through discarded. Then the seeds were incubated in absolute ethanol for 1 min, centrifugated for 1 min at max. speed, and the flow-through discarded. An additional centrifugation step of 2 min ensured that no residual ethanol was left. For drying the column was opened under a hood for ~ 5 min.
Large quantities of *A. thaliana* seeds were sterilized by chloride treatment. Seeds were transferred to Eppendorf tubes or Falcon tubes and placed with open lids in an exsiccator. Then 5 ml of fumy 37 % HCl were added to 100 ml 12 % sodium-hypochloride solution (chlorine bleach) in the exsiccator so that yellow-greenish vapours were forming and the solution was bubbling heavily. The lid of the exsiccator was closed immediately and vacuum was generated to get an air tight seal. The seeds were incubated for 4-6 h.

2.2.5 Maintenance of Pathogens

2.2.5.1 Maintenance of Pseudomonas syringae

Pseudomonas syringae pv. *tomato* strains described in 2.1.2.1 were streaked onto selective NYGA agar plates containing rifampicin (50 µg/ml) and/or kanamycin (50 µg/ml) from -80° C DMSO stocks. Streaked plates were incubated at 28° C for 48 h before using the bacteria for spray inoculation.

2.2.5.2 Maintenance of Hyaloperonospora arabidopsis

Hyaloperonospora arabidopsis (*H.a.)* isolates were maintained as mass conidiosporangia cultures on leaves of their genetically susceptible *Arabidopsis* ecotypes over a 7 day cycle (s. 2.1.2.2). Leaf tissue from infected seedlings was harvested into a 50 ml Falcon tube 7 days after inoculation. Conidiospores were collected by vigorously vortexing harvested leaf material in sterile dH_2O for 15 sec and after the leaf material was removed by filtering through miracloth (Calbiochem) the spore suspension was adjusted to a concentration of 4×10^4 spores/ml dH_2O using a

Neubauer counting cell chamber. Plants to be inoculated had been grown under short day conditions as described above. *H.a.* conidiospores were applied onto two week-old seedlings by spraying until imminent run-off using an aerosol-spray-gun. Inoculated seedlings were kept under a propagator lid to create a high humidity atmosphere and incubated in a growth chamber at 18° C and a 10 h light period. For long term storage *H.a.* isolate stocks were kept as mass conidiosporangia cultures on plant leaves at -80° C.

2.2.6 Pathogen infection assays and quantification

2.2.6.1 Pseudomonas growth assay

Bacterial infections were performed as previously described (Zipfel et al., 2004). In brief, PtoDC3000 cultures were grown for two days on NYGA broth agar plates containing rifampicin (50 µg/ml) and kanamycin (50 µg/ml). Bacteria were then scratched from the plates and directly transferred into a solution of 10 mM $MgCl_2$ with 0.04 % Silwet L-77 (Lehle Seeds, USA) until reaching an optical density of OD_{600} = 0.2 equal to 10^8 cfu/ml (for two-week-old plants an OD_{600} of 0.1 and 0.02 % Silwet L-77 was used). Plants were surface sprayed with the bacterial suspension. For the qualitative assay two-week-old plants were used, and the disease symptoms were recorded at 5-6 dpi. For the quantitative growth assay leaves were harvested 3 and 72 h after infection from four-week-old plants and surface sterilized (30 s in 70 % ethanol, followed by 30 s in sterile dH_2O). Two leaf discs from two different leaves were taken per plant by using a cork borer (∅ 0.5 cm) for excision, and ground in 10 mM $MgCl_2$ with a microfuge tube plastic pestle. After grinding of the tissue, the samples were thoroughly vortex-mixed and diluted 1:10 serially. Samples were finally plated on NYGA broth agar plates containing rifampicin (50 µg/ml). Plates were placed at 28° C for 2 days, after which the colony-forming units were counted. For each line six plants were analyzed. The experiment was repeated at least three times per sample.

2.2.6.2 Peronospora sporulation assay

To determine sporulation levels, seedlings were harvested 5-6 days after inoculation in a 50 ml Falcon tube and vortexed vigorously in 5 to 10 ml water for 15 sec. While the conidiospores were still in suspension, 12 µl were removed twice and spores were counted under a light microscope using a Neubauer counting cell chamber. For each

tested *A. thaliana* wild-type or mutant line, nine jiffy pots containing each approximately 10-20 seedlings were infected per experiment. Seedlings of three pots (~30-60 seedlings) were pooled and harvested spores were counted with sporulation levels expressed as the number of conidiospores per gram fresh weight. For each line three replicates were counted. The experiment was repeated at least three times per sample.

2.2.7 Molecular biological methods

2.2.7.1 Isolation of genomic DNA from Arabidopsis

Genomic DNA from *A. thaliana* cotelydons was isolated according to manufacturer's instructions with REDExtract-N-Amp^{TM} Plant PCR Kit (Sigma-Aldrich, Deisenhofen, Germany). The extraction could be performed in half the volume recommended. 2 µl genomic DNA of this quick preparation was used in subsequent PCR reactions for map based cloning.

Genomic DNA from *A. thaliana* used for sequencing analysis was isolated according to Edward's isolation protocol (Sambrook and Russel, 2001).

Edwards buffer: 200 mM Tris/HCl (pH7.5), 250 mM NaCl, 25 mM EDTA, 0.5% (w/v) SDS

2.2.7.2 Isolation of total RNA from Arabidopsis

Total RNA was prepared from three to six week-old plant material. Liquid nitrogen frozen samples (approximately 50 mg) were grinded with mortar and pestle. RNA was extracted with the RNeasy Plant Mini Kit (Qiagen, Hilden, Germany) according to manufacturer's instructions. All RNA extracts were adjusted to the same concentration with H_2O. Samples were stored at -20° C.

2.2.7.3 Polymerase Chain Reaction (PCR)

Standard PCR reactions were performed using *Taq* DNA polymerase (Amplicon, Copenhagen, Denmark) according to the manufacturer's instructions. All PCR reactions were carried out using a Peltier Thermal Cycler PTC-225 (GMI Inc., Ramsey, USA). A typical PCR reaction mix and conditions are shown below (for RT-PCR lower cycle numbers 20-25x were used, for mapping higher cycle numbers 40x):

Reaction Mix (20 µl):

Template DNA (genomic, plasmid)	2 µl
dNTPs (10 mM)	0.4 µl
10 x PCR buffer NH_4 (Amplicon)	2 µl
Primer (fwd + rev; 10 µM each)	2 µl
Taq-Polymerase (Amplicon) (5U/µl)	0.2 µl
25 mM $MgCl_2$	0.8 µl
H_2O	12.6 µl

PCR program:

1x	94°C 4 min
20-40x	94°C 30 s
	55°C 30 s
	72°C 30 s (1 kb /min)
1x	72°C 5 min
	16°C hold

2.2.7.4 Reverse-transcription polymerase chain reaction (RT-PCR)

RT-PCR was carried out in two steps. SuperScript™ II RNase H^- Reverse Transcriptase (Invitrogen, Karlsruhe, Germany) was used for first strand cDNA synthesis by combining 1 - 1.5 µg template total RNA, 1 µl oligodT primer, 5 µl dNTP mix (each dNTP 2.5 mM) in a volume of 13.5 µl (deficit made up with dH_2O). The sample was incubated at 65° C for 10 min to destroy secondary structures before cooling on ice. Subsequently, the reaction was filled up to a total volume of 20 µl by adding 4 µl of 5x reaction buffer (supplied with the enzyme), 2 µl of 0.1 M DTT and 0.5 µl reverse transcriptase. The reaction was incubated at 42° C for 60 min before the enzyme was heat inactivated at 70° C for 10 min. For subsequent normal PCR, 1 µl of the above RT-reaction was used as cDNA template.

2.2.7.5 Restriction endonuclease digestion of DNA

Restriction digests were carried out using the manufacturer's recommended conditions. Typically, reactions were carried out in 0.5 ml tubes, using 1 µl of restriction enzyme per 10 µl reaction. All digests were carried out at the appropriate temperature for a minimum of 1 h.

2.2.7.6 Gel-electrophoresis

DNA fragments were separated by agarose gel electrophoresis in gels consisting of 1 – 4 % (w/v) agarose (Bio-Budget Technologies GmbH, Krefeld, Germany) in TAE

buffer. Agarose was dissolved in TAE buffer by heating in a microwave. Molten agarose was cooled to 50° C before 2.5 µl of ethidium bromide solution (10 mg/ml) was added. The agarose was pored and allowed to solidify before being placed in TAE in an electrophoresis tank. DNA samples were loaded onto an agarose gel after addition of 2 µl 6x DNA loading buffer to 10 µl PCR reaction. Separated DNA fragments were visualised by placing the gel on a 312 nm UV transilluminator and photographed.

Agarose gel: 1 or 4 % (w/v) agarose, 0.2 µg/l ethidium bromide in 1x TAE buffer
10 x TAE (Tris/acetate/EDTA) buffer: 0.4 M tris, 0.01 M EDTA-sodium-salt, 0.2 M acetic acid
6x DNA loading buffer: 50% (v/v) glycerol, 0.1% (w/v) xylene cyanol, 0.1% (w/v) bromphenol blue

2.2.8 Biochemical Methods

2.2.8.1 Total protein extraction from Arabidopsis

One to two frozen *Arabidopsis* leaves (approximately 1 cm²) were grinded in liquid nitrogen. 100 µl protein extraction buffer was added and samples were boiled for 5 min at 95°C under shaking. Cell debris were pelleted by centrifugation at 4°C at 13 000 rpm for 10 min. 40 µl supernatant was transferred to a new Eppendorf tube and mixed with 10 µl 5x loading buffer. After boiling the samples for 5 min at 95°C, 40 µl were loaded on 7 % SDS-PAGE.

2x protein extraction buffer: 100 mM Tris-HCl (pH 6.8), 2 % SDS
5x loading buffer: 2.5 % bromphenol blue, 20 % glycerol, 4 % SDS, 10 % DTT, 200 mM Tris-HCl (pH 6.8)

2.2.8.2 SDS-Polyacrylamidgelelectrophoresis (SDS-PAGE)

To separate proteins under denaturing conditions according to their size, SDS-PAGE according to Laemmli was performed (Laemmli, 1970). Protean 3 mini gels (1.5 mm; BIO-RAD, München, Germany) were used and 20-40 µl protein samples were loaded including a protein standard (6.5 µl, Precision Plus Protein Standard; BIO-RAD, München, Germany). The gels were run at 20 to 30 mA in 1 x SDS-running buffer until the sample running front reached the gel bottom (1-1.5 h).

Separating gel (12 %):	PUG	7.5 ml
	Acrylamid	12 ml
	dH_2O	10.5 ml
	10 % APS	150 µl
	TEMED	50 µl
Stacking gel:	POG	2.5 ml
	Acrylamid	1.5 ml
	dH_2O	6 ml
	10 % APS	100 µl
	TEMED	20 µl

PUG (separating gel buffer): 1.5 M Tris-HCl (pH 8.8), 0.4 % SDS
POG (stacking gel buffer): 0.5 M Tris-HCl (pH 6.8), 0.4 % SDS

10x SDS-running buffer: 250 mM Tris/HCl, 2.5 M glycine, 1 % SDS

2.2.8.3 Western blot analysis

Semi-dry blotting of the gels onto a PVDF membrane (Imobilon, Milipore, USA) was performed in BIO-RAD Trans-Blot SD Semi-Dry transfer cell. Briefly, the PVDF membrane was activated by incubation in MeOH for 15 s and then incubated for 10 min in AB2 buffer. The semi-dry blot contained one layer of extra-thick blotting paper (BIO-RAD, USA) rinsed in AB1, a second extra-thick blotting paper in AB2, followed by the activated membrane and the polyacrylamid gel, which was washed in CB buffer. Finally, a third extra-thick blotting paper incubated in CB covered the stack. Proteins were transferred to the membrane for 1 h at 25 V.

Anode buffer 1 (AB1): 300 mM Tris, 20 % MeOH
Anode buffer 2 (AB2): 25 mM Tris, 20 % MeOH
Cathode buffer (CB): 25 mM Tris, 40 mM □-amino-n-carpic acid, 20 % MeOH

2.2.8.4 Immunodetection of proteins

Following the blotting procedure, the membranes were blocked in 5 % (w/v) milk for 1 h at room temperature and incubated with the primary antibody dilution o/n at 4°C. Then, the membranes were washed three times for 5 min in 1 x TBS-T before incubation with the secondary alkaline phosphatase-coupled antibody for 1 h at room temperature and subsequently washed three times for 5 min in 1 x TBS-T. For detection the blots were incubated with chemi-luminescence detection solution (CDP-Star, Roche Diagnostics GmbH, Mannheim, Germany) and light emission was documented on x-ray films (Hyperfilm, Amersham Pharmacia, Freiburg, Germany).

As protein loading control the membranes were stained with coomassie dye. Briefly, the membranes were washed in H_2O and incubated for 5 min in coomassie staining solution. Destaining was achieved by washing the membranes twice in destaining solution I for 5 min and washed in H_2O before imaging for documentation.

Coomassie staining solution: 0.25 % coomassie brilliant blue, 50 % MeOH,
Destaining solution I: 50 % MeOH
Blocking solution: 5 % milk powder in 1 x TBS-T
TBS-T (tris buffer saline- tween 20): 140 mM NaCl, 2.5 mM KCl, 25 mM Tris-HCl (pH 7.4), 0.05 % Tween 20

2.2.8.5 Binding assay

Chemical binding studies were performed as described (Bauer et al., 2001). Briefly, plant homogenates were prepared by grinding 140 mg fresh mass and re-suspending it in 700 µl binding buffer. Samples containing 100 µl plant extract were incubated with 0.6 nM ^{125}I-Tyr-flg22 and with (nonspecific binding) or without (total binding) 1 µM unlabeled flg22. After incubation on ice for 10 min, free label was separated from bound label by vacuum filtration. Radioactivity was determined by γ-counting. Specific binding was calculated by subtracting nonspecific from total binding.

2.2.8.6 In-gel MAP kinase assay

Seeds were grown on MS plates for 7 days and transferred to liquid MS medium (24 well plates) for further 10 days growth. MS liquid medium was refilled in the wells (1-2 ml) and after 2 h, flg22 solution was added (end-concentration: 100 nM). Samples were harvested at indicated time points after flg22 treatment by drying the seedlings, cutting the roots, transferring them to 2 ml tubes, and freezing them in liquid nitrogen within 2 min. Separating and stacking gels were prepared as follows:

<u>11.25 % Separating Gels (2 mini gels):</u>

Acrylamide:bis- (30 %:0.8 %)	3	ml
1.5 M Tris-HCl (pH 8.8)	2	ml
Water	2.4	ml
MBP (5 mg/ml)	0.4	ml
10 % SDS	0.08	ml
10 % APS	0.08	ml
TEMED	0.008	ml

Solution for separating gels was mixed and poured into a space between glass plates (0.75 mm glass plates). Immediately, 1 ml of iso-propanol was added. After 1 h of polymerization, the iso-propanol was discarded and the stacking gel prepared.

<u>Stacking gels (2 mini gels)</u>:

Acrylamide:bis- (30 %:0.8 %)	1	ml
0.5 M Tris-HCl (pH 6.8)	1	ml
Water	1.94	ml
10 % SDS	0.04	ml
10 % APS	0.17	ml
TEMED	0.005	ml

Stacking gel solution was mixed and added on top of the separating gels. Then the well spacers were placed, and the gel polymerized at RT for 1 h.

Frozen leaf tissue was grinded in liquid nitrogen with a pestle and 100 mg were weighed in 2 ml tubes, 150 µl of extraction buffer were added, and re-suspended by vortexing. After a centrifugation step at 14 000 rpm for 20 min at 4°C, the supernatant was transferred to a new tube (30 µl aliquots, rest supernatant was stored at - 80°C). Then 15 µl of loading buffer was added to 30 µl of supernatant and vortexed, boiled for 5 min, and 15 µl of the sample was loaded on denaturing SDS-polyacrylamid gel containing myelin basic protein (MBP) as substrate (8 µl of protein ladder was loaded). The gel was run at 20 mA per gel (stacking gel) and 30 mA per gel (separating gel) for 1-1.5 h (running buffer Tris-Glycin-SDS)

Extraction buffer (20 samples):

1 M Tris-HCl (pH 7.5)	150 µl
0.5 M EGTA	30 µl
0.5 M EDTA	30 µl
1 M DTT	6 µl
0.1 M AEBSF (Pefabloc)	6 µl
Protease Inhibitor for plants (SIGMA)	80 µl
1 M NaF	30 µl
1 M Na3VO4	15 µl
1 M ß-glycerophosphate	150 µl
H_2O	2503 µl
	3000 µl

Loading buffer:

0.5 M Tris-HCl (pH 6.8)	2.5 ml
100 % glycerol	6 ml
10 % SDS	3.2 ml
BPB	1 mg
Water	20 ml

Before use 250 µl of 1 M DTT were added to 300 µl of the above solution and mixed by vortexing.

After the SDS-PAGE run, the protein gels were washed and re-naturated and incubated with radioactively labelled ^{32}P-ATP. Several washing steps followed.

Washing steps (2 mini gels):

Buffers	Buffer contents	Washing steps	Speed
F	5 ml 1 M Tris-HCl (pH 7.5) 100 µl 1 M DTT 20 µl 1 M Na_3VO_4 1 ml 1 M NaF 0.1 g BSA 2 ml 10 % Triton X 100 @ 200 ml with H_2O	3 x 30 min, RT	45 rpm
G	5 ml 1 M Tris-HCl (pH 7.5) 200 µl 1 M DTT 20 µl 1 M Na_3VO_4 1 ml 1 M NaF @ 200 ml with H_2O	2 x 30 min, 4 °C over night, 4 °C	45 rpm

H	2.5 ml HEPES 20 µl 0.5 M EGTA 400 µl 3 M $MgCl_2$ 100 µl DTT 10 µl 1 M Na_3VO_4 @ 100 ml with H_2O	1 x 30 min, RT	45 rpm
Radioactivity	20 ml buffer H 40 µl 100 µM ATP 2 µl y-^{32}P-ATP (5 µCi/µl) / 2 mini gels	1 x 90 min, RT	92 rpm
1 % phosphoric acid	11.76 ml phosphoric acid (86%) @ 1 l with H_2O	3 x shortly, RT, 15 ml 6 x 30 min, RT, 50 ml	45 rpm
H_2O		20 min, RT, 50 ml	45 rpm

Then the gels were put in an autoclaving bag and a screen was put on the gels in a cassette for 1 h and/or overnight. Subsequently, the screen was scanned with a phosphor imager (Typhoon 8600 Phosphor imager und Image Eraser, molecular dynamics, Sunnyvale, USA). Image processing was performed with AdobePhotoshop8.0 (Adobe Systems Inc., San Jose, CA, USA).

2.2.9 Bioassays to monitor PAMP responses

2.2.9.1 Seedling Fresh Weight

Seedling fresh weight was assayed as previously described (Gomez-Gomez et al., 1999). In brief, seedlings grown for five days on MS agar plates were transferred to liquid MS medium containing the peptides indicated. After 7-10 days the effect of the different peptides on seedling growth was analyzed by weighing (fresh weight).
For genetic screening seedling growth was performed directly on plates. After five days of growth on MS plates, 1 µM peptide solution was added and growth differences were observed eight days later.

2.2.9.2 Reactive Oxygen Species (ROS) detection

Oxidative burst analysis in *A. thaliana* leaf pieces was performed following standard procedures (Gomez-Gomez et al., 1999). The assay measures active oxygen species released by leaf tissue by H_2O_2-dependent luminescence of luminol (Keppler et al., 1989). In brief, leaves of *A. thaliana* were cut into ~1 mm slices and incubated overnight in H_2O. Slices were transferred into microtiter plates (OptiPlate-96 F, Perkin

Elmer, Waltham, USA) containing 100 µl H_2O supplied with 20 µM luminol and 1 µg horseradish peroxidase (Sigma-Aldrich, Deisenhofen, Germany). Luminescence was measured in a luminometer (Centro LB 960 microplate luminometer, Berthold Technologies, Bad Wildbad, Germany) for 35 min after addition of peptide solutions.

2.2.9.3 Analysis of callose deposition

Callose staining was performed as previously described (Gomez-Gomez et al., 1999). In brief, callose deposition was analyzed in fully expanded leaves of 4- to 6-week-old *A. thaliana* plants. Leaves were vacuum-infiltrated with a 1 ml syringe containing H_2O, 2 µM flg22, or 2 µM elf18 peptide solution and harvested after 20-24 h. Then the leaves were cleared in acetic acid/ethanol 1:3 (v:v) over night, subsequently washed in H_2O and stained in aniline blue solution o/n. Stained material was mounted in 50 % glycerol and examined using ultraviolet epifluorescence with a Zeiss Axiophot2 fluorescence microscope (Carl Zeiss MicroImaging GmbH, Jena, Germany).

Aniline blue staining solution: 150 mM KH_2PO_4, 0.01% (w/v) aniline blue, pH9.5 (KOH pellets)

2.2.9.4 Ethylene measurement

Ethylene biosynthesis in *A. thaliana* leaf pieces was measured as previously described (Bauer et al., 2001). In brief, leaves of six-week-old *A. thaliana* plants were cut in 2-3 mm slices and incubated over night in H_2O. Ten leaf slices were transferred per glass tube containing 1 ml H_2O. After the addition of 2 µM aqueous peptide solution (flg22 or elf18) the vials were rapidly closed with rubber septa and placed horizontally on a shaker (100 rpm) at RT. Ethylene accumulating in the free air was measured by gas chromatography (GS MS) after 4-6 h for flg22 and 6-8 h for elf18 treatment (injection volume: 100 µl).

2.2.10 *In-vivo* imaging techniques

2.2.10.1 Fluorescence microscopy

Fluorescence microscopy was performed with a Zeiss Axiophot2 fluorescence microscope (Carl Zeiss MicroImaging GmbH, Jena, Germany) equipped with UV light source and a digital camera (AxioCam MRc5). Detached leaves of four to six-week-old plants were mounted in 50 % glycerol on microscopic slides for imaging.

Epifluorescense was analyzed with a 5x objective. Images were processed using the software Axiovision von Zeiss (Carl Zeiss MicroImaging GmbH, Jena, Germany).

2.2.10.2 Confocal laser scanning microscopy

Confocal laser scanning microscopy was performed with a Leica TCS SP2 AOBS (Leica Microsystems, Bensheim, Germany) microscope equipped with an Argon/Helium-Neon laser and diode laser of 405 nm. Detached leaves of two to three weeks old plants were mounted in H_2O on microscopic slides for imaging. Excitation of the samples was performed at 488 nm for GFP. Emission spectra were taken from 490 to 560 nm for GFP. Images were processed using the Leica Confocal Software Version 2.61 and Adobe PHOTOSHOP 8.0 (Adobe Systems Inc., San Jose, CA, USA).

2.2.10.3 Automated confocal laser imaging technology (Opera)

Confocal high throughput imaging was performed with the Opera microscope (Perkin Elmer, Hamburg, Germany), which contains four laser based excitation sources 405, 488, 561, 635 nm. Additionally, it is equipped with three 1.3 MPixel CCD cameras with a nipkov disk. Excitation of the samples was performed at 488 nm for GFP. The emission spectrum was taken from 502 to 577 nm.

2.2.10.3.1 Preparation of leaves for high-throughput screening with the Opera

For high-throughput imaging leaves were prepared in 96-well sensoplates with glass bottom (Greiner Bio-One GmbH, Essen, Germany). For leaf preparation a particular stamp was used containing 96 pins with a soft tissue out of neoprene on top to prevent damage of the leaves. A fine film of Vaseline® was distributed on the neoprene tissue to render it sticky. Detached cotyledons of two-week-old *A. thaliana* plants were placed upside up onto the stamp. Both cotyledons of each plant were imaged. Due to technical reasons the pins at the margins were left free, resulting in 60 leaves from 30 plants on the stamp. The fully loaded stamp was then turned upside down and inserted into a water filled 96-well microplate with an optical glass bottom. After 5 min the plate was ready for imaging. Since the Opera microscope is an inverted microscope the stamp could be left on the plate during imaging.

2.2.10.3.2 Image processing and automated analysis

For the automated screen certain areas of the leaf had to be defined for imaging. For the reference line FYVE-GFP, five areas per leaf were defined. Because two leaves per plant were processed, up to ten images per plant could be analyzed for their endosomal content (~30 cells per image), which was sufficient for reliable quantification. Due to the curvature of the leaves images of a consecutive series of 21 planes (z-stack) with a distance of 1 µm were taken per area. Thus, in total 105 images were taken per leaf.

The images were automatically analyzed with the Acapella Software. To merge the three-dimensional stack of 21 optical planes, an image projection was performed, resulting in a two-dimensional pseudo image. Subsequently, the pseudo-image was analyzed with a pattern-recognition script, specifically identifying FYVE-GFP labelled endosomes. The script was developed in collaboration with Perkin Elmer (Meyer, 2008) and further modified (with the help of Kurt Stüber (bioinformatician) and Sebastian Schaaf (bachelor student)). Several parameters such as cell boundary recognition or large spot detection were already implemented for pictures of 20 x magnification. However, in our study we used larger magnification (40 x objective) to visualize smaller objects (endosomes). Moreover, a different transgenic *Arabidopsis* line with different fluorescence signal intensities was used. Therefore, the Acapella script parameters had to be optimized accordingly. Manual inspection of object recognition revealed that quantitative differences in endosomal numbers could be detected reliably und unbiased. Besides the analysis of FYVE-GFP endosomes, also the number and size of epidermal leaf cells were analyzed, resulting in 33 output parameters, which are listed and described in (Table 6).To facilitate and fasten the analysis of the output results we generated a script for graphical presentation of the output data with respect to the different parameters. Six parameters were chosen that were depicted routinely in graphics for the genetic screen (highlighted in Table 1).

Table 6: Description of the Output Parameters Measured During the Automated high-throughput Imaging. Parameters (1-8) were first calculated per individual stack (5 stacks per leaf). Subsequently, average parameters (9-30) per leaf (whole well; stack 1-5) and per seedling (two leaves; 10 stacks) were calculated (31-33). Parameters that were needed to calculate respective parameters per seedling are marked in dark blue. Parameters that were routinely depicted in graphics during the genetic screen are highlighted in grey. SD: standard deviation.

	output parameter (per stack)	description
1	Number of valid cells in stack	Number of recognized cells per picture; cells that were too big (> 40 000 pixel) or small (< 800 pixel) were excluded (possibly false recognitions)
2	Number of valid spots in stack	Number of spots within recognized cells
3	Number of spots in and out of cells in stack	Total number of spots per stack
4	Percents of inner spots in stack	If >25 % of spots lie within recognized cells, parameter average number of spots/image area is calculated.
5	Average area of cells in stack	Average area of cells in pixel (+SD)
6	Percents of found cell area in stack	
7	Average number of spots in cells in stack	Average number of spots in cells in stack (+SD)
8	Average number of spots per recognized area	
9	Number of leaf cells in whole well	Sum of cells of good pictures
10	Average cell area in whole well	Average area of cells in all good pictures (+SD)
11	Number of spots in whole well	Sum of spots found within recognized cells in all pictures
12	Total cell area in well	Sum of recognized cell area of all pictures per well
13	Percentage of total cell area in well	
14	Number of stomata	Number of recognized stomata per picture
15	Average intensity of spots	Average brightness of spots per picture
16	Average area of spots	Average area of spots per picture
17	Average length of spots	Average length of spots per picture
18	Average half width of spots	Average half width of spots per picture
19	Average width to length ratio of spots	Average width to length ratio of spots (+SD)
20	Average roundness of spots	Average roundness of spots (+SD)
21	Average contrast of spots	Average contrast of spots (+SD)
22		
23	Average area of cells	Average area of cells in pixel (+SD)
24	Average cell area in whole well	Average area of cells in all good pictures (+SD)
25	Average number of spots in cells	Average number of spots per recognized cell (+SD)
26	Average number of spots per cell in whole well	Average number of spots per cell in all good pictures (+SD)
27	Average peak intensity of spots	
28	Total number of stacks analyzed	
29	Number of valid stacks in well	Number of stacks with good (valid) pictures in well
30	Percentage of valid stacks in well	
31*	Average number of spots per 100 % image area	Average number of spots per 100 % image area per seedling
32*	Average number of found spots per image	Average number of found spots (in and out of recognized cells) per image per seedling
33*	Average number of spots per cell	Average number of spots per cell per seedling

* Parameter 31 was calculated as follows:

$$\text{Average number of spots/100 \% image area} = \frac{100 * \sum(\text{number of valid spots in stack})}{\sum(\text{percents of found cell area in stack})}$$

Paramter 32 was calculated as follows:

$$\text{Average Number of found spots per image} = \frac{\text{number of spots in and out of cells in stack}}{\text{number valid stacks in well 1 and well2}}$$

Parameter 33 was calculated as follows:

$$\text{Average number of spots per cell} = \frac{\sum(\text{number of valid spots in stack})}{\sum(\text{number of valid cells in stack})}$$

2.2.11 Software

2.2.11.1 DNA sequence analysis

DNA sequences were determined by the MPIZ DNA core facility on Applied Biosystems (Weiterstadt, Germany) Abi Prism 377, 3100 and 3730 sequencers using BigDye-terminator v3.1 chemistry. Premixed reagents were from Applied Biosystems. Subsequent sequence analysis was performed using VectorNTI (Invitrogen, Karlsruhe, Germany). PCR products were purified with the Nucleospin Extract-Kit (MACHEREY-NAGEL) ensuring sufficient amount at appropriate concentration to be directly sequenced. Alignments were conducted with the AlignX or ConticExpress programs of Vector NTI Advance 10 (Invitrogen, Karlsruhe, Germany), whereas Primer Design and restriction fragment analysis was done in the main program Vector NTI.

Annotated DNA sequences, mapping primer, and SNP information were obtained from online genome databases listed below (Table 7).

Table 7: Web Resources

Database	Specification.	Web page
NCBI	National Centre for Biotechnology Information	http://www.ncbi.nlm.nih.gov/
TAIR	The Arabidopsis information resource	http://www.arabidopsis.org/
BAR	The Bio-Array Resource for Arabidopsis Functional Genomics	http://bbc.botany.utoronto.ca/
MSAT	The V.A.S.T lab-Variation and Abiotic Stress Tolerance	http://www.inra.fr/internet/Produits/vast/msat.php
SNP	WeigelWorld- polymorph tools	http://polymorph.weigelworld.org/
RIL/SNP	Genetic/Genotyping Resources	http://www.naturalvariation.org/

2.2.11.2 Statistical analysis

For statistical analyses Excel was used to perform a two-sided heteroescdastic t-test to determine the statistical significance of the difference between two sample means. Systat Version 11 (2004, Systat Software GmbH, Erkrath, Germany) was used to determine the statistical significance of the difference between two sample means measured in repeated experiments. For analysis of pathogen infection assays we transformed data by taking the logarithmus of the count to meet assumptions of

ANOVA. Subsequently, a pairwise comparison (Tukey corrected) was performed. Statistical significant differences were observed when the p-value was <0.05.

2.2.11.3 Image processing

For general picture processing Adobe PHOTOSHOP 8.0 and Adobe ILLUSTRATOR 11.0.0 (Adobe Systems Inc., San Jose, CA, USA) were used.

The Leica software 'Leica Confocal Software', Version 2.61 (Leica Microsystems Heidelberg GmbH, Germany) was used to process images taken with the Leica Confocal microscope.

The Zeiss software 'AxioVision' Version 4.4 (Zeiss, Jena, Germany) was used to take pictures with the Zeiss fluorescence microscope.

The software 'Acapella' Version 2.0 (Perkin Elmer Cellular Technologies, Germany) was used to process the images taken with the Opera microscope.

3 RESULTS

In order to identify new components of PAMP signaling, we performed a combinatorial genetic approach of forward genetic screening and mutant candidate analysis. We further hypothesized that new PAMP signaling components would be linked with endocytic trafficking and therefore balanced our screens between typical PAMP responses and cell biology.

3.1 NATURAL VARIATION OF THE FLS2 MEDIATED FLAGELLIN RESPONSE

To reveal new components of PAMP signaling previous successful genetic screening was refined (Gomez-Gomez and Boller, 2000), since it only led to the identification of the *fls2* mutant. In order to enhance sensitivity of the response to flg22 by seedling growth inhibition, the crosstalk between flg22 and UV-B was used. The screen is based on observations made by Logemann and Hahlbrock revealing that pathogen defense overrides UV-B protection in parsley cell culture through an inversely light-regulated ACE type gene promoter element (Logemann and Hahlbrock, 2002). Accordingly, wild-type plants that are responsive to flg22 fail to turn on their UV protection pathway, which leads to lower growth. In contrast, flg22-insensitive mutants are able to activate their UV defense and grow normally. Also, ecotype variation was thought to further enhance the possibility identifying novel components (Bauer et al., 2001).

Thus, we applied the flg22/UV-B crosstalk screen to the Nordborg and Koornneef collection comprising 180 *A. thaliana* ecotypes (Suppl. Table 1). Nine-day-old seedlings were treated for 4 h with 10 nM flg22 followed by 6 h UV-B light. Since all ecotypes exhibit different growth rates, controls with no or individual stress treatments were included for each ecotype. Initially, 36 ecotypes were selected as flg22-insensitive and were further subjected to various flg22 responses. We measured seedling growth in liquid medium upon 100 nM flg22 treatment and identified five out of 36 ecotypes (Suwon, Sij-1, Cvi-0, Kas-1 and Got-22) that showed strong flg22 insensitivity (Fig. 4). We further tested the 36 ecotypes for their responsiveness towards the bacterial PAMP EF-Tu (elf18), and identified one ecotype (Nes-1) as elf18-insensitive (data not shown).

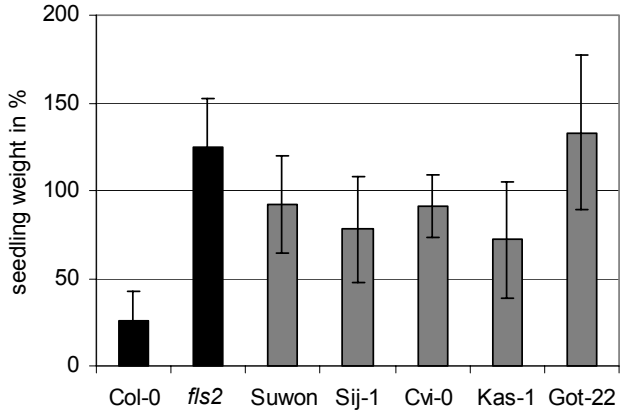

Fig. 4: Seedling Growth of flg22-Insensitive Ecotypes. Fresh weight of plants without flg22 was set to 100 %, and fresh weight after seven days of 100 nM flg22 treatment was calculated accordingly. Error bars indicate 6 replicates.

To test at which level the five candidate ecotypes were affected in flg22 signaling, we measured ROS production as early flg22 response (Fig. 5). We included Col-0 as positive control and Ws-0 as negative control (natural *fls2* mutant). The ecotypes Suwon, Sij-1 and Cvi-0 failed to mount an oxidative burst, but Kas-1 and Got-22 exhibited a normal flg22-triggered oxidative burst.

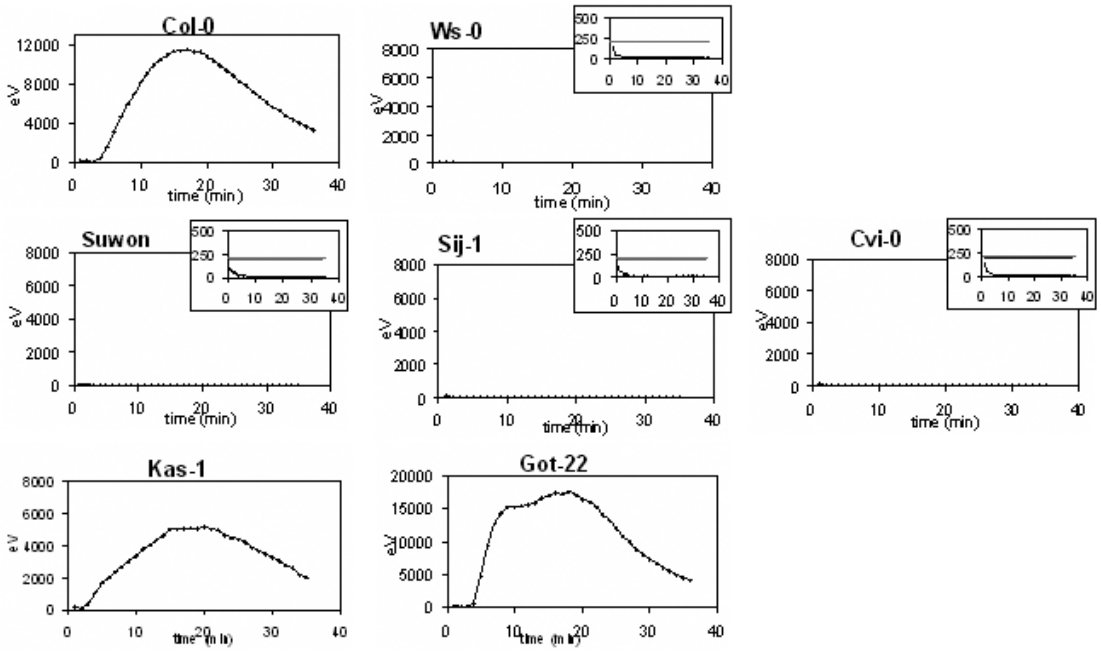

Fig. 5: Characterization of flg22-Insensitive Ecotypes. Generation of ROS. Oxidative burst is measured in eV luminescence after addition of 1 µM flg22 for 35 min. For each ecotype six leave pieces were analyzed from which one representative curve is shown. The experiment was repeated three times with similar results.

Next we monitored flg22-induced callose deposition as a downstream response. Col-0 showed a strong deposition of callose after 24 h of 1 µM flg22 treatment, while Ws-0 did not (Fig. 6). The ecotypes Sij-1, Suwon and Got-22 did not accumulate any callose, whereas Kas-1 exhibited a weak callose deposition.

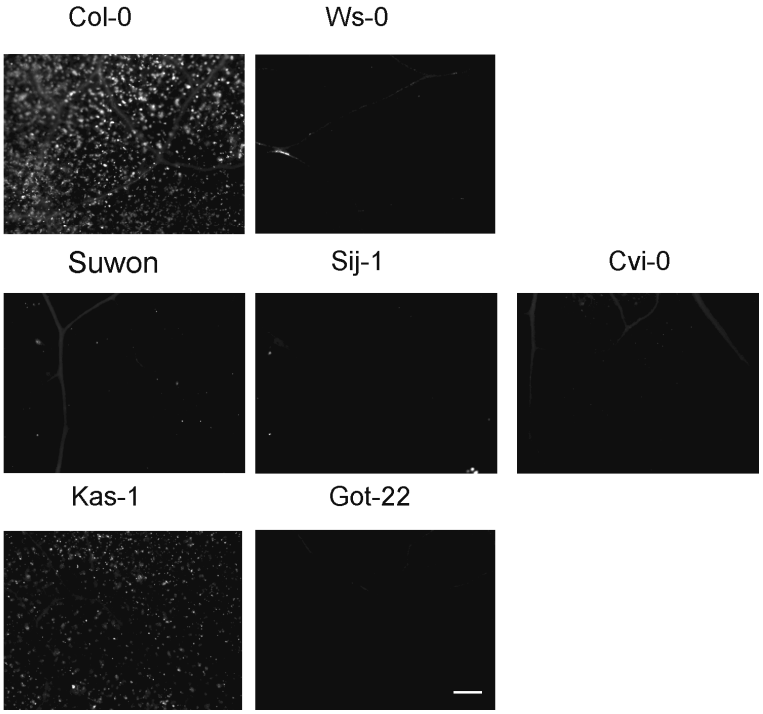

Fig. 6: Characterization of flg22-Insensitive Ecotypes. Callose Deposition upon 2 µM flg22 Treatment. Leaves were first destained with acetic acid ethanol and then stained with aniline blue. Callose deposits were visualized using a fluorescence microscope (5x objective). Three independent experiments showed similar results. Bar: 200 µm.

To exclude that the candidate ecotypes carry mutations in the *FLS2* gene we performed a sequence analysis of the respective ecotypes (Fig. 7).

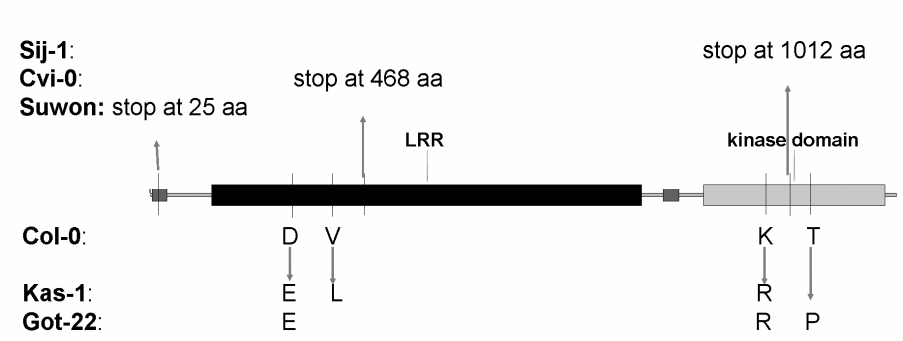

Fig. 7: Schematic Representation of FLS2 Amino Acid Sequence Differences within flg22-Insensitive Ecotypes. Suwon, Sij-1 and Cvi-0 carry 1 and 5 bp deletions, respectively, leading to premature stop codons, whereas Kas-1 and Got-22 carry three polymorphic differences.

The ecotype Suwon carries a 5 bp deletion leading to a premature stop codon after 25 aa. Cvi-0 has a 1 bp deletion in the LRR-domain leading to a stop codon after 468 aa, and Sij-1 has a 1 bp deletion in the kinase domain resulting in a stop codon at 1012 aa. The ecotypes Kas-1 and Got-22 carry three amino acid differences, respectively, compared to Col-0 derived FLS2. Whether the polymorphic differences in Kas-1 and Got-22 lead to a non-functional FLS2 protein cannot be excluded at the moment. However, western blot analysis revealed that FLS2 protein is expressed in Kas-1 and Got-22 (data not shown).

Suppl. Table 1: List of 180 Ecotypes Analyzed in the flg22/UV-B Screen. Confirmed candidates are highlighted in grey. + flg22-sensitive; - flg22-insensitive; n.d. not determined; * not enough seeds; $^{\Delta}$ confirmed in later experiments

ecotypes	flg22/UV-B screen	confirmed	ecotypes	flg22/UV-B screen	confirmed	ecotypes	flg22/UV-B screen	confirmed
Ag-0	+		Cvi-0	-	-	HR-5	+	
AK	+		Daejon	+		Jea	+	
Alc-0	+		Dra-0	+		Ka-0	-	+
Amel-1	+		Driel*	-	n.d.	Kas-1	-	-
An-1	+		Eden-1	-	+	Kas-2	+	
Ang	+		Eden-2	+		Kil-0	+	
Ann-1	-	+	Edi-0	-	+	Kin-0	+	
Aq-0	+		Ei-2	+		Kl-2	+	
Baa-1	+		Ei-2	+		Kn-0	+	
Bay-0	+		Eil-2	+		Knox-10	+	
Be-0	+		Ely-1a*	-	n.d.	Knox-18	-	+
Bil-7	+		Ema-1	+		Konchezero	+	
Bl-1	+		En-2	+		Kondara	+	
Bla-10	+		Eri	+		Kvo-1	+	
Blh-1	+		Es-0	+		Kz-1	+	
Boot	+		Est-0	+		KZ-13	+	
Bor-1	+		Est-1*	-	n.d.	Kz-9	+	
Bor-4	+		Fab-2	+		Ler-1	+	
Br-0	-	+	Fab-4	+		Lim	-	+
Bs-1	-	+	Fei-0	+		LL-0	+	
BSO-1a*	-	n.d.	Fi-1	+		Lm-2	+	
Bur-0	+		Fuk	-	+	Lov-1	-	+
Byn	+		Ga-0	+		Lov-5	-	+
C24	+		Ga-0	+		Lp2-2	+	
Cal-0	+		Gd-1*	-	n.d.	Lp2-6	-	+
Calamin	+		Ge-0	+		Lz-0	+	
Can-0	+		Got-22	-	-	Mr-0	+	
Car-1	+		Got-7	+		Mrk-0	+	
Cerv-1	-	+	Gre-0	+		Ms-0	+	
Chat-1	-	+	Gu-0	+		Mt-0	+	
Chi-0	+		Gu-0	+		Mz-0	+	
CIBC-17	+		Gy-0	+		Nd-1	+	
CIBC-5	+		Gy-0	+		Nes-1	-	+
CS 22491	+		Hey	-	+	NFA-10	+	
Ct-1	+		HR-10	+		NFA-8	+	

ecotypes	flg22/UV-B screen	confirmed
No-0	+	
Nok-3	+	
Omo2-1	-	+
Omo2-3	-	+
Orn	+	
Oy-0	+	
Pak-3	+	
Per-1	+	
Pet-0	+	
Pna-10	+	
Pna-17	+	
Pro-0	+	
Pu2-23	+	
Pu2-7	+	
Ra-0	+	
Ren-1	+	
Ren-11	+	
Ri-0	+	
RIB-1	+	
RLD-1	+	
Rmx-A02	+	
Rmx-A180	+	
Rome-1	+	
RRS-10	+	
RRS-7	+	
Rsh-0	+	
Sah-0	-	+
Sakhdara	+	
Sapporo	-	+
Sav-0	+	
Se-0	+	
Sei-0	-	+
Sf-2	+	
Sij-1	-	-
Sorbo	+	
Spr1-2	+	
Spr1-6	+	
Sq-1	+	
Sq-8	+	
St-0	+	
Stor	-	+
Strand	-	+
STW-0	+	
Suwon	-	-
Tamm-2	+	
Tamm-27	-	+
Te-0	+	
Terlet*	-	n.d.
Tha-1	+	
Ts-1	+	
Ts-5	+	
Tschag	+	
Tsu-0	-	+
Tsu-1	+	
Uk-2	+	
Ull2-3	+	
Ull2-5	-	+
Uod-1	-	+
Uod-7	+	
Van-0	+	
Var2-1	+	
Var2-6	+	
Vil-0	+	
Wa-1	-	+
Wag-1	-	+
Wei-0	+	
Wha-2	+	
Ws-2$^{\Delta}$	-	-
Wt-0	+	
Yam	+	
YK	+	
Yo-0	+	
Zdr-1	-	+
Zdr-6	+	
Zu-1	+	

Total # screened	180	
flg22-insensitive	43	
re-screened		36
confirmed		6

3.1.1 Concluding Remarks

In this study, we identified three *Arabidopsis* ecotypes, Sij-1, Suwon and Cvi-0, with clearly impaired flg22 responses, which carried premature stop codons in their *FLS2* alleles. Two ecotypes expressing *FLS2* variants, Kas-1 and Got-22, were identified that were only affected in some flg22-triggered responses. To determine whether the amino acid differences in Kas-1 and Got-22 are relevant for FLS2 function or are due to ecotype variations, the neighbouring amino acid sequences were inspected. One of the amino acid differences resides in the LRR domain, but does not affect conserved residues of the LRR motif (Fig. 7). The other amino acid differences are located in the kinase domain, respectively. Previously, a *FLS2* mutant allele, *fls2-24*, was identified that contains a point mutation in the 10th LRR domain, resulting in disrupted flg22 binding (Gomez-Gomez and Boller, 2000; Gomez-Gomez et al., 2001). However, early flg22 responses were unaffected in Kas-1 and Got-22, suggesting that flg22 binding is unlikely to be altered. Another *FLS2* mutant allele, *fls2-17*, carries a point mutation in a conserved residue in the kinase domain (Gomez-Gomez and Boller, 2000; Gomez-Gomez et al., 2001). In contrast to *fls2-24*, the *fls2-17* mutant failed to accumulate FLS2 protein (Robatzek et al., 2007). Kas-1 and Got-22 carry each one difference outside conserved regions of the kinase, whereas Got-22 has one additional amino acid difference affecting the kinase active site. It could be possible that Kas-1 encodes a novel yet unidentified component of the flg22 signaling cascade.

Analyzing variation within *A. thaliana* revealed an unexpected high number of naturally occurring *fls2* mutants. Out of 181 ecotypes we now know seven flg22-insensitive accessions, of which five are *fls2* mutants (Cvi-0, Sij-1, Suwon, Ws-0, and Ws-2). This represents a total of 4 % flg22-insensitive ecotypes, and they do not display any preferred geographical location. In line with this, in a recent study Dunning *et al.* sequenced 11 *A. thaliana* accessions and tested 23 accessions for flg22 responses, and independently found three ecotypes with premature stop codons (Cvi-0, Dra-0, and Po-0) (Dunning et al., 2007). In the flg22/UV-B crosstalk screen Cvi-0 was also identified, while Dra-0 was not and Po-0 was not included in the ecotypes screened. Unfortunately, the flg22/UV-B crosstalk screen mostly resulted in identification of additional *FLS2* alleles, thus a second forward genetic screen with a mutant population was performed.

Our findings strongly suggest that loss-of FLS2 function has appeared several times independently indicative of ongoing selection of FLS2 evolution. However, the relatively high number of naturally occurring *fls2* mutants also implies that loss-of FLS2-function might have had an evolutionary advantage at a given time. Another explanation would be that loss-of FLS2 function might be the cost for the ongoing counter-evolution between plants and microbes. It was reported that pathogens can evade flagellin perception by altering their flagellin sequence (Felix et al., 1999; Pfund et al., 2004; Sun et al., 2006). As a consequence, plants vary their *FLS2* sequence to maintain the ability to detect flagellin of pathogens (Dunning et al., 2007). In the case these variations result in loss-of FLS2 function, the build in repertoire of PRRs in plants provides reasonably protection even in the absence of one functional PRR.

3.2 GENETIC ANALYSIS OF *ARABIDOPSIS* DEFENSE SIGNALING IN RESPONSE TO PAMPS

In order to dissect PAMP signaling in *Arabidopsis* and to identify novel components of the flg22/FLS2 pathway, a forward genetic screen was employed. The seedling growth inhibition response in the presence of flg22, an easy screenable phenotype, has been successfully used to identify FLS2 (Gomez-Gomez and Boller, 2000). In addition, mutants of the FLS2 co-receptor *bak1* also displayed reduced sensitivity to flg22 in seedling growth assays (Chinchilla et al., 2007b). Here, we modified the seedling growth assay to allow high-throughput screening of a large set of mutated La-er population.

3.2.1 Isolation of flg22-Insensitive (*fli*) Mutants

Approximately 40 000 M_2 seeds of gamma-irradiated La-er plants were screened for reduced flg22 sensitivity by seedling growth on plates (Suppl. Fig. 1). Similar to previous observations (Gomez-Gomez et al., 1999) wild-type plants with a functional *FLS2* gene displayed a seedling growth arrest, whereas mutant plants such as *fls2* did not show this severe growth reduction on plates. Seedlings exhibiting increased growth compared to wild-type in the presence of flg22 were selected as flg22-insensitive candidates. Initially selected 675 putative candidates were further tested for early and late flg22 responses. A total of 642 candidates exhibited a flg22-triggered oxidative burst, likely representing other alleles than *fls2* or *bak1* mutants. Furthermore, 265 candidates were impaired in flg22-triggered callose deposition, suggesting that they were affected in PAMP signaling rather than developmental growth differences. In the M_3 generation 70 candidates could be confirmed, referred to as *fli* mutants (for flg22-insensitive), of which three *fli* mutants were chosen for further analysis.

3.2.2 Late PAMP Responses are Severely Reduced in *fli* Mutants

Seedling growth of *fli1*, *fli3* and *fli6* appeared mostly wild-type-like in the absence of any stimulus, but is significantly different when flg22 was applied (Fig. 8A). In the control treatment, the *fli* mutants have a similar size as wild-type (La-er) and *fls2-17* mutant seedlings. Notably, in the presence of flg22 *fli* mutants display an intermediate

phenotype; the size of aerial parts and roots are in between those of wild-type and *fls2-17* mutants, suggesting that only a subset of flg22 responses is affected.

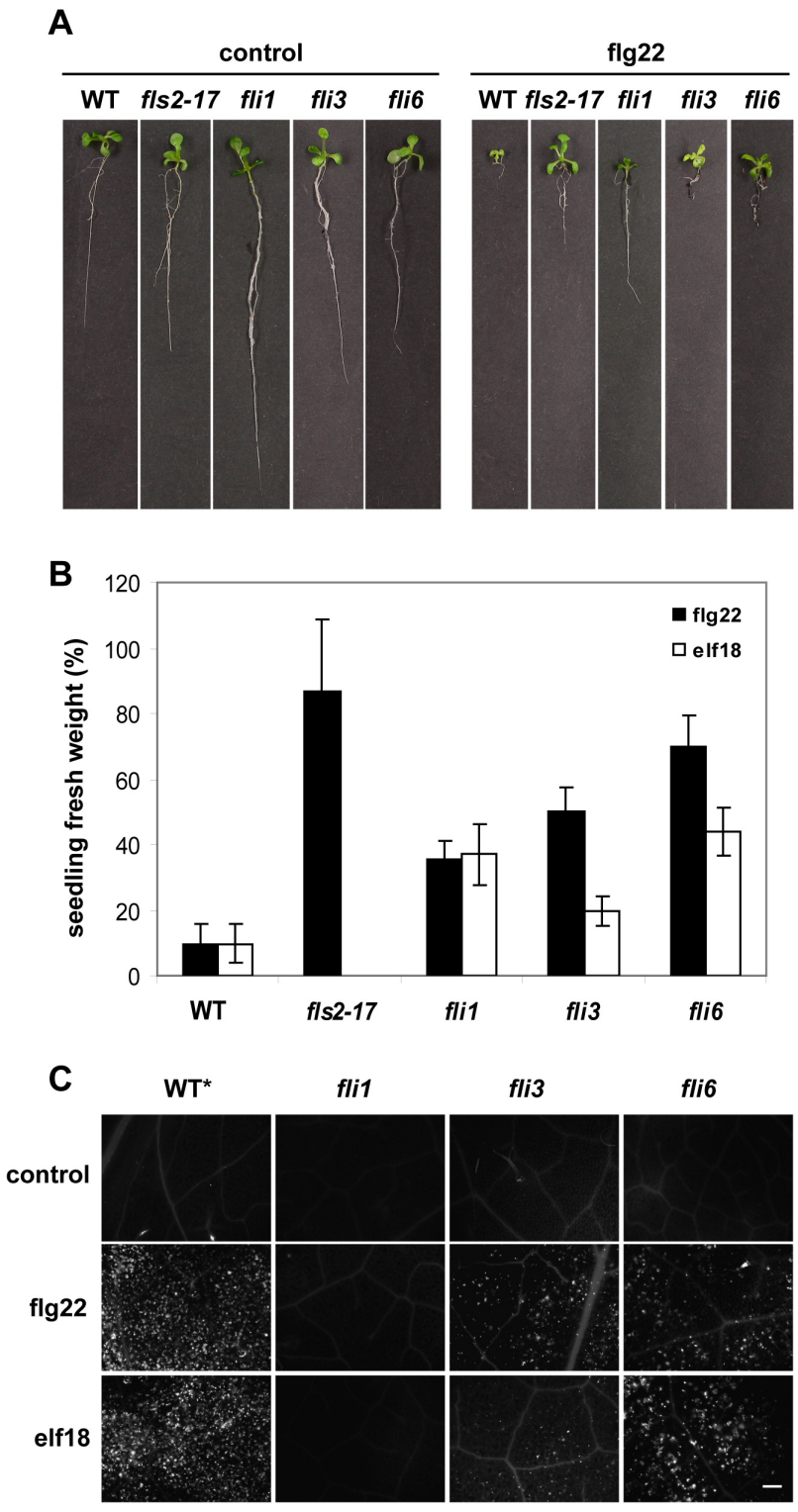

Fig. 8: Late PAMP Responses are Severely Reduced in *fli1*, *fli3* and *fli6* Mutants. (A) flg22-triggered seedling growth inhibition upon flg22 or elf18 treatment is severely reduced in *fli* mutants. Five-day old

seedlings were supplied with 1 µM flg22 and grown for eight days. Representative pictures of four independent experiments are shown. (B) Quantification of seedling growth. Fresh weight of seedlings without flg22 or elf18 was set to 100 % and fresh weight after PAMP treatment was calculated accordingly. Bars and error bars show the average and standard deviation of ten samples. The experiment was repeated twice. (C) Callose deposition was analyzed in leaves infiltrated with 2 µM flg22 or 2 µM elf18 for 24 h. Control leaves were infiltrated with H_2O. Callose deposits were visualized by aniline blue staining and fluorescence microscopy. WT: La-er. WT*: Col-0. Similar callose deposition was observed in WT compared to WT* (data not shown). Bar: 200 µm. Three independent experiments showed similar results.

Distinct differences can be observed between *fli1*, *fli3* and *fli6*. While in *fli3* and *fli6* aerial parts and roots are similarly affected in growth reduction, *fli1* displays a more pronounced growth reduction in the roots (Fig. 8A). To quantify the observed growth differences, the average fresh weight of ten samples was calculated (Fig. 8B), thereby confirming previous observations. In addition, responses to elf18 were tested and revealed that *fli1* and *fli6* also display a reduced seedling growth inhibition towards elf18, while for *fli3* the observed difference was not significant.

Next we monitored callose deposition in the *fli* mutants upon flg22 or elf18 stimulus. While *fli1* was almost completely impaired and accumulated no callose upon both PAMP treatments, *fli3* and *fli6* still showed a weak callose response (Fig. 8C). No differences were detected in the responses towards flg22 or elf18. Therefore, we conclude that the *fli* mutants are impaired in a shared PAMP signaling event.

3.2.3 Pathogen Proliferation is Altered in *fli* Mutants

To determine whether the selected candidates would also be affected in their immune responses, four- to five-week-old *fli* mutants were spray inoculated with *Pseudomonas syringae* pv. *tomato* DC3000 (PtoDC3000) and a disarmed strain lacking two effector proteins PtoDC3000ΔAvrPto/AvrPtoB (Zipfel et al., 2004; Rosebrock et al., 2007). *Fli1* allowed clearly enhanced multiplication of both bacterial strains; its observed susceptibility occurred in the same magnitude than *fls2* mutants (Fig. 9A+B). By contrast, *fli6* appeared less susceptible compared to *fls2* but still significantly enhanced to wild-type plants, while *fli3* was not altered in bacterial resistance (Fig. 9A+B). In previous qualitative spray inoculation of two-week-old *fli* mutants, *fli1* already

exhibited the strongest disease symptoms of the tested *fli* mutants (data not shown). Together, this provides evidence that *fli1* and *fli6* contribute to plant innate immunity.

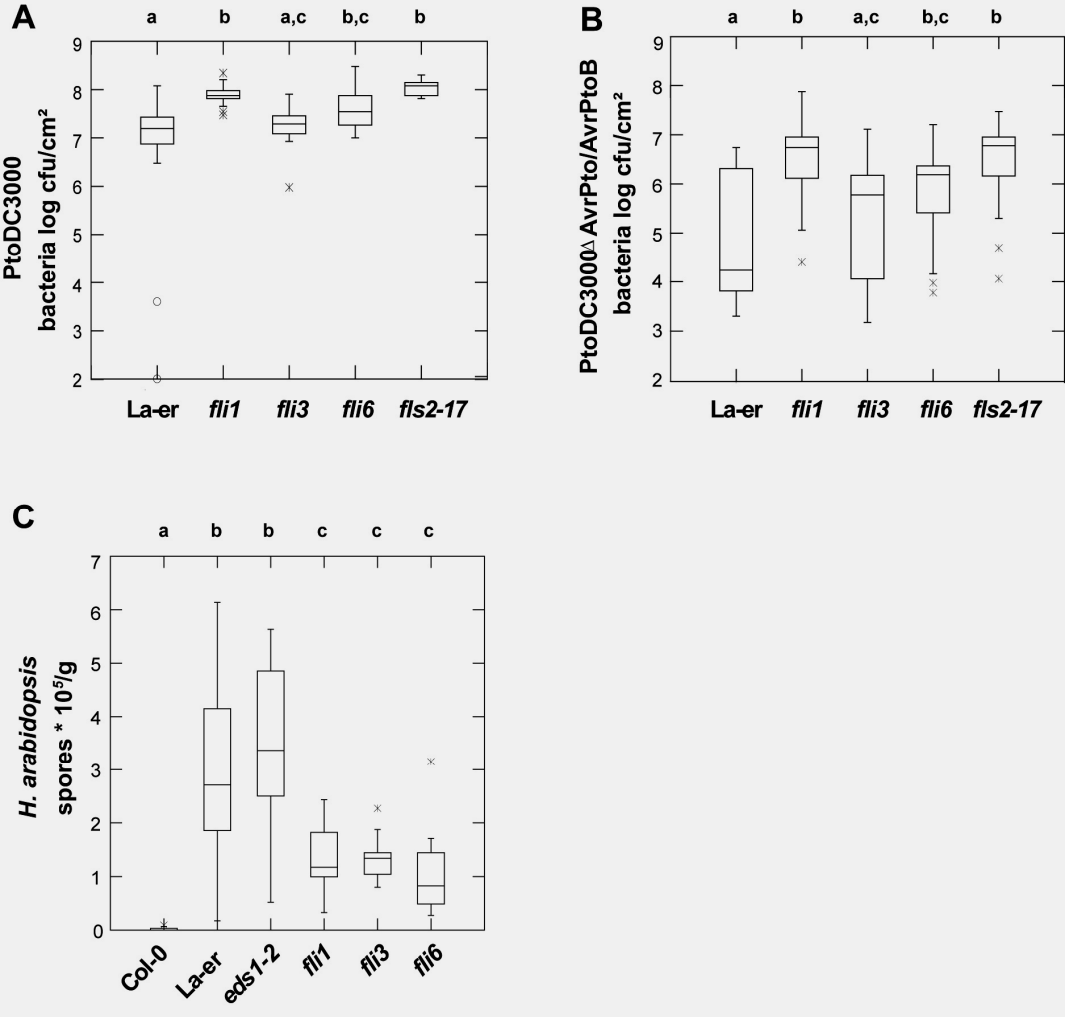

Fig. 9: Pathogen Proliferation in *fli1*, *fli3* and *fli6* Mutants. (**A**) Susceptibility to PtoDC3000 and (**B**) Susceptibility to PtoDC3000ΔAvrPto/AvrPtoB. Bacterial growth was analyzed at 4 dpi. Each box represents six technical and four biological replicates; error bars the standard error of the mean (SEM). **(C)** Susceptibility to *Hyaloperonospora arabidopsis* (previously *H. parasitica*) strain Cala2. Each box represents three technical and four biological replicates; error bars the SEM. Statistical analysis was performed using pairwise comparison (Tukey corrected). Different letters indicate statistically significant differences between sample means ($p < 0.007$).[1]

To determine whether other plant-pathogen interactions were compromised in *fli1*, *fli3* and *fli6*, they were infected with *oomycete* spores of *Hyaloperonospora arabidopsis*

[1] Data presented in Fig.9A+B was obtained with technical help of Heidrun Häweker.

(previously *H. parasitica*) (*H.a.*) cv. Cala2, the causal agent of downy mildew (Chou, 1970). Surprisingly, the tested *fli* mutants were significantly more resistant than wild-type (La-er) (Fig. 9C). Together with the impaired callose deposition in the *fli* mutants, this prompted us to analyze the accumulation of pathogen-inducible secondary metabolites in *fli1*. Recently, indol-3-ylmethylamine and raphanusamic acid were shown to play an important role in antifungal defense (Bednarek et al., 2009; Clay et al., 2009). However, analysis of flg22-triggered accumulation of raphanusamic acid revealed similar levels in *fli1* compared to wild-type seedlings (Suppl. Fig. 4). Notably, unlike the *fls2* mutant, *fli1* exhibits not only enhanced susceptibility to *Pseudomonas* but also increased resistance to *H. arabidopsis.*

3.2.4 Immediate Early PAMP Responses are Unaffected in *fli* Mutants

A number of immediate early PAMP responses were investigated in the *fli* mutants. Analysis of PAMP-triggered oxidative burst revealed that *fli1*, *fli3* and *fli6* were able to produce ROS upon flg22 as well as elf18 treatment (Fig. 10A). Also, *fli1*, *fli3* and *fli6* inducibly generated the stress hormone ethylene at wild-type levels and signaling MAP kinases were activated (Fig. 10B+C). Finally, we tested whether early defense gene expression is altered in *fli1*, *fli3* and *fli6*. RT-PCR analysis was performed to monitor transcript levels of the well characterized marker genes *WKRY22*, *WRKY29* and *FRK1* (Asai et al., 2002; Navarro et al., 2004). Flg22-elicited up-regulation of *WRKY22*, *WRKY29* and *FRK1* expression in *fli* mutants was indistinguishably compared to wild-type seedlings. This suggests that immediate early PAMP responses and signaling are not affected in *fli* mutants.

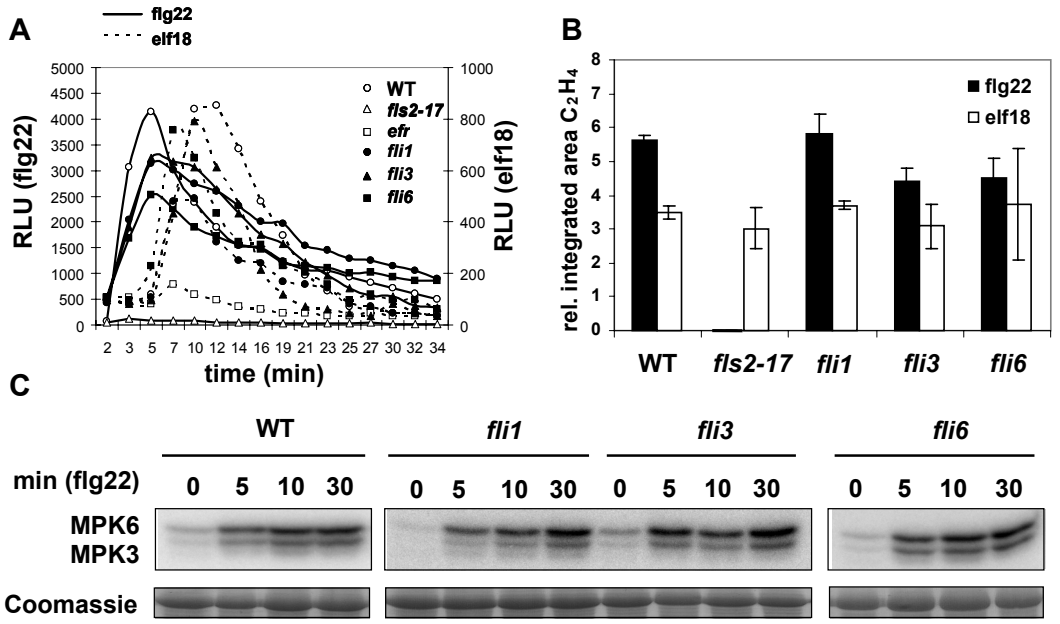

Fig. 10: Immediate Early PAMP Responses and Signaling are Unaffected in *fli1, fli3* and *fli6* Mutants. (A) ROS are generated in *fli* mutants upon PAMP treatment. The experiment was repeated with six technical and three biological replicates, of which representative curves are shown.[2] **(B)** Ethylene (C_2H_4) is synthesized in *fli* mutants upon PAMP perception. Bars and error bars depict the median and standard deviation of three independent replicates.[3] **(C)** MAP kinases are activated in *fli* mutants upon flg22 perception. Three independent experiments showed similar results.

3.2.5 Molecular Characterization of *fli* Mutants Reveals Novel Components

The *FLS2* and *BAK1* genes were sequenced in the *fli* mutants to exclude that mutations or deletions in the flg22 receptor or co-receptor itself are responsible for the observed phenotypes. No base-pair differences from the La-er derived *FLS2* or *BAK1* sequences were detected. Furthermore, FLS2 protein levels were analyzed (Suppl. Fig. 3A). No difference in protein abundance and size was observed in *fli* mutants. Binding of radiolabeled flg22 was not impaired in *fli1, fli3* and *fli6* mutants (Suppl. Fig. 3C). In addition, BAK1 protein levels and size were wild-type-like in *fli1* mutants (Suppl. Fig. 3B). These data support that the *fli* mutants are likely affected in yet unknown components of PAMP signaling.

[2] Data presented in Fig. 10A was obtained with technical help of Petra Köchner.
[3] Data presented in Fig. 10B was kindly provided by Sophia Mersmann.

To isolate the genes responsible for the observed phenotypes of *fli1* and *fli3*, mapping populations were generated by crossing with Col-0. In parallel, backcrosses to La-er were set up. In genetically confirmed F1 siblings of the Col-0 crosses, flg22-triggered callose deposition was analyzed to determine the genetic inheritance. *Fli1* exhibited recessive behavior, while *fli3* appeared dominant (Table 8).

Table 8: Genetic Analysis of *fli1* and *fli3* Mutants. Segregation data (WT: wild-type, mutant phenotype) was evaluated with chi-square analysis (χ^2) using the null hypothesis (n.h.) indicated. Chi-square probabilities (P) are indicated. P > 0.05 indicates non-significant deviation from hypothesis. n.d. = not determined. pheno = phenotyping. 1 = callose deposition, 2 = seedling growth, 3 = PtoDC3000.

	F1 segregation			F2 segregation					
Cross	WT	mutant	pheno	WT	mutant	Ratio	n.h.	χ^2; P	pheno
Col-0 x *fli1*	14	0	1	59	17	3.5 : 1	3:1	0.3; >0.8	3
				51	17	3 : 1	3:1	0 ; >0.95	3
*fli*1 x Col-0	2	0	1	55	23	2.4 : 1	3:1	0.8; >0.5	3
				55	24	2.3 : 1	3:1	1.2; >0.5	3
				56	10	5.6 : 1	3:1	3.3; >0.1	1
				83	9	9.2 : 1	3:1	11.3; >0.001	1
La-er x *fli1*	n.d.	n.d.	n.d.	151	41	3.7 : 1	3:1	1.3; >0,5	3
				130	29	4.5 : 1	3:1	4.5; >0,2	3
				148	37	4.0 : 1	3:1	4.0; >0,3	3
Col-0 x *fli3*	3	8	1	39	101	1 : 2.6	1:3	0.61; >0.7	1
				28	110	1 : 3.9	1:3	1.63; >0.3	1
				63	131	1 : 2.1	1:3	5.7; >0,05	2
				30	147	1 : 4.9	1:3	6.0; >0,05	2
La-er x *fli3*	n.d.	n.d.	n.d.	53	201	1 : 3.8	1:3	2.3; >0,3	2
				50	165	1 : 3.3	1:3	0.4; >0,8	2

In the *fli3* F2 progeny only two out of eight individual crosses exhibited a genetic inheritance of 1:3 in the seedling growth response. Map-based cloning failed therefore to identify a region that showed a co-segregation with the tested SSLP markers.

By contrast, recessive segregation could be confirmed for the *fli1* F2 progeny. Three out of four individual crosses revealed genetic inheritance of 3:1 ratio. It is worth to note that most robust phenotyping was obtained by PtoDC3000 infection, and was therefore used for subsequent rough mapping analysis. Bulk segregant linkage analysis (Lukowitz et al., 2000) was used to assign an approximate chromosomal position to the mutant *fli1* loci. First results suggest that *fli1* co-segregates with the SSLP marker MSAT 2.28 located on the lower arm of chromosome II (Supp. Fig. 5).

3.2.6 Supplementary Material

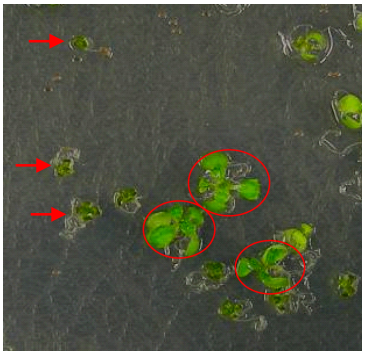

Suppl. Fig. 1: Seedling Growth Inhibition. Seedlings were grown on plates for five days and were subsequently treated with 1 µM flg22 solution for another eight days. Small seedlings with a functional FLS2 respond with a typical growth arrest (red arrows). Seedlings exhibiting a *fls2*-like growth in the presence of flg22 were selected as mutant candidates (red circles).

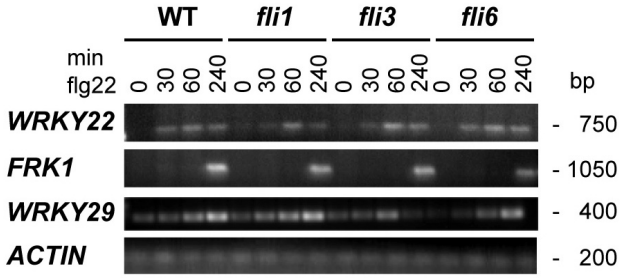

Suppl. Fig. 2: *Fli* Mutants Inducibly Express Early-flg22 Responsive Genes such as *WRKY22*, *WRKY29* and *FRK1*. RT-PCR analysis was conducted with samples treated for 0, 30, 60 and 240 min with 1 µM flg22. As a control constitutive expression of *Actin* is shown. The experiment was repeated four times with similar results.

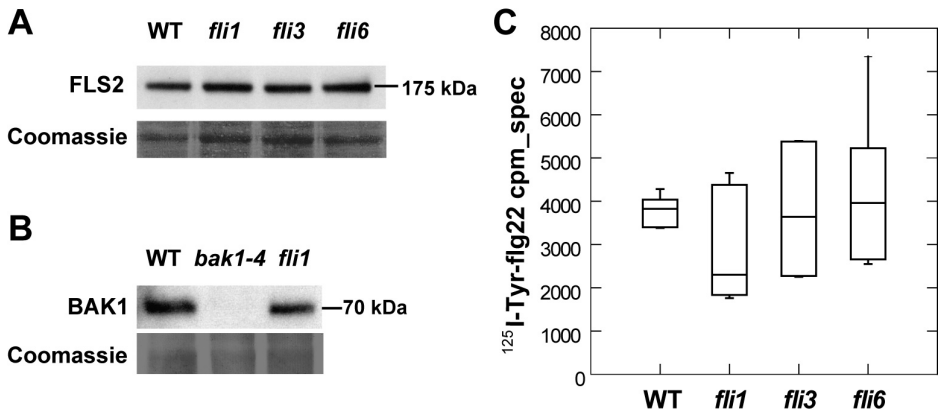

Suppl. Fig. 3: Molecular Analysis of *fli* Mutants. (A) *Fli* mutants express wild-type-like FLS2 protein levels. Western blot was revealed with α-FLS2 antibodies. (B) *Fli1* shows wild-type-like BAK1 protein levels. Immunoblotting was revealed with α-BAK1 antibodies. (C) *Fli* mutants bind ^{125}I-Tyr-flg22 peptide. Total and unspecific binding (in cpm) was measured in homogenates of six individual plants for wild-type (La-er) and the mutant lines *fli1*, *fli3*, and *fli6*. The specific binding was calculated by subtracting the flg22-competed from total binding. Bars represent three technical and two biological replicates; error bars the standard error of the mean.[4]

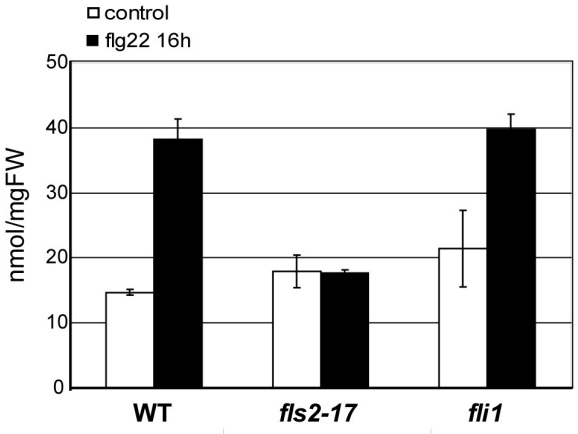

Suppl. Fig. 4: *Fli1* Produces Raphanusamic Acid upon flg22 Treatment. Accumulation of secondary metabolite raphanusamic acid in *Arabidopsis* genotypes 16 h after 1 µM flg22 treatment. FW: fresh weight. Bars and error bars represent the average and standard deviation of three samples.[5]

[4] Data presented in Suppl. Fig. 3B was kindly provided by Sophia Mersmann and data in Suppl. Fig. 3C by Madlen Vetter.
[5] Data presented in Suppl. Fig. 4 was obtained in collaboration with Dr. Pawel Bednarek.

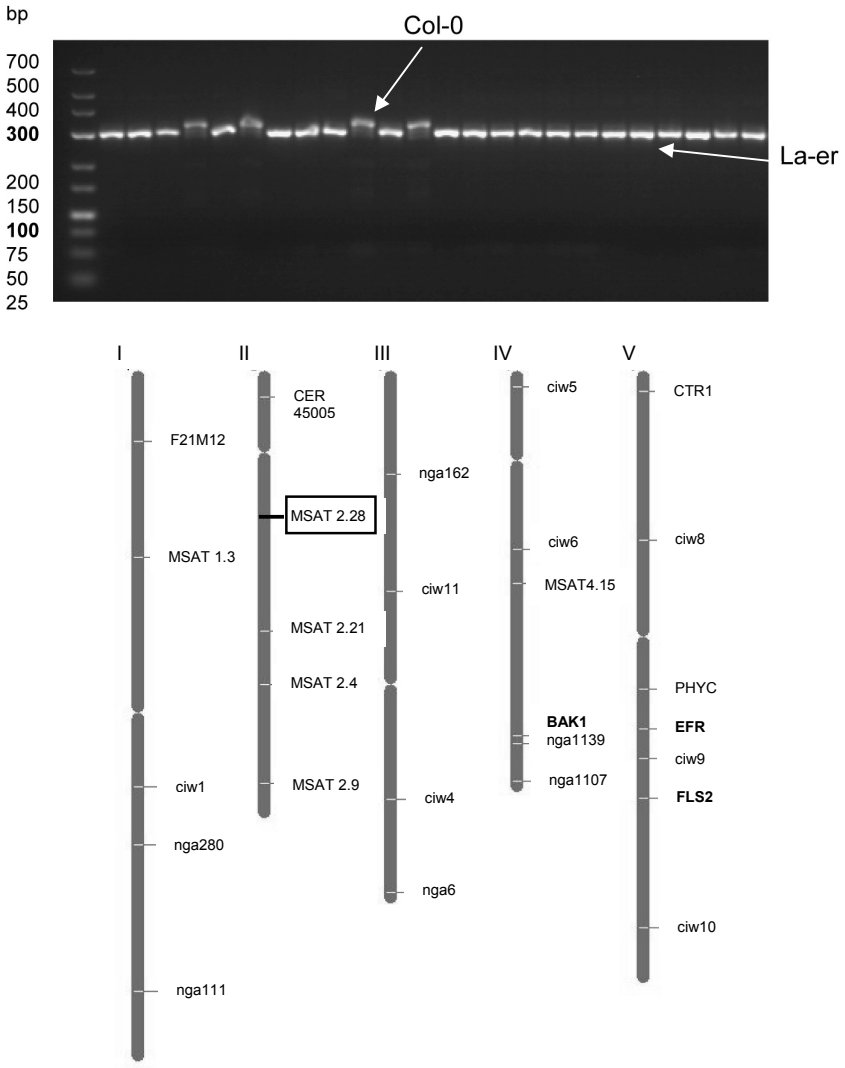

Supp. Fig. 5: Rough Mapping Position of *fli1*. Co-segregation of SSLP marker MSAT 2.28 with mutant phenotyped F2 *fli1*xCol-0 plants (PCR with single DNA samples). La-er specific band: 300 bp; Col-0 specific band: 319 bp. Positions of used rough mapping markers as well as of FLS2, EFR, and BAK1 are indicated on the *Arabidopsis* chromosome map.

3.2.7 Concluding Remarks

Although PAMP perception and signaling became a focus within the past years, many components contributing to PTI remain to be identified. Moreover, PTI is genetically poorly defined, while biochemical evidence exists for typical defense responses such as ROS production, MAP kinase activation, or gene expression changes (Gomez-Gomez et al., 1999; Asai et al., 2002; Navarro et al., 2004). In addition, the relevance of individual defense responses for the establishment of disease resistance is not known. To identify novel signaling components and to dissect the role of individual defense responses, previous screening conditions were refined, since they only led to the identification of the *fls2* mutant (Gomez-Gomez and Boller, 2000). With this modified genetic screen, a number of flg22-insensitive, *fli*, mutants were indeed identified. Although characterization of *fli* mutants revealed unaffected early PAMP responses, they were impaired in late responses such as callose deposition. Notably, *fli* mutants were found to be more susceptible to bacterial and more resistant to oomycete infection. We only detected the hyper-susceptible phenotype of *eds1-2* towards the oomycete *H. arabidopsis* cv. Cala2 in one out of four experiments probably due to seed contamination or a suboptimal time point for harvesting. Nevertheless, the increased resistance of the *fli* mutants was consistent. Thus, we conclude from our data that loss of downstream PAMP responses is sufficient to affect overall outcome of resistance. Future mapping analysis of *fli* mutants should lead to new insights into regulation of PAMP responses and signaling and reveal the contribution of individual responses to disease resistance.

Interestingly, *fli* mutants exhibit impaired responses towards two different PAMPs, flg22 and elf18, which was similarly observed for *bak1* mutants (Chinchilla et al., 2007b). Contrary to the *fli* mutants, *bak1* mutants, however, displayed clearly reduced oxidative burst and MAP kinase activation in response to both PAMPs, while *fli* mutants appeared unaffected in early PAMP responses. Notably, most physiological and molecular analysis was performed with liquid grown seedlings, a growth condition which failed to reveal the typical *fli* phenotype as observed on plates. Possibly uptake or diffusion of flg22 differs between the methods. This could also implement tissue-specificities in roots and leaves. Therefore, there might be unexpected differences due

to the condition used. However, *fli1*, *fli3* and *fli6* did not reveal any obvious developmental phenotypes, while *bak1* mutants showed a semidwarfed phenotype (Li et al., 2002). This lack of severe pleiotropic phenotypes in *fli* mutants is not surprising since callose was found not be a major component of unstressed plant cell walls (Stone and Stone, 1992; Nishimura et al., 2003).

The powdery mildew-resistant mutant, *pmr4* (*gsl5*), exhibits strongly reduced callose deposition upon wounding, pathogen attack and flagellin treatment (Vogel and Somerville, 2000; Jacobs et al., 2003; Nishimura et al., 2003; Kim et al., 2005). Paradoxically, absence of *PMR4* (i.e. callose) confers broad-spectrum resistance towards fungal and oomycete pathogens. We therefore tested whether *FLI1* might be the callose synthase *PMR4*. However, current data argues against this hypothesis: (1) *pmr4* transcript levels are unaltered in *fli1* (data not shown); (2) *pmr4* does not show a reduced growth inhibition effect upon PAMP treatment on plates (data not shown); (3) *PMR4* is located on chromosome IV (Vogel and Somerville, 2000) while *fli1* was mapped to chromosome II; and (4) although *pmr4,* like *fli1,* exhibits more resistance towards the oomycete *H. arabidopsis* (Vogel and Somerville, 2000), *pmr4* was reported to be significantly more susceptible than *fls2* mutants towards TTSS-deficient PtoDC3000 bacteria (Kim et al., 2005). In contrast, *fli1* displayed comparable bacterial growth towards PtoDC3000 like *fls2* mutants. It has to be noted, however, that *pmr4* mutants display elevated salicylic acid levels (Nishimura et al., 2003). Taken together, we hypothesize that *FLI1* is rather a regulatory component influencing the activity of an unknown protein involved in late PAMP responses.

3.3 ENDOCYTOSIS MUTANTS IN PAMP-TRIGGERED IMMUNITY

There is evidence that flg22-triggered endocytosis of FLS2 contributes to flg22 signaling (Robatzek et al., 2006). To further address the role of endocytosis in PTI, available T-DNA insertion lines in known components of the endocytic pathway with only minor developmental defects were selected (Tab.3). Most lines carried insertions in components of the ESCRT I machinery, important for intracellular trafficking of mono-ubiquitinated proteins to MVBs (Alam and Sundquist, 2007). In *Arabidopsis,* ESCRT I-III genes were identified by homology to their counterparts in yeast and mammals (Spitzer et al., 2006; Winter and Hauser, 2006). To date, only one ESCRT I component, ELCH, has been functionally characterized in *Arabidopsis*, and revealed a role in cytokinesis (Spitzer et al., 2006). The positive regulator *lip5* of AAA-ATPase SKD1, which is involved in the release of ESCRT components from MVBs, was included (Haas et al., 2007). Furthermore, Rab5 GTPase mutants *ara6*, *ara7* and *rha1* were selected. Rab GTPases are key regulators of vesicular transport and are known markers for early and late endosomes (Ueda et al., 2001; Ueda et al., 2004). The *gnl1-1* mutant, an ARF GEF (Richter et al., 2007; Teh and Moore, 2007), and the Rab5 GEF *vps9a-2*, which activates Rab5 GTPases in *Arabidopsis,* were studied (Goh et al., 2007). GEFs regulate vesicle formation by activating their GTPase substrates on distinct donor membranes and are essential for vesicle trafficking (Zerial and McBride, 2001; Shin and Nakayama, 2004). GNL1 has been implicated in Golgi trafficking as well as selective internalization of PIN2 from the plasma membrane (Teh and Moore, 2007). Furthermore, GNL1 is BFA-resistant (Richter et al., 2007; Teh and Moore, 2007). Since FLS2 endocytosis was not inhibited by BFA, we hypothesized that a BFA-resistant ARF GEF could be involved in regulation of FLS2 endocytosis. In order to test the selected endocytic components for a potential role in PAMP signaling, early and late flg22 responses as well as resistance to pathogens were analyzed.

3.3.1 Flg22 Responses are Not Altered in Endocytosis Mutants

Fls2 mutant variants impaired in endocytosis were preferentially affected in late flg22 responses (Robatzek et al., 2006). Perception of flg22 typically triggers responses such as the production of ROS and callose deposition (Gomez-Gomez et al., 1999), and were

therefore investigated in the endocytosis mutant collection (Fig. 11). All tested single T-DNA insertion lines of ESCRT I components displayed wild-type-like flg22 responses but the *elch* mutant. This is likely explainable because the *elch* mutant is in the Ws-2 background, a natural *fls2* mutant. Similarly, only *vps37-1 elch* and *vps37-2 elch*, as well as the triple mutant *vps28-2 vps37-1 elch* exhibited full flg22 insensitivity. These lines failed to accumulate FLS2 protein (data not shown), which confirms their Ws-2 *fls2* mutant phenotype.

In further analysis, quantitative assays were used to identify also weaker phenotypes. It could be shown that *fls2* mutant variants or *bak1* null mutants resulting in reduced sensitivity to flg22 in seedling growth, also displayed impaired FLS2 endocytosis (Robatzek et al., 2006; Salomon and Robatzek, 2006; Chinchilla et al., 2007b). Therefore, seedling growth in response to 20 nM and 1 µM flg22 was performed with the endocytosis mutant collection (Fig. 12). The *vps9a-2* mutant was not included since it did not grow in liquid culture. Besides a confirmation of previous data, only *vps28-1 elch* and *gnl1-1* exhibited a partially reduced flg22 sensitivity but not as strong as observed in the *bak1* mutant.

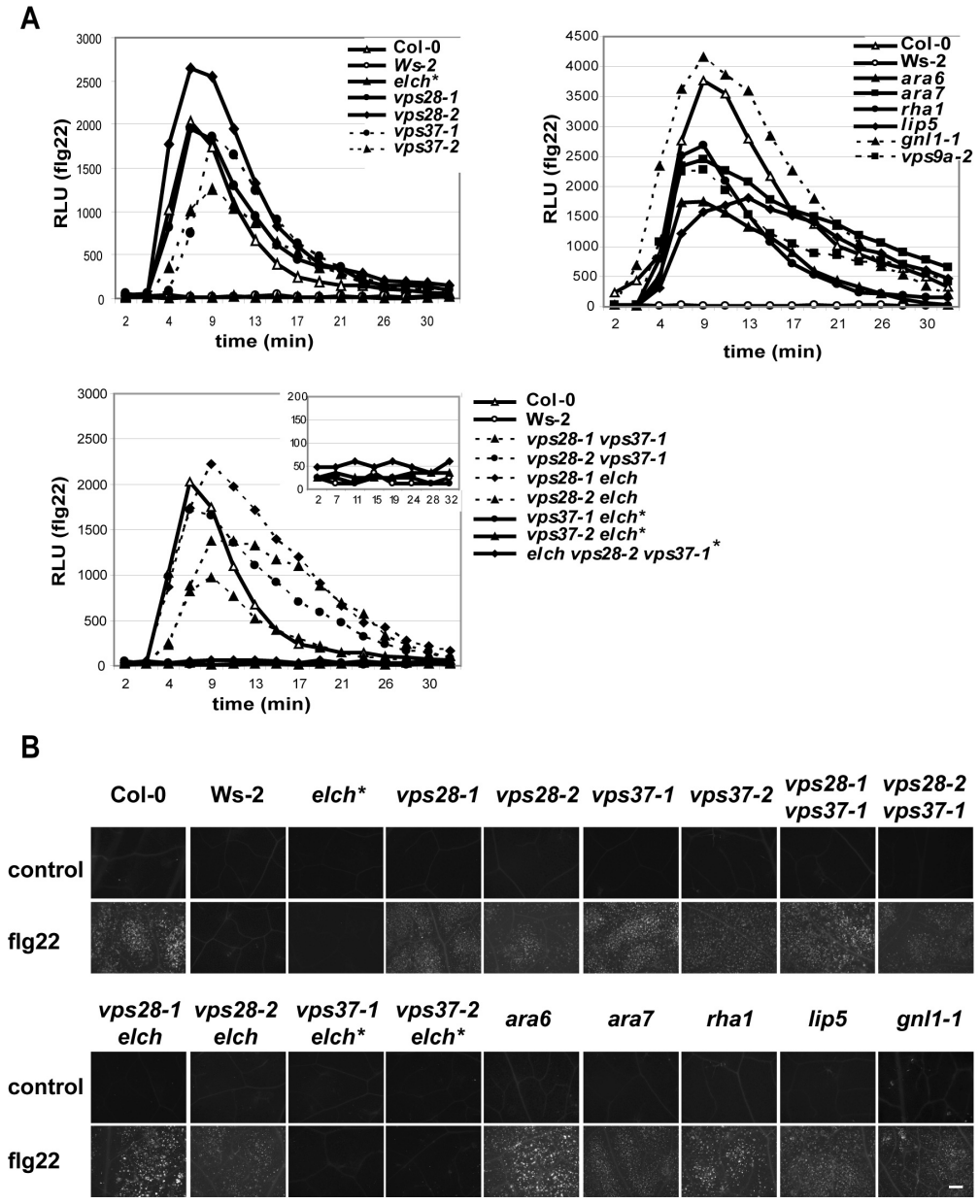

Fig. 11: Flg22 Responses in Endocytosis Mutants. (A) ROS are generated in most endocytosis mutants upon flg22 treatment. Representative curves of six technical replicates and three biological replicates are shown. **(B)** Callose deposition is wild-type-like in most endocytosis mutants. Callose deposits were visualized by aniline blue staining and fluorescence microscopy. * indicates lines that failed to accumulate FLS2 protein. Bar: 200 µm. Two independent experiments revealed similar results.

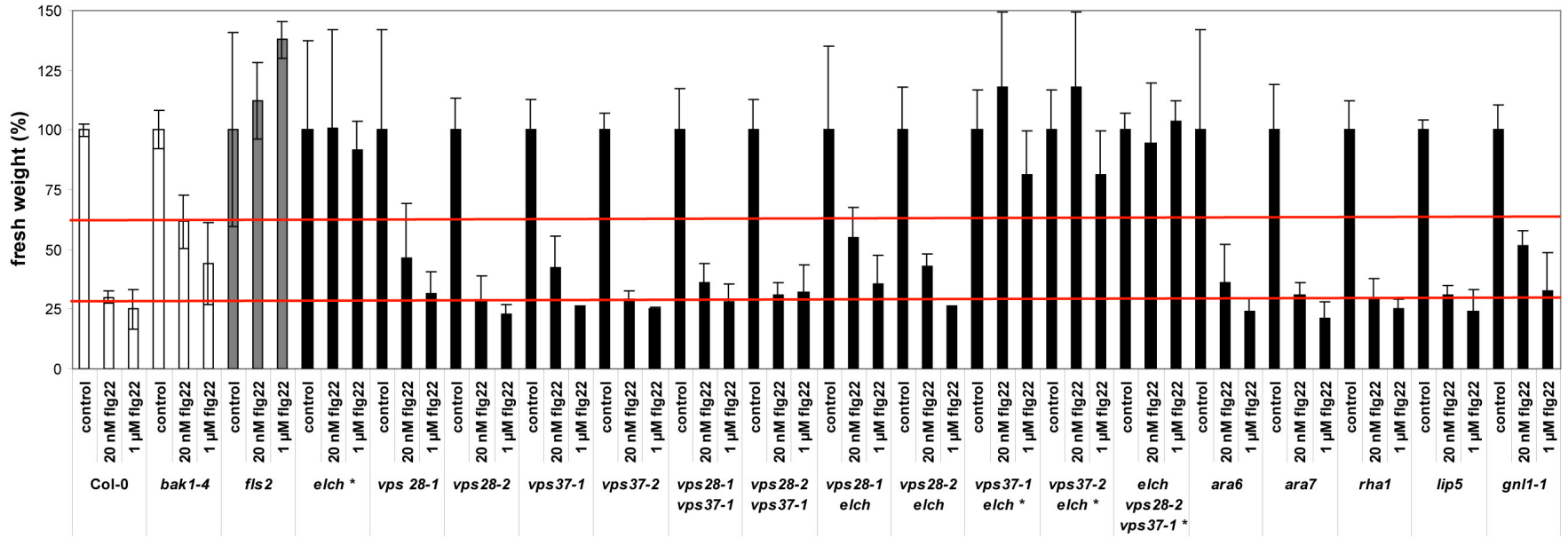

Fig. 12: Seedling Growth Response to flg22 is wild-type-like in Most Tested Endocytosis Mutants. Fresh weight of control treated seedlings was set as 100% and seedling weight upon 20 nM or 1 µM flg22 was calculated accordingly. * indicates lines that failed to accumulate FLS2 protein. Bars and error bars depict the average and standard deviation of six replicates.

3.3.2 Endocytosis Contributes to Disease Resistance towards Bacteria

To analyze a more general role of endocytosis in plant immunity, the endocytosis mutant collection was subjected to infection with PtoDC3000 and PtoDC3000ΔAvrPto/AvrPtoB (Table 9). Disease was monitored by leaf yellowing and wilting (de Torres et al., 2006), which was strongest in Ws-0 and nearly absent in Col-0. Most mutants displayed to some extent enhanced susceptibility to bacterial infection. As before, *elch* mutants including double and triple mutant variants that failed to accumulate FLS2 protein exhibited a clear Ws-like phenotype. In addition, *vps28-2*, *vps37-1*, *vps28-1 elch* and *gnl1-1* mutants were as susceptible as Ws-0, suggesting a role for endocytic traffic in resistance to bacteria.

Table 9: Endocytosis Mutants are More Susceptible to Bacterial Infection. Two-week-old seedlings were sprayed with PtoDC3000 or PtoDC3000ΔAvrPto/AvrPtoB and disease symptoms (DS) were scored at 5 dpi. Three independent experiments with six replicates revealed similar results. Mutants exhibiting DS comparable to Ws-0 are highlighted in grey. - no DS; + weak DS; ++ strong DS; +++ very strong DS; * lines that failed to accumulate FLS2 protein.

	PtoDC3000	PtoDC3000ΔAvrPto/AvrPtoB
Col-0	+/-	-
Ws-0	+++	++
*elch**	+++	++
vps28-1	++	++
vps28-2	+++	++
vps37-1	+++	+
vps37-2	++	+
vps28-1 vps37-1	++	+
vps28-2 vps37-1	++	+
vps28-1 elch	+++	++
vps28-2 elch	++	+
*elch vps28-2 vps37-1**	+++	++
ara6	+	-/+
ara7	+	-/+
rha1	+	-/+
lip5	++	-/+
gnl1-1	+++	++

3.3.3 Concluding Remarks

To better understand the role of endocytosis in flg22 signaling and PTI, a number of T-DNA insertion lines in known components of the endocytic pathway with only minor developmental defects were studied. Our findings revealed that flg22-triggered responses were mostly unaffected. However, the ESCRT I components *vps28-1*, *vps37-1*, and *vps28-1 elch* displayed enhanced disease symptoms upon bacterial infection. Thus, our study suggests for the first time a role of the ESCRT machinery in plant immunity. Importance of the ESCRT complex for essential cellular functions is demonstrated by the fact that T-DNA insertion lines of ESCRT II components are lethal in *Arabidopsis* (Swen Schellmann, personal communication) and could therefore not be studied. To date, only one ESCRT I component, ELCH, was functionally characterized and was shown to be important for cytokinesis (Spitzer et al., 2006). Besides ESCRT I components, we also identified another endocytic regulator, GNL1, in our candidate gene approach. We observed that *gnl1-1* mutants exhibited a partially reduced sensitivity towards flg22 in seedling growth and enhanced proliferation of bacteria. These findings imply that GNL1 might be involved in the regulation of FLS2 endocytosis probably by regulating the selective internalization of FLS2 from the PM. However, further studies need to be performed to support this hypothesis.

Although our preliminary data provided evidence for endocytic traffic contributing to plant immunity, a candidate reverse genetic approach is limited. T-DNA insertion lines may cause severe pleiotropic phenotypes, or are not phenotypically affected due to redundancy. Also, homology searches across kingdoms might be restricted. This might explain why no flg22-insensitive mutant was identified. Notably, also seedling growth in response to elf18 was largely unaffected and failed to reveal an elf18-insensitive candidate (data not shown). Moreover, current data suggest that multiple endocytic routes are operational in plant cells, which are specifically regulated by different components as was shown for the polar localization of different PIN proteins regulated by BFA-sensitive or –insensitive ARF GEFs (Paciorek et al., 2005; Dhonukshe et al., 2007; Kleine-Vehn et al., 2008). Therefore, specific regulators of the FLS2/flg22 pathway might not have been included in the endocytosis mutant collection.

Taken together, this study could assign a role for some ESCRT I components and an ARF-GEF in plant defense confirming our hypothesis that molecular components mediating subcellular trafficking are important for plant innate immunity. Individual differences in the susceptibility rate were observed suggesting that the tested components fulfil distinct yet maybe redundant functions.

3.4 GENETIC ANALYSIS OF ENDOCYTOSIS IN *ARABIDOPSIS*

In order to learn more about general endosome biogenesis, trafficking, and subsequently to gain insights into FLS2 receptor endocytosis, a high-throughput genetic screen for mutants affected in endocytosis was established. A chemically mutagenized population of the FYVE-GFP endosomal marker line (Voigt et al., 2005) was inspected for quantitative differences in endosome numbers, which yielded 12 mutants, referred to as *fel* (FYVE-endosome levels).

3.4.1 Quantitative Analysis of Endosomes

For the genetic screen we selected the La/FYVE-GFP line, which labels early and late endosomes (Voigt et al., 2005). Proteins containing FYVE domains specifically bind to phosphoinositol 3-phosphate typically found in endosomal membranes (Gaullier et al., 1998). The FYVE domain was named after the four proteins in which this zinc-finger domain was first identified: Fab1p, YOTB, Vac1p and EEA1 (Stenmark et al., 1996). A GFP-reporter construct containing two tandemly fused FYVE domains from the mouse Hrs (hepatocyte growth factor-regulated tyrosine kinase substrate) protein was validated as an endosome-specific marker in plants by co-localization of DsRed-FYVE with the Rab GTPases Ara6-GFP, and YFP-Rha1 as well as with the lipophilic dye FM4-64 (Voigt et al., 2005). We hypothesized that this line would also mark FLS2 endosomes, since wortmannin, which interferes with phosphoinositol 3-kinase (Vanhaesebroeck et al., 1997), inhibits FLS2 endocytosis. For the quantitative analysis of endosomes an automated confocal microscope (Opera) was employed (Perkin Elmer, former Evotec). The Opera imaging systems allows the automated analysis of leaves in 96-well microtiter plates and subsequent automated image analysis with the adapted Acapella software. A time-course experiment treating the La/FYVE-GFP line with 10 µM flg22 for 10, 30 and 60 min indicated slightly more endosomes upon 10 or 30 min treatment (Suppl. Fig. 8). This is in accordance to the kinetics of FLS2 endocytosis and suggests that a sub-pool of the FYVE-GFP vesicles is formed in response to flg22.

Automated high-throughput quantitative confocal microscopy was optimized to recognize cell patterning and FYVE-GFP endosomes of the used reference line (for details see 2.2.10.3).[6] Briefly, individual z-sections were automatically merged to produce a pseudo-image of the epidermal cell layer (
Suppl. Fig. **6**). During this step images that are not in focus are excluded. Further bioinformatic analysis recognizes cells and vesicles (Suppl. Fig. 7). Calculated numbers were used to produce graphic tables (Suppl. Fig. 9). The average value of FYVE-GFP endosomes of the reference line: endosomes/image area: 545 ± 125 (n=20); endosomes/cell: 14 ± 9 (n=50)[7] with cells/image area: 27 ± 4 (n=10)[8]. Therefore, putative mutants with <200 or >800 endosomes/image area were selected in our genetic screen.

3.4.2 Mutants with Altered FYVE-GFP Endosome Levels

In total, 13 600 M_2 plants of the EMS-mutagenized La/FYVE-GFP line were inspected. However, we encountered a high rate of silencing in these lines (~40 %). Therefore, informative pictures were gained only for 8100 M_2 plants (from 170 M_2 families) out of which 228 putative mutants (at least 97 individual mutants) were initially selected (Table 10) and grouped into three different classes (Fig. 13).

[6] Software was optimized with the help of Kurt Stüber, Sebastian Schaaf, Dorit Meyer and Olavi Ollikainen (Perkin Elmer, fomer Evotec).
[7] Manual calculation of endosomes per cell.
[8] Manual calculation of cells per image area.

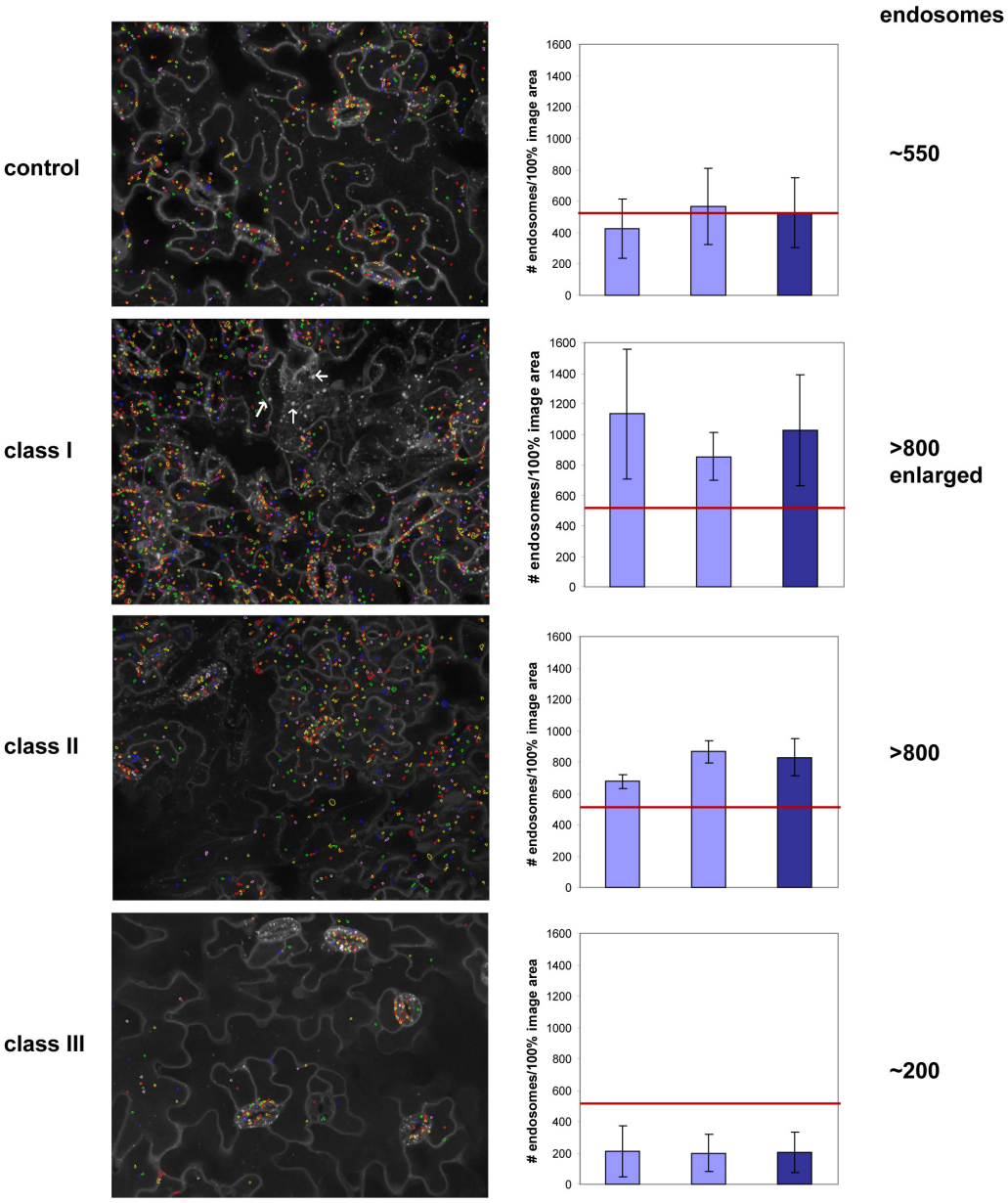

Fig. 13: Classes of M_2 Mutant Candidates Displaying Different FYVE-GFP Endosome Levels. Control: parental line (~550 endosomes/image area); class I: increased number and enlarged endosomes (>800 endosomes/image area); class II: increased number of endosomes (>800 endosome/image area); class III: reduced number of endosomes (~200 endosome/image area). Arrows point to enlarged endosomes. Light blue bars represent average endosome values per leaf, dark blue bars per plant. Red line marks average value of parental line.

Table 10: Overview of Selected *fel* Mutants. Respective M_2 and M_3 phenotypes are indicated. Numbers in brackets indicate how many mutants were initially grouped in a different class. No GFP signal indicates how many mutants exhibited silencing in the M_3 generation.

		M_2 phenotype						
		fertility					growth	
mutant class	total #	high amount of seeds	low amount of seeds	sterile (no seed set)	lethal	no data	short siliques	dwarf
I: increased # + enlarged endosomes	23	9	7	3	0	4	1	5
II: increased # endosomes	142	83	35	5	9	10	4	25
III: reduced # endosomes	63	41	12	7	0	3	6	6
Total #	228	133	54	15	9	17	11	36

		M_3 phenotype		
	total #	WT-like	M_2-like	no GFP signal
I: increased # + enlarged endosomes	10	8	2	0
II: increased # endosomes	52	46	4 (+1)	1
III: reduced # endosomes	35	27	5	3
Total #	97	85	12	4

Class I mutants display an increased number together with an enlargement of some endosomes, class II mutants contain increased number of endosomes, and class III mutants reduced number of endosomes. In total, most candidates (58 %) produced a high number of seeds. Although some candidates exhibited defects in fertility (35 %), or growth (21 %), the majority of mutants were suitable for phenotypic analysis in plant immunity.

A total of 12 *fel* mutants were confirmed in the M_3 generation (Fig. 14 and Table 10). In the following, *fel4* with increased and enlarged and *fel5* with reduced endosomal numbers were further characterized.

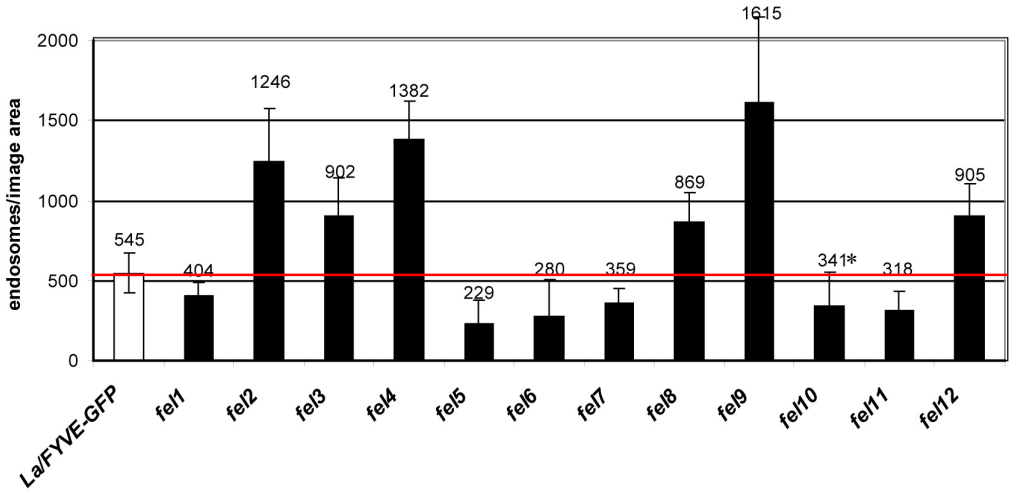

Fig. 14: Identified *fel* Mutants. Calculation of average number of endosomes/100 % image area. Bars and error bars depict average and standard deviation of n=15-30 individual plants (*n=5 due to low seed production). Red line marks mean value of reference line (La/FYVE-GFP).

Phenotypic analysis of M_4 progeny of *fel4* and *fel5* revealed growth retardation compared to the reference line (Fig. 15). Importantly, the number of cells per image area was in the range of the reference line (La/FYVE-GFP: 27 ± 4; *fel4*: 26 ± 5; *fel5*: 26 ± 6). This suggests that differences in endosomal numbers of *fel4* and *fel5* are likely not due to altered cell numbers. At later stages of development, *fel4* exhibits a striking left-handed twist of the hypocotyl and side shoots, while *fel5* appears bush-like. Moreover, the siliques of *fel4* are shorter and curved, while the siliques of *fel5* are shorter and thicker. Interestingly, also *fel5* shows a left-handed twist of rosette leaf petioles (clockwise orientation viewed from above). This is comparable to the phenotype of a transgenic line expressing GFP-tagged microtubules (GFP-MAP4) (Marc et al., 1998). This GFP-MAP4 microtubule marker line was described before to exhibit twisting of petals, petioles and roots, however in right-handed direction (Thitamadee et al., 2002). Similar observations were made with a transgenic *Arabidopsis* line expressing GFP-tagged α-tubulin (GFP-TUA6) (Ueda et al., 1999). Therefore, Hashimoto *et al.* conclude that moderate defects in microtubule functions generate helical growth (Shpak et al., 2005). However, no differences in La-er derived *TUA4* and *TUA6* sequences were detected in *fel4* and *fel5*. Moreover, root skewing was analyzed with and without propyzamide, a tubulin inhibitor known to enhance skewing phenotypes. La/FYVE-GFP exhibited slight bending to the left, which was not changed by propyzamide treatment, and appeared similar to *fel4* and *fel5* (data not shown). This

suggests that alterations of the tubulins itself are not likely to be responsible for the *fel4* or *fel5* endosomal phenotype.

The subcellular phenotype of *fel4* and *fel5* was further investigated by conventional confocal microscopy (Fig. 16). Interestingly, while *fel4* and *fel5* phenotypes could be confirmed in epidermal leaf cells, endosomal numbers in root cells appeared wild-type-like. This raises the possibility that the observed phenotypes maybe tissue-specific in particular for *fel5*. Moreover, mobility and trafficking of endosomes in *fel4* and *fel5* root cells was indistinguishable from the parental line, supporting that the cytoskeleton may not be affected. Treatment of cotelydons for 1 h with 50 µM wortmannin, a phosphoinositol 3-kinase inhibitor, resulted in strongly reduced FYVE-GFP-labeled endosomes in *fel4* and the parental line and revealed larger vesicles at the PM. Previous studies characterizing the tandem FYVE-GFP fusion construct reported enlargement of FYVE-GFP-labeled endosomes upon wortmannin treatment in root hairs of stably transformed *Medicago truncatula* (Voigt et al., 2005). Another study observed disappearance of FYVE-GFP from endosomes to the cytosol and nucleus within few minutes of wortmannin treatment in stably transformed BY-2 cells and reappearance of labeling on membrane structures after 1-2 h (Vermeer et al., 2006). Again the authors noted that the labeled vesicles appeared larger. To exclude possible overexpression of the FYVE-GFP transgene RT-PCR analysis comparing the FYVE-GFP mRNA levels in La/FYVE-GFP, *fel4* and *fel5* was performed, which revealed similar transcript levels (data not shown). These results suggest that the FYVE-GFP labeled structures are of endocytic nature, which supports that indeed endosomal mutants have been identified.

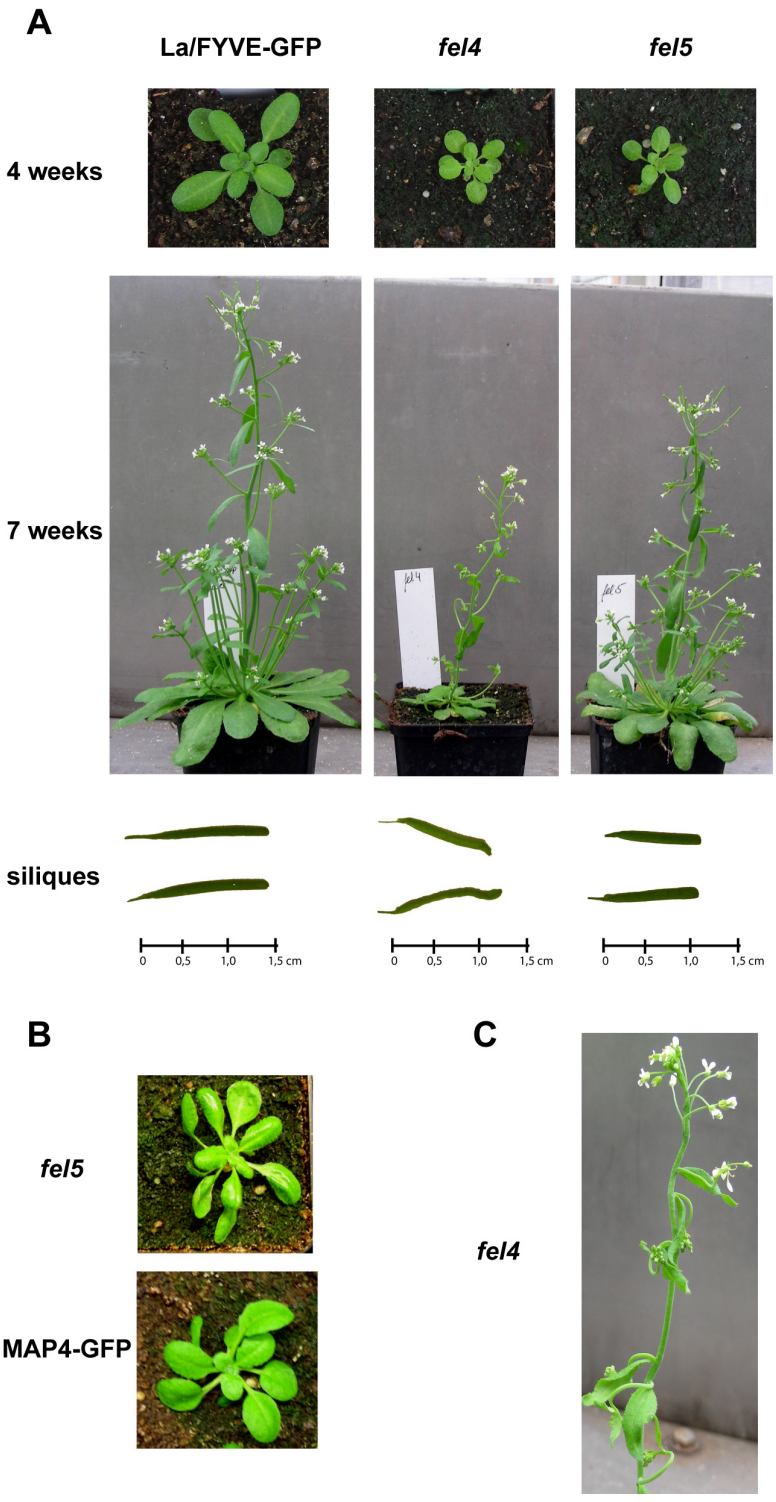

Fig. 15: Phenotypic Characterization of *fel4* and *fel5*. Mutant plants were grown under the same growth conditions and compared to the parental La-er/FYVE-GFP line. **(A)** Representative pictures of 4-week-old rosette leaves, 7-week-old plants and siliques. **(B)** Close-up view of 4-week-old *fel5* and the transgenic microtubulin marker line p35S::GFP-MAP4. **(C)** Close-up view of twisting phenotype of 7-week-old *fel4*.

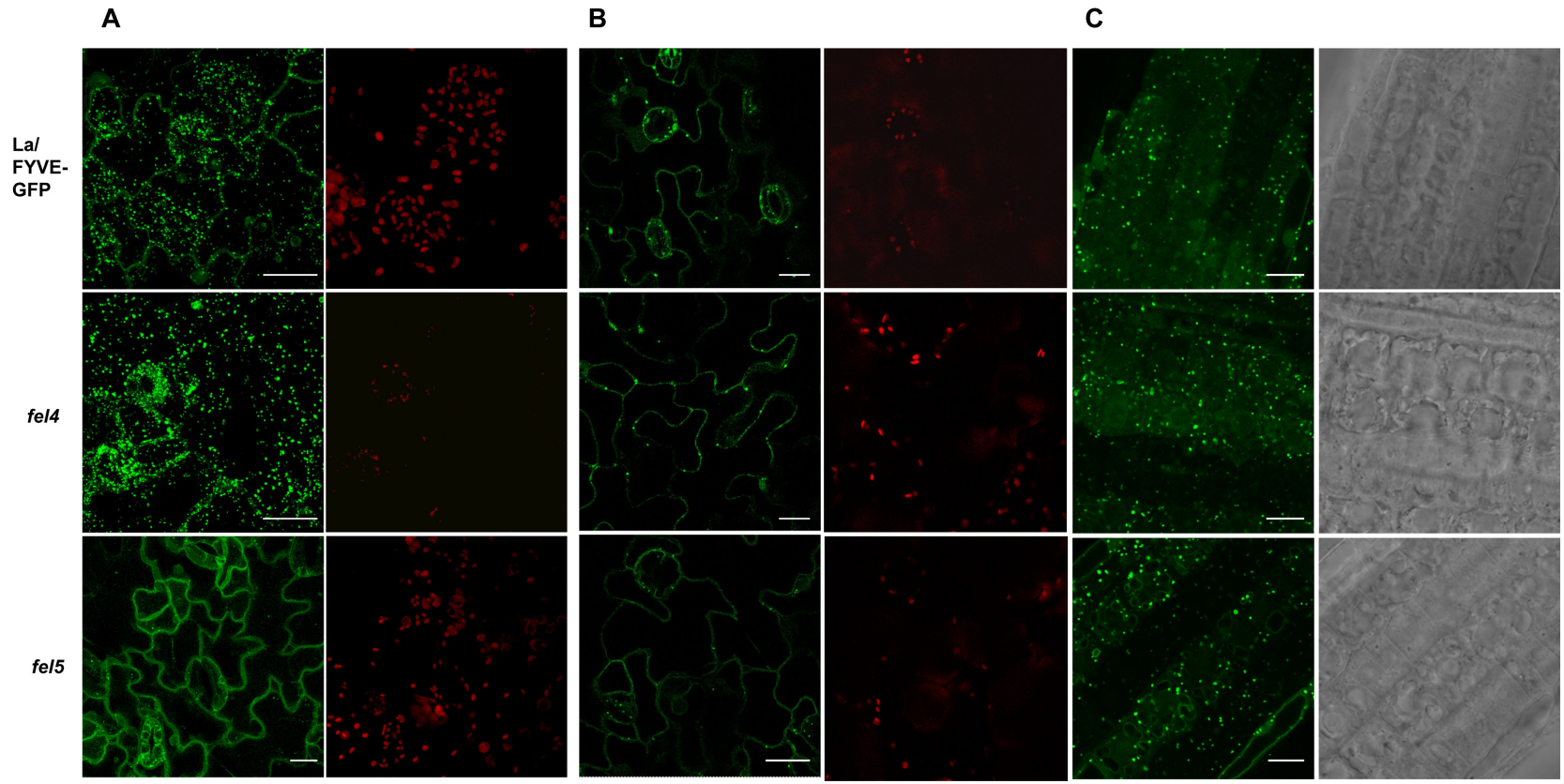

Fig. 16: Microscopic Analysis of *fel4* and *fel5*. Images were taken with a confocal laser scanning microscope (Leica). **(A)** Expression of FYVE-GFP in two-week-old cotelydons. 14 images a 1 µm distance were merged. *fel4* shows more and enlarged endosomes, while *fel5* shows almost no endosomes compared to La/FYVE-GFP. **(B)** Strongly reduced FYVE-GFP-labeled endosomes in two-week-old cotelydons after 1 h wortmannin (50 µM) treatment in La/FYVE-GFP, *fel4* and *fel5*. Single images are depicted. **(C)** Subcellular localization of FYVE-GFP in two-week-old root cells. La/FYVE-GFP, *fel4* and *fel5* display similar levels of FYVE-GFP-labeled endosomes. Two independent experiments showed similar results. Bar: 20 µm.

3.4.3 Molecular Characterization of *fel4* and *fel5*

To identify the genes conferring the altered FYVE-GFP endosomal patterns in *fel4* and *fel5*, the mutants were crossed to a Col/FYVE-GFP line to generate corresponding mapping populations. The Col/FYVE-GFP line (Vermeer et al., 2006) exhibits an average of 350 endosomes/image area (Suppl. Fig. 10). Genetically confirmed F1 siblings were subjected to quantitative confocal imaging (Table 11). All F1 progeny of crossed *fel4* revealed a recessive behavior, while crosses of *fel5* were indicative of a dominant inheritance.

Table 11: Genetic Analysis of *fel4* and *fel5* Mutants. Segregation data were evaluated with chi-square analysis (χ^2) using the null hypothesis (n.h.) indicated. Chi-square probabilities (P) are indicated. P > 0,05 indicates non-significant deviation from hypothesis.

	F1 segregation		F2 segregation				
cross	WT	mutant	WT	mutant	ratio	n.h.	χ^2; P
Col/FYVE-GFP x *fel4*	16	0	74	22	3.4 : 1	3:1	0.2; >0,8
			107	13	8.2 : 1	3:1	12.8; >0,0001
fel4 x Col/FYVE-GFP	8	0	115	16	7.2 : 1	3:1	11.4; >0,0001
La/FYVE-GFP x *fel4*	10	0	31	9	3.4 : 1	3:1	0.1 ; >0.95
fel4 x La/FYVE-GFP	16	0	22	6	3.6 : 1	3:1	0.2 ; >0.9
Col/FYVE-GFP x *fel5*	2	5	28	100	1 : 3.6	1:3	0.7; >0,7
			25	89	1 : 3.6	1:3	0.6; >0,7
			20	86	1 : 4.3	1:3	2.1; >0,2
La/FYVE-GFP x *fel5*	5	7	24	5	1 : 4.8	1:3	0.9 ; >0.5
fel5 x La/FYVE-GFP	1	14	20	7	1 : 2.8	1:3	0 ; >0,95

Analysis of the F2 progeny revealed a recessive inheritance of *fel4* for one out of three crosses, and indicated a dominant inheritance for all three tested *fel5* crosses (Table 11). It has to be noted that for F1 and F2 progeny of *fel5* crosses correct endosomal phenotyping was challenging due to low differences between the Col/FYVE-GFP (~350; Suppl. Fig. 10) and the mutant *fel5* line (~250). Notably, the previously

described twisting phenotype did not co-segregate with the endosomal phenotype of *fel4* or *fel5*. The F2 population of *fel4* x Col/FYVE-GFP revealed even larger endosomal structures than the *fel4* mutant (Fig. 17). However, to some extent these enlarged structures were also detected in F2 *fel5* x Col/FYVE-GFP, although not as big, indicating they might result from ecotype crosses. Re-analyzing Col/FYVE-GFP plants revealed that already in the parental line one can observe larger endosomal structures (Suppl. Fig. 10). Backcrosses with the reference line La/FYVE-GFP validated the recessive inheritance for *fel4*, while it revealed a recessive behavior for *fel5* (Table 11).

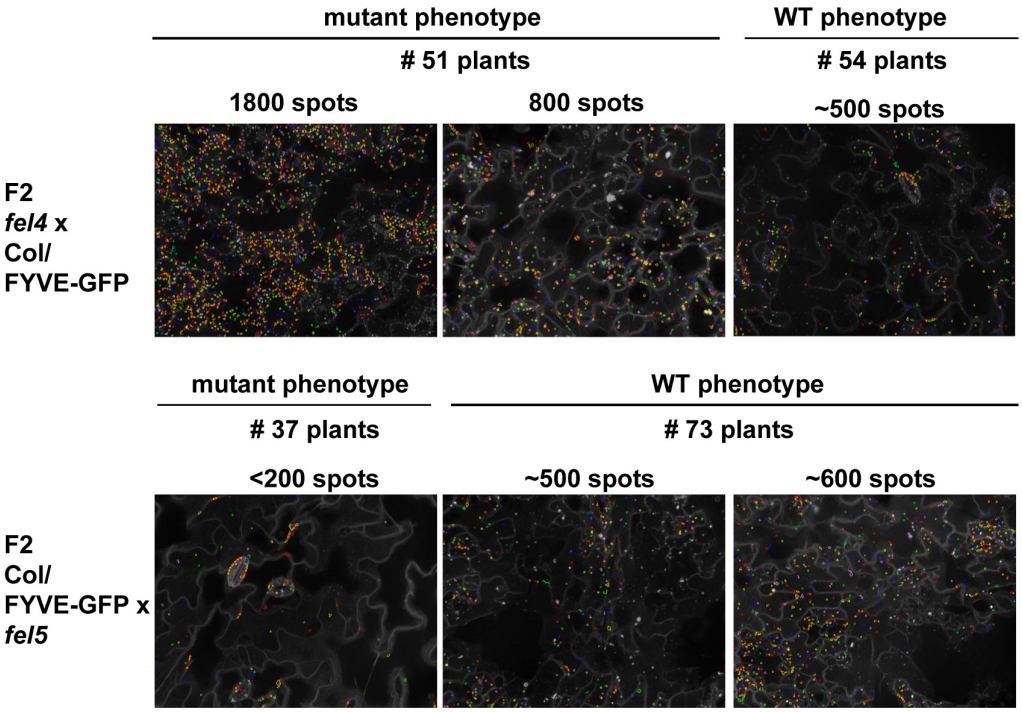

Fig. 17: Endosomal Phenotype of F2 Crosses of *fel4* and *fel5*. F2 offspring of the *fel4* x Col/FYVE-GFP and the reciprocal cross resulted in the isolation of 52 plants with mutant phenotype (increased endosomal numbers) and 323 wild-type-like plants. F2 offspring of the Col/FYVE-GFP x *fel5* allowed isolation of 331 plants with mutant phenotype (reduced endosomal numbers) and 122 wild-type like plants. Numbers of phenotyped plants from which DNA was isolated for rough mapping analysis are indicated.

Probably due to the high rate of false positives in phenotyping F2 progeny of *fel5* crosses, no co-segregation of any marker with *fel5* was detected in a bulk segregant approach (Lukowitz et al., 2000). By contrast, similar analysis revealed two rough mapping positions, on chromosome I and III, for *fel4* (data not shown).

3.4.4 Supplementary Material

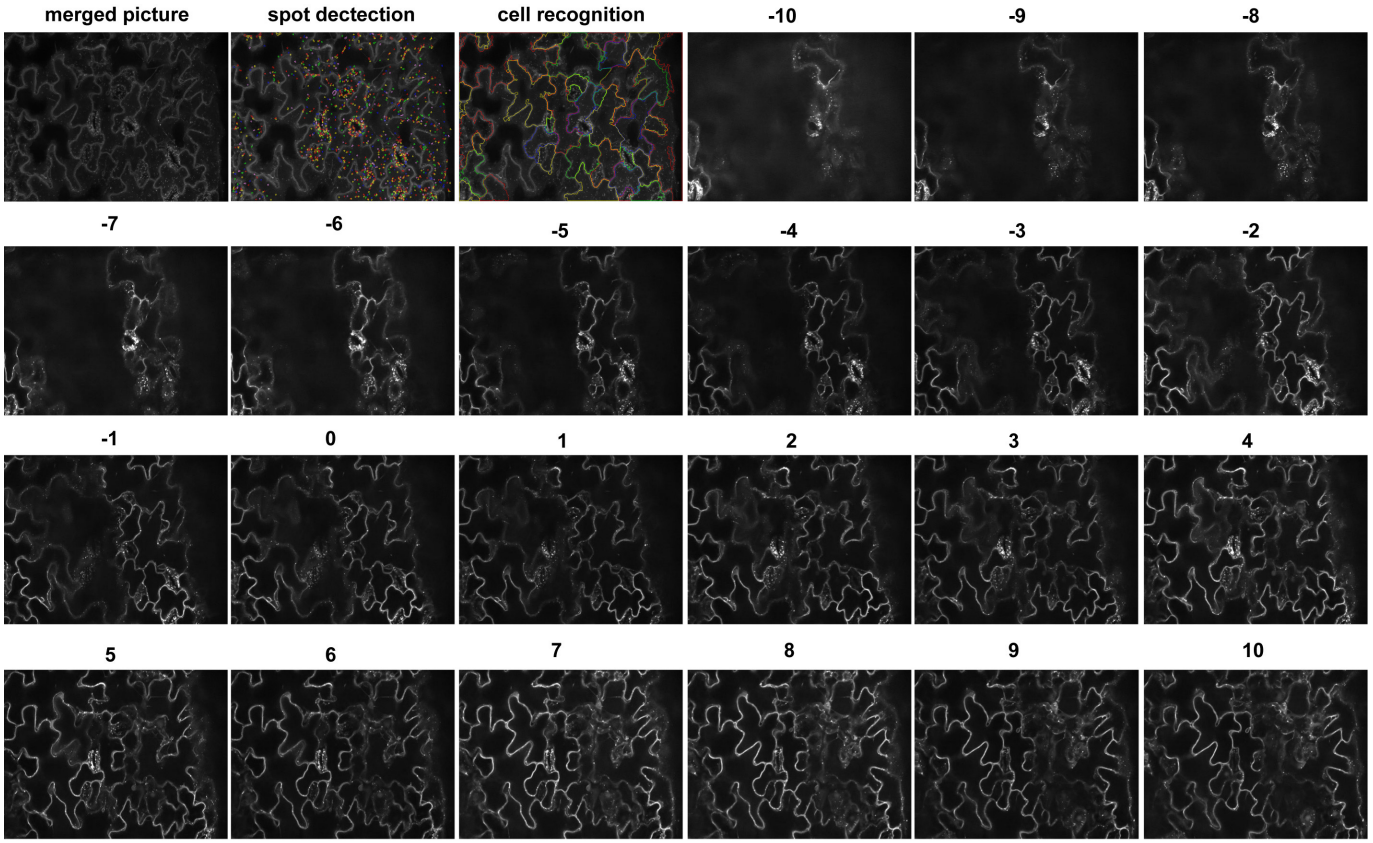

Suppl. Fig. 6: Images Obtained by Automated Confocal Microscopy. 21 images a 1µm distance (10 pictures below and above the set height at 0) are merged to a pseudo-image by the software Acapella. Areas that are not in focus are neglected. Spot (endosome) detection and cell recognition within the merged picture are also operated by the software Acapella.

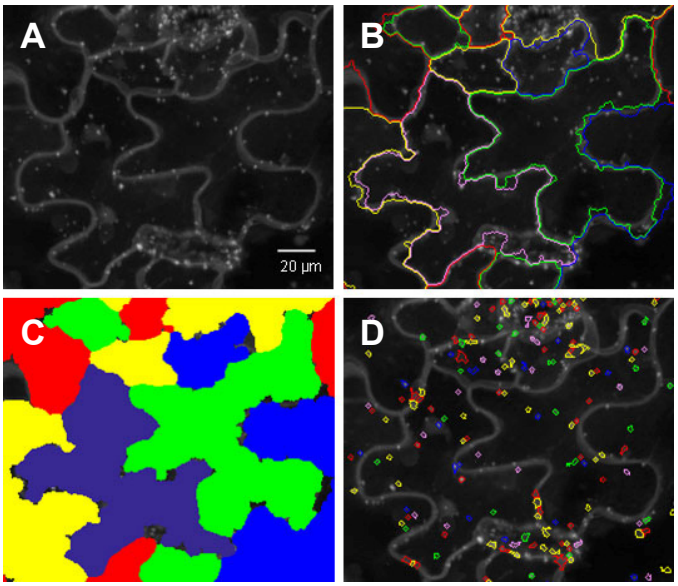

Suppl. Fig. 7: Detailed Images Generated by Software Analysis. (A) Merged picture. **(B)** Colored lines label recognized cell boundaries. **(C)** Colors represent recognized cell areas. **(D)** Colored spots resemble counted endosomes. Images were obtained by automated confocal microscopy (Opera) and Acapella software analysis. Color coding is random. Scale bar: 20 µm.

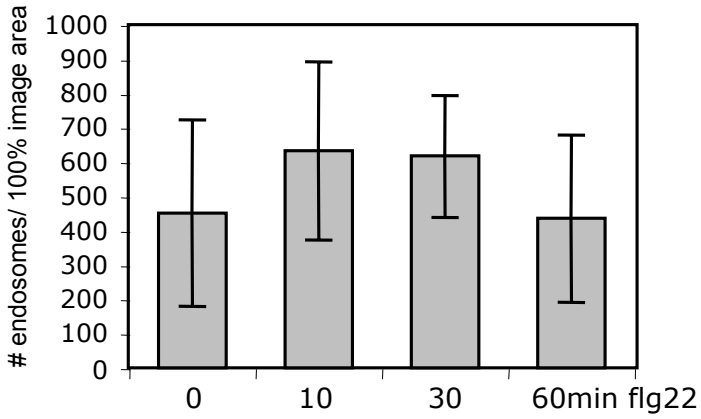

Suppl. Fig. 8: Quantitative Analysis of the Reference Line (La/FYVE-GFP) upon 0, 10, 30, and 60 min flg22 Treatment. Data was obtained by automated confocal microscopy (Opera) and subsequent Acapella software analysis. Bars and error bars represent the average and standard deviation of 10 replicates.

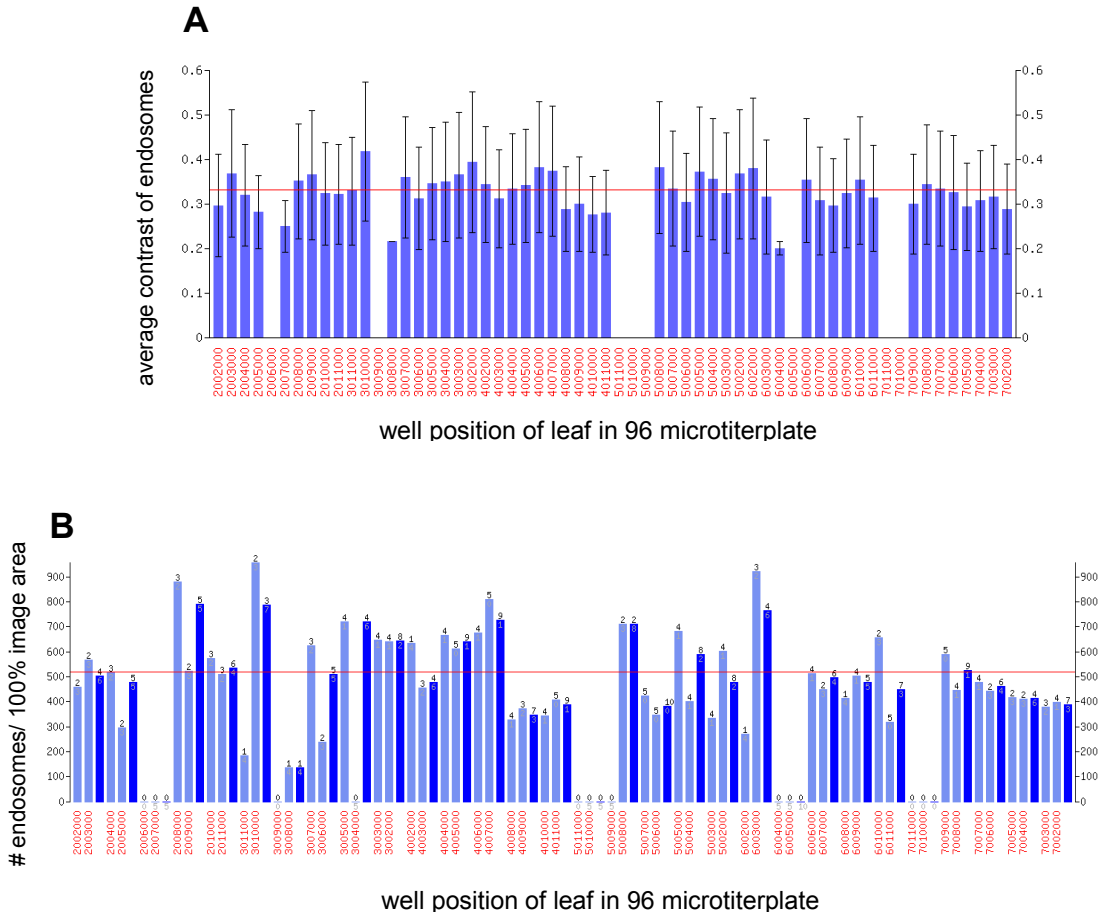

Suppl. Fig. 9: Quantitative Analysis of the Reference Line (La/FYVE-GFP). (A) Average contrast of spots (similar roundness, size). **(B)** Average number of spots per image area (similar spots per cell, total spots). Light blue bars: average value per leaf. Dark blue bar: average value per plant. Numbers above bars represent the number of valid pictures that were used to calculate the mean values. Numbers below the bars state how many pictures could not be used for the calculation (e.g. images that were out of focus). Red line indicates mean values of reference line.

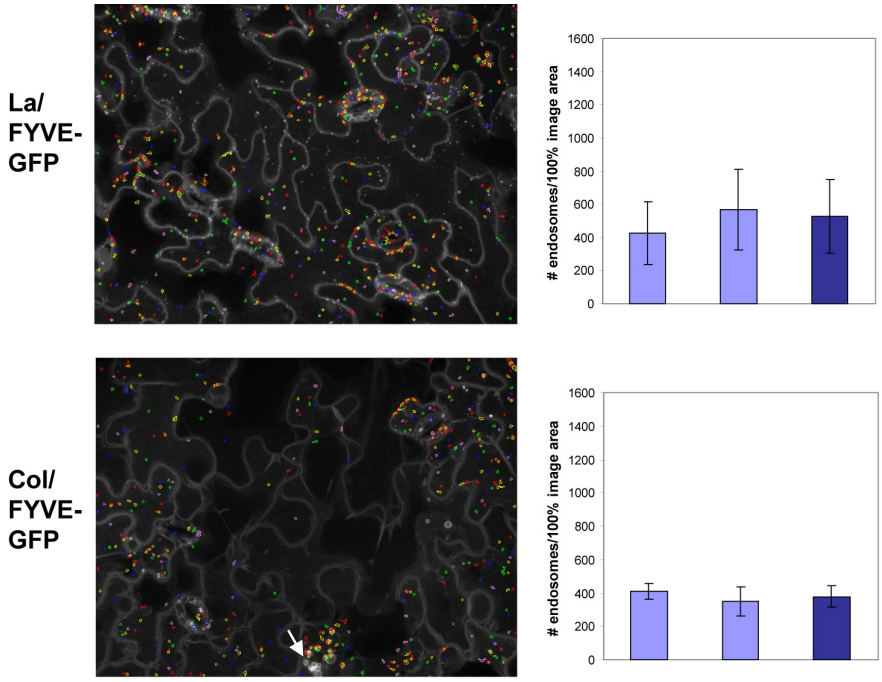

Suppl. Fig. 10: Analysis of the Reference Lines La/FYVE-GFP and Col/FYVE-GFP. Graphs illustrate the average number of endosomes found in the respective seedling shown on the left. La/FYVE-GFP contains ~550 endosomes/image area, while Col/FYVE-GFP contains ~350 endosomes/image area including some enlarged endosomes (arrowhead). Light blue bars: average value per leaf. Dark blue bar: average value per plant.

3.4.5 Concluding Remarks

To identify components involved in endosome biogenesis, trafficking and regulation, a high-throughput genetic screen was established detecting quantitative differences in endosomal levels in living plant tissue. In this study, an automated confocal microscope (Opera) was employed to analyze endosomes in *Arabidopsis* epidermal leaf cells at subcellular resolution. The success of this novel screening method was validated by screening 8 100 M_2 plants of an EMS-mutagenized FYVE-GFP endosomal marker population. In total, 12 *fel* mutants were confirmed in the M_3 generation and sorted into three distinct mutant classes: (1) increased number together with some enlarged endosomes, (2) increased number of endosomes, and (3) reduced number of endosomes. Here, we described the further characterization of *fel4* with increased and some enlarged, and *fel5* with reduced endosomes. Current data suggests that defects of the cytoskeleton are unlikely to be responsible for the endosomal *fel* phenotypes. Treatment with the inhibitor wortmannin supported the endocytic nature of FYVE-labeled endosomes in *fel4* and *fel5*. Moreover, we observed an unexpected layer of tissue-specificity of the *fel* endosomal phenotype, in particular for *fel5*.

Fel mutants will be challenged with different pathogens to identify endocytic regulators involved in plant immunity. Preliminary results for *fel4* and *fel5* suggest slightly increased susceptibility to PtoDC3000 infection compared to the parental line. Interestingly, the parental line is already more susceptible than wild-type, indicating that changes in endocytic processes (here: overexpression of a FYVE-domain containing protein) affect plant immunity. *Fel4* and *fel5* displayed recessive inheritance, and preliminary rough mapping data indicates co-segregation of *fel4* with markers on chromosome I and III. One potential limitation of mapping endosomal levels could lie in the quantitative nature of this phenotype, which might be influenced by ecotype specific variation or more than one gene. In fact, we observed differences between the La/FYVE-GFP and the Col/FYVE-GFP line. Although these differences might be due to different ecotype backgrounds, we cannot rule out that subtle differences in the FYVE-GFP constructs themselves are responsible for this finding. Both lines were stably transformed with a N-terminal GFP-tagged tandem FYVE construct under the control of the Cauliflower mosaic virus (CaMV) 35S-promoter. Moreover, the FYVE

domain was derived from the mouse Hrs protein in both constructs (Voigt et al., 2005; Vermeer et al., 2006). Another possibility might be that the position of the transgene in the genome influences the expression of the transgene.

4 DISCUSSION

4.1 PAMP PERCEPTION AND SIGNALING

Although PAMP perception and signaling became a focus within the past years, many components contributing to PTI remain to be identified. A considerable overlap in responses to different PAMPs has been observed in plants (Thilmony et al., 2006; Zipfel et al., 2006; Ferrari et al., 2007), indicating that different PAMPs activate a conserved set of defense responses (Jones and Dangl, 2006) Nevertheless, especially early signaling events differ in kinetics and intensity between individual PAMPs (Garcia-Brugger et al., 2006). Elf18 and flg22 trigger similar PAMP responses and induce the same set of genes (Zipfel et al., 2006), of which ~30% or ~50% are also regulated by peptidoglycan or chitin, respectively (Navarro et al., 2004; Gust et al., 2007; Schwessinger and Zipfel, 2008). Comparable observations were made analyzing the responses to flagellin and oligogalacturonides, oligosaccharides derived from the plant cell wall (Denoux et al., 2008). While early transcriptional responses are similar, transcriptional programs diverge over time resulting in different late PAMP responses (Denoux et al., 2008). Moreover, it is not understood how specificity arises when the same signaling components are activated by different PAMPs or how an active receptor complex triggers a number of different responses. To date, the only genetically confirmed components of PAMP signaling are the ligand-binding receptors (PRRs), the co-receptor BAK1, the NADPH oxidase RBOHD, the MAP kinase MKK1, and the callose synthase PMR4 (Gomez-Gomez and Boller, 2000; Asai et al., 2002; Nishimura et al., 2003; Kim et al., 2005; Meszaros et al., 2006; Torres et al., 2006; Zipfel et al., 2006; Chinchilla et al., 2007b).

Flg22 signaling is conserved within species, indicating its important role in PTI (Felix et al., 1999; Hann and Rathjen, 2007; Robatzek et al., 2007; Takai et al., 2008). Inspecting a collection of *A. thaliana* accessions we identified Sij-1, Suwon, and Cvi-0 with clearly impaired flg22 responses, which carried premature stop codons in their *FLS2* alleles. Two ecotypes expressing *FLS2* variants compared to flg22-sensitive Col-0, Kas-1 and Got-22, were hampered in some flg22-triggered responses. Together, analyzing natural variation revealed mostly novel *FLS2* mutant alleles. This suggests

that downstream components of PAMP signaling are likely to be evolutionary conserved, and may only be detected by quantitative or time wise resolution.

We therefore applied a traditional genetic approach and identified *fli1* to *fli8,* which expressed FLS2 at wild-type-like levels and carried no mutation within the *FLS2* and *BAK1* sequences. Thus, we potentially isolated a novel set of flg22-insensitive mutants. ROS production in *fli1-fli8* was indistinguishable from wild-type, while callose deposition was strongly reduced, suggesting that we potentially indeed identified signaling components that affect only a subset of PAMP responses. The *fli* mutant phenotype correlates with enhanced susceptibility to bacterial infection. Notably, *fli* mutants were not only more susceptible to bacterial but also more resistant to oomycete infection. These findings imply that loss of downstream responses can affect the overall outcome of basal resistance. Importantly, we detected no obvious developmental phenotype in *fli1-fli8*, indicating defense responses are not constitutively active in these mutants. Dissecting PAMP signaling in more detail revealed that *fli1*, *fli3*, and *fli6* responded like wild-type in generating ROS, expressing early PAMP-inducible genes, producing ethylene, activating MAP kinases, but callose deposition was clearly reduced. It therefore appears evident that different PAMP responses can be uncoupled, which raises the question about the role of individual responses in plant immunity.

To date, a number of compounds important for PAMP-triggered callose deposition are known (Clay et al., 2009). PMR4/GSL5 was shown to be the callose synthase required for wound, papillary and PAMP-triggered callose formation (Jacobs et al., 2003; Nishimura et al., 2003; Vogel et al., 2004; Kim et al., 2005). In addition, the essential compounds glutathione and ascorbate, the transported metal ion cadmium, and the secondary metabolite 4-methoxy-indol-3-ylmethylglucosinolate are necessary for callose deposition (Clay et al., 2009). Flg22-triggered callose response in *Arabidopsis* seedlings required three pathways: ethylene- and MYB51-dependent indol-3-ylmethylglucosinolate (I3G) biosynthesis, CYB81F2-dependent 4-methoxylation of I3G, and the PEN2-, PCS1-, and PEN3-mediated hydrolysis of 4-methoxy-I3G (Clay et al., 2009). Classically, glucosinolates are known to function as insect deterrents. Recent studies, however, unravelled additional roles for hydrolytic products of glucosinolates in PAMP-mediated defense responses (Clay et al., 2009) and in broad-spectrum antifungal defense (Bednarek et al., 2009). The *fls2* receptor mutant, the ethylene

signaling mutant *ein2-1,* the indole glucosinolae (IGS) biosynthesis mutant *cyp81F2-1*, and the IGS hydrolytic mutant *pen2-1* were slightly more susceptible to PtoDC3000 infection in seedlings (Clay et al., 2009). This finding suggests a role for glucosinolate-dependent callose deposition contributing to PAMP-induced growth restriction of PtoDC3000. This is supported by the fact that PtoDC3000 bacteria actively suppress callose deposition (Hauck et al., 2003). Although it could be shown that the callose synthase mutant *pmr4-1* contributes to TTSS-deficient PtoDC3000 growth suppression (Kim et al., 2005), a higher susceptibility in response to PtoDC3000 was not observed (Clay et al., 2009), probably due to elevated SA levels in the mutant (Nishimura et al., 2003). Since *fli1* is clearly more susceptible to PtoDC3000 infection and exhibits almost no PAMP-induced callose deposition it appears to be distinct to the *pmr4-1* mutant. Notably, levels of raphanusamic acid, which correlate with indol-3-methylamine (Bednarek et al., 2009), as well as I3G and 4-methoxy-I3G, required for callose deposition (Clay et al., 2009), were wild-type-like in *fli1* mutants. This suggests that components involved in callose deposition are impaired in *fli1*. The *fli1* mutation is recessively inherited and seems to co-localize with markers on chromosome II, while *pmr4* locates to chromosome IV.

Interestingly, the *pmr4-1* mutant still showed some faint callose deposits in seedlings (Clay et al., 2009). This suggests that another callose synthase might contribute to a minor extent to flg22-triggered callose deposition (Clay et al., 2009). However, analysis of other callose synthases, encoded by glucan synthase-like (*GSL*) genes, argues against involvement of another callose synthase (Nishimura et al., 2003). *Bak1* mutants were still able to deposit callose in response to flg22 (Clay et al., 2009). This implies that a related member of the SERK family could substitute for the co-receptor BAK1/SERK3 indicating that FLS2 could form receptor complexes with different partners depending on the response mediated. BRI1, which also forms a complex with BAK1, was additionally described to interact with SERK1 (Karlova et al., 2006) and functional redundancy was reported for SERK1 and SERK2 (Albrecht et al., 2005; Colcombet et al., 2005). Moreover, we cannot rule out that there might be BAK1-dependent and -independent flg22 signaling routes downstream of receptor activation.

Fli mutants exhibit impaired responses towards two different PAMPs, flg22 and elf18, which was similarly observed for *bak1* mutants (Chinchilla et al., 2007b). Interestingly,

bak1 mutants are hyper-susceptible to necrotrophic pathogens (Kemmerling et al., 2007). Moreover, *N. benthamiana* silenced for *NbBAK1* is more susceptible to bacterial and *H. arabidopsis* infection (Heese et al., 2007), whereas *bak1* mutants in *Arabidopsis* do not support increased bacterial growth but display spreading necrosis upon PtoDC3000 infection (Kemmerling et al., 2007). This difference could be due to additional silencing of SERK family members in *N. benthamiana*, which in *Arabidopsis* could substitute for *BAK1*. In *fli* mutants spreading necrosis was not detected, suggesting that different components are affected compared to *bak1* mutants.

Fli mutants exhibit clearly reduced flg22-triggered seedling growth inhibition. Recently, stabilization of DELLA proteins, plant growth repressors, was shown to contribute to flg22-induced growth inhibition (Navarro et al., 2008). A quadruple *della* mutant exhibited enhanced resistance to PtoDC3000 and *H. arabidopsis* cv. Cala2, while displaying enhanced susceptibility to the necrotrophs *Botrytis cinerea* and *Alternaria brassicicola* (Navarro et al., 2008). Since *fli* mutants are more susceptible to PtoDC3000 and more resistant to *H. arabidopsis*, they differ from the *della* mutants. Typically resistance or susceptibility towards bacterial infection correlates with resistance or susceptibility to other biotrophic pathogens. Thus, the increased resistance of *fli* mutants to *H. arabidopsis* was unexpected. A dual role of callose in plant immunity has been discussed before (Nishimura et al., 2003). While callose deposition is thought to be effective against bacterial infections, fungi often utilize callose for their own purposes.

Callose deposition does not only play a role in plant immunity, but also occurs at specific stages of plant cell wall development, upon wounding and physiological stresses. Recently, GSL8 was shown to be required for cytokinesis, cell patterning, and seedling maturation (Chen et al., 2009). GSL1 and GSL5 are important for plant and pollen development and fertility (Enns et al., 2005), whereas GSL10 functions in male gametogenesis (Huang et al., 2009). The callose synthase mutant *calS12* was reported to form reduced papillary callose and to be more resistant to *H. arabidopsis* (Dong et al., 2008). Morphological distinct types of callose were observed depending on the bacterial infection. Whereas TTSS-deficient bacteria or PAMPs induce small deposits, bacteria capable of injecting effectors triggered larger deposits of callose (Ham et al., 2007). Furthermore, callose deposition upon bacterial or fungal attack differs. While bacterial

infection induces wide-spread callose deposition in the whole leaf, fungal attacks lead to specific focal accumulation of callose, so called papillae, underneath the attacked site (Kwon et al., 2008). Whether *FLI1* is involved in callose deposition upon other stimuli than plant basal immunity remains to be addressed.

4.2 ENDOCYTOSIS IN PLANT IMMUNITY

Endocytosis regulates membrane homeostasis and thereby has important roles in plant development and immunity. In our candidate mutant approach, we detected enhanced susceptibility of *vps28-2*, *vps37-1*, and *vps28-1 elch* to bacterial infection, all of which are components of the ESCRT I complex. *VPS28-1* and *VPS28-2* are two different genes that were identified due to their homology to the mammalian *VPS28* ESCRT I component (Spitzer et al., 2006). The ESCRT machinery sorts ubiquitylated proteins for degradation. To achieve this three main functions need to be fulfilled by ESCRT components: (1) ubiquitylated cargo is recognized, thus preventing recycling and retrograde trafficking; (2) the endosomal membrane is deformed, allowing cargo to be sorted into endosomal invaginations; and (3) the final abscission of the endosomal invagination is catalyzed, forming intraluminal vesicles within MVBs, which contain the sorted cargo (Raiborg and Stenmark, 2009). ESCRT I components do not themselves recognize mono-ubiquitylated proteins but are an essential linker within the ESCRT complex by binding to ESCRT 0, which recognizes mono-ubiquitylated proteins, and ESCRT II, which binds to ESCRT III. ESCRT II and III then mediate the internalization of the cargo into the MVB. In mammals, ESCRT components have been shown to play an important role in cytokinesis, autophagy, neurodegenerative disorders, cancer, and bacterial diseases (Raiborg and Stenmark, 2009). A recent study reported that knockdown of certain ESCRT components in mammalian cells including the ESCRT I proteins TSG101 (homolog to ELCH) and VPS28 (homolog to VPS28-1 and VPS28-2) restricted bacterial growth (Philips et al., 2008), which supports our finding that ESCRT I components contribute to immunity in *Arabidopsis*.

Unexpectedly, we did not detect an ESCRT I mutant with clearly impaired flg22 responses. We assumed that ESCRT components could be involved in regulating FLS2 trafficking for the following reasons: first, the FLS2 receptor contains a PEST-like motif, implicated in mono-ubiquitination in animals, and secondly, FLS2 endosomes are

targeted for degradation to the lytic vacuole (Robatzek et al., 2006). Maybe due to the redundancy of ESCRT I components we did not observe a flg22 phenotype or the specific ESCRT component involved in FLS2 endocyotosis was not included. Nevertheless, bacterial infection revealed a higher susceptibility of some ESCRT I components, suggesting that a different PRR important for mediating PTI gets ubiquitinated and is subsequently targeted by the ESCRT machinery. Therefore, identifying the substrate of VPS28-2, VPS37-1, or VPS28-1 ELCH should shed more light on other components regulated by the endocytic machinery.

Recently, it was reported that parasitic nematodes alter the localization of PIN proteins to facilitate infection (Grunewald et al., 2009). Since it is known that GNOM, an ARF GEF, is responsible for asymmetric PIN localization (Geldner et al., 2003), the authors speculate whether the nematodes directly or indirectly target GNOM. This would not be surprising since GNOM is already targeted by a fungal toxin BFA, a widely used inhibitor of endocytic trafficking in plants. Here, we observed enhanced susceptibility towards bacterial infection of a related protein GNL1, encoding a BFA-insensitive ARF GEF (Richter et al., 2007; Teh and Moore, 2007), and also detected a partial insensitivity in flg22 responses. Because FLS2 trafficking appears BFA-insensitive (Robatzek et al., 2006), reduced flg22 sensitivity in *gnl1* mutants suggest a role for GNL1 in FLS2 endocytosis. However, BFA was reported to mainly act in root meristem cells (Robinson et al., 2008) and therefore we cannot exclude the possibility of a BFA-sensitive FLS2 trafficking in roots. Notably, endocytic trafficking of the co-receptor BAK1 is sensitive to BFA, implying that FLS2 and BAK1 enter into different trafficking routes, which are under the control of different ARF GEFs. Interference with host vesicle trafficking emerges as a successful strategy for fungal and bacterial pathogens to enhance virulence. Characterization of effector proteins of PtoDC3000 revealed that the secreted protein HopM1 targets AtMIN7, an ARF GEF, for degradation (Nomura et al., 2006), implying that endocytic regulators are important for plant defense. Recently, another study reported that AvrPto interacts with a small GTPase RabE1d, which regulates Golgi to PM traffic (Speth et al., 2009). RabE co-suppression in *Arabidopsis* did not confer increased susceptibility, but expression of a constitutive active RabE1d-Q74L variant resulted in enhanced resistance to PtoDC3000 (Speth et al., 2009). By contrast, *Atmin7* mutant plants allow enhanced proliferation of

PtoDC3000 and are impaired in callose deposition (Nomura et al., 2006). These findings suggest that interference with host vesicle trafficking affects plant immunity.

Quantitative confocal imaging was applied to a genetic screen and allowed the isolation of 12 *fel* mutants exhibiting altered FYVE-GFP labeled endosomal numbers. The FYVE domain specifically binds to phosphoinositol 3-phosphates (Gaullier et al., 1998), which accumulate preferentially in endosomal membranes (Gillooly et al., 2001). According to their subcellular phenotype, the *fel* mutants were grouped into three distinct classes: (1) increased number together with some enlarged endosomes, (2) increased number of endosomes, and (3) reduced number of endosomes. Two fel mutants, *fel4* and *fel5*, were characterized in more detail. The *fel4* mutant revealed not only clearly increased numbers of FYVE-labeled vesicles but also enlarged vesicles. The endocytic nature of these structures was confirmed by Wortmannin treatment, which led to a significant decrease in FYVE-labeled vesicles. Increased endosomal numbers in *fel4* could result from a higher rate of endocytic uptake, reduced recycling or reduced turnover of cargo. BFA treatment accelerates endocytic uptake of cargo to so-called BFA compartments. However, the effect of BFA in root cells could not be studied in *fel4*, because it failed to express FYVE-GFP in meristematic root cells. It has to be noted that BFA does not inhibit trafficking of all endocytic compartments and displays different effects in different tissues, hinting at tissue-specific vesicle components (Robinson et al., 2008). The fel4 phenotype in roots could be further studied with additional endocytic tracers such as FM4-64. Interestingly, enlarged endosomes were not detected in root cells of *fel4*. In a screen for vacuolar biogenesis mutants, *bub* (bubble-bath) mutants with increased numbers of small vacuolar vesicles in cotyledons were identified (Avila et al., 2003), the same tissue in which the *fel* endosomal phenotype is detected. In the *fel5* mutant we observed strongly reduced endosomal numbers, which became most apparent in expanded pavement cells of leaf epidermis. However, endosomal numbers appeared unaltered in roots, which unravels an unexpected layer of tissue-specificity of vesicular trafficking.

Initially both *fel4* and *fel5* mutants displayed growth of twisted organs indicative of interference with the tubulin cytoskeleton network. Mutations in the α-tubulin (TUA) or β-tubulin (TUB) e.g. in the *lefty* mutants were reported to cause either right-handed or left-handed twisted growth depending on the mutation (Thitamadee et al., 2002; Ishida and Hashimoto, 2007). In addition, microtubule markers such as GFP-MAP4 exhibit

helical growth (Thitamadee et al., 2002). However, we can exclude a role of tubulin, in particular due to the lack of co-segregation along the endosomal phenotype. Moreover, vesicle traffic appeared highly mobile (data not shown), which further hints at *fel4* and *fel5* possibly not affected in components of the cytoskeleton. Other developmental characteristics of the *fel* mutants observed were a reduced growth rate, low seed production and a reduced germination rate in *fel4* and *fel5*. *Fel4* exhibited also slight dwarfism, while *fel5* developed additional outgrowth of secondary inflorescence giving rise to a bush-like appearance. These findings are not surprising since mutants involved in regulation of vesicle trafficking often exhibit various degrees of developmental defects or are lethal. One example is GNOM, which displays defects in the apical-basal axis formation in the embryo and variable fusions or deletions of the cotyledons and hypocotyl (Mayer et al., 1993; Geldner et al., 2003). GNL1 exhibits short and bushy growth combined with not fully opened floral organs and increased ovule abortion (Teh and Moore, 2007). To assess whether *fel4* and *fel5* would be impaired in plant immunity, pathogen infections assays spraying two- to three-week-old *fel* mutants were conducted and suggested slightly increased susceptibility to PtoDC3000 compared to the parental line (data not shown). It is noteworthy that the parental line already displayed more disease symptoms than wild-type, indicating that changes in endocytic processes (transgenic expression of the FYVE-domain) affects plant immunity.

Analysis of mapping populations generated by crossing *fel4* and *fel5* to its parental La/FYVE-GFP and to a Col/FYVE-GFP line, respectively, revealed a recessive inheritance for *fel4* and *fel5*. First mapping results of *fel4* detected two loci, on chromosome I and III, which co-segregated with the endosomal phenotype (data not shown). Genetic mapping by the help of expressing a subcellular marker could encounter some limitations, e.g. silencing of the transgene, the transgene locus itself or different levels of transgene expression in the different ecotype backgrounds. Nevertheless, a number of reports described the application of genetic screening based on subcellular markers, some of which led indeed to the successful isolation of mutants (Avila et al., 2003; Logan et al., 2003; Tamura et al., 2005; Teh and Moore, 2007; Boulaflous et al., 2008; Tanaka et al., 2009). Avila et al. searched for mutants defective in vacuolar biogenesis with the help of a GFP fusion to a tonoplast intrinsic protein, and identified four mutant classes: *bub* mutants with increased numbers of small vacuoles in the cell, *agg* mutants containing large aggregates of GFP fluorescence, *tvs* mutants

showing vacuoles transected by transvacuolar strands and other mutants with unique defects e.g. in the regular pattern of the cotyledon epidermal cell (Avila et al., 2003). In a screen employing a soluble vacuolar marker, Tamura et al. successfully isolated a Golgi membrane protein, KATAMARIN1/MURUS3 required for endomembrane organization (Tamura et al., 2005). Using a mitochondria-targeted protein resulted in the isolation of mutants with altered mitochondrial morphology, and the *fmt* mutant was mapped successfully (Logan et al., 2003). In the background of a endoplasmic reticulum marker line mutants affected in the Golgi apparatus were identified (Boulaflous et al., 2008). Mutants defective in membrane trafficking to the PM were searched by monitoring the intracellular accumulation of a secreted GFP, thereby GNL1 was isolated (Teh and Moore, 2007). The only screen for endocytotic and not secretory mutants was recently reported and was based on internalization/accumulation of PIN1 in BFA compartments in roots (Tanaka et al., 2009). The responsible gene of the *ben1* (BFA-visualized endocytic trafficking defective1) mutant was isolated, which encoded *Atmin7* (Tanaka et al., 2009). Another allele of *ben1*, *min7*, has been shown to impair callose deposition. Interestingly, *min7* therefore is able to interfere with secretory and endocytic traffic. Moreover, *min7* mutant plants were more susceptible to PtoDC3000 (Nomura et al., 2006), indicating that searching for endocytosis mutants indeed enables also the isolation of mutants with altered disease resistance. To date, most of the reported fluorescence-based imaging mutant screens were monitored for qualitative differences. By contrast, our quantitative approach for altered endosomal numbers appeared to also result in the identification of specific mutant alleles such as *fel4* and *fel5*, which are better suitable for pathogen infection. Our genetic screen at the subcellular level was equally successful as other mutant surveys based on fluorescent imaging. Taken together, we developed a novel tool combining cell biology and genetic approaches, which allowed us to identify a set of interesting endocytosis mutants. Further mutant analysis will therefore gain better insights into membrane trafficking in plants and its contribution to immune responses.

The current understanding of endocytosis in diverse plant processes provides evidence for signaling from endosomes (Russinova et al., 2004; Robatzek et al., 2006; Geldner et al., 2007). Advantages of endosome-based signaling discussed in mammals are induced proximity of signaling components, to function as signaling platforms that recruit scaffolding proteins and signaling mediators, to fulfil a “memory function”, i.e. signals

are prolonged beyond the ligand exposure at the PM, and to serve as vehicles for physical transport of a signal (e.g. to the nucleus) (Sorkin and Goh, 2009). Similar concepts could apply to endosomal signaling in plants. In line with this, Geldner and Robatzek postulate that endosomal signaling in plants evolved as a necessary adaptation to (1) high density of different receptors per PM surface area and (2) differences in signaling depending on the position relative to the nucleus (Geldner and Robatzek, 2008). Endosomal signaling is thought to solve these problems by (1) generating additional surfaces for signaling and (2) providing highly mobile signaling stations and generating cytoplasmic streaming (Geldner and Robatzek, 2008). Moreover, endocytosis of PRRs in plant immunity provides a mechanism to prevent continuous immune responses by the clearance of PAMPs from the apoplast. Together, it is therefore tempting to speculate that "signalosomes" constitute a general concept in plant immunity to modulate immune responses. This is further supported by the finding that most RLKs and RLPs, including BRI1 and BAK1, contain the endocytosis motif Yxx□, the di-Leu motif or like FLS2 a PEST-like motif (Geldner and Robatzek, 2008).

4.3 FINAL REMARKS

In this study we aimed at elucidating the contribution of endocytosis to plant immunity and at identifying additional PAMP signaling components. To date, many signaling components involved in PTI are yet unknown. However, several studies provide some insights into PRR activation and signaling. The first step in PAMP signaling constitutes ligand binding to its cognate receptor, thereby activating the receptor and triggering multiple downstream responses. Different models for ligand-receptor activation for plant RLKs are discussed. Phosphorylation of an accessory protein for downstream signaling and stability was shown for XB3, an E3 ubiquitin ligase, required for XA21 signal transduction in rice (Wang et al., 2006). Another study reports trans-phosphorylation of two RLKs after heterodimerization e.g. for RLK5 (Horn and Walker, 1994). Other possibilities are autophosphorylation of a RLK upon ligand binding as shown for CrRLK1 (Schulze-Muth et al., 1996), or interaction of a RLK with a receptor-like cytoplasmic kinase and subsequent transphosphorylation as recently demonstrated for BRI1 and BAK1 (Yun et al., 2009). Moreoer, RLPs can interact with RLKs to transduce the signal as demonstrated for the interaction of CLV3 with CLV1/2

(Jeong et al., 1999). FLS2 forms heterodimers with BAK1 upon ligand binding (Chinchilla et al., 2007b).

In plants, one well characterized example is the BRI1/BAK1 receptor complex mediating brassinosteroid (BR) signaling. BR perception results in hetero-dimerization of BR1 and BAK1 and subsequent phosphorylation of the cytoplasmic kinase domains, which is required for BR signal transduction (Li and Nam, 2002; Li et al., 2002). Recently, transphosphorylation of BRI and BAK1 was demonstrated (Wang et al., 2008; Yun et al., 2009). BRI1 also forms homodimers via an autoinhibitory C-terminal domain (Wang et al., 2005). Upon BR binding to the extracellular domain of BRI1, the C-terminal domain is released, thereby activating the kinase domain and promoting the formation of multimeric complexes with BAK1 (Wang et al., 2005). Although BRI1 and BAK1 are classified as serine/threonine protein kinases, autophosphorylation of tyrosine residues in the cytoplasmic domain was lately reported for BRI1, indicating that BRI1 is a dual-specificity kinase (Oh et al., 2009). Tyrosine kinase activity was also described for the pollen-expressed receptor kinase PRK1 (Mu et al., 1994) and for SERK1, which is expressed during embryogenesis (Shah et al., 2001). This suggests that tyrosine signaling should be considered with other plant receptor kinases including FLS2. BRI1 does not only form a complex with BAK1/SERK3 but was also reported in a complex with SERK1 (Karlova et al., 2006).

BAK1 is a multifunctional co-receptor involved in BR signaling (Li and Nam, 2002; Li et al., 2002), in plant immunity (Chinchilla et al., 2007b; Heese et al., 2007) and in programmed cell death (He et al., 2007; Kemmerling et al., 2007). Different receptor complexes are formed depending on the pathway involved, e.g. BRI1/BAK1 mediates BR signaling while FLS2/BAK1 plant immunity. Recently, BAK1 was shown to contribute to *Verticillium* wilt resistance mediated by the LRR-RLK Ve1 in tomato, implying BAK1/Ve1 complex formation (Fradin et al., 2009). These diverse functions of BAK1 could be controlled by site-specific phosphorylation (Wang et al., 2008). It would also be plausible that BAK1 only supports phosphorylation of ligand-binding receptors to such thresholds that they are able to activate downstream molecules. Interestingly, to date no ligands have been described for SERK receptors, indicating that they fulfil a general role as co-receptors in diverse biological processes.

Plant LRR-RLKs have an organization of functional domains similar to mammalian receptor tyrosine kinses (RTK) and transforming growth factor-ß (TGF-ß) serine/threonine receptor kinase. Therefore, receptor activation of plant RLKs is often compared to models of the animal RTK or TGF-ß receptor families. In mammals, RTKs are known to form homo- or heterodimers between related RTKs upon ligand binding, which leads to phosphorylation of the respective kinase domains and activation. (Schlessinger, 2002; Burgess et al., 2003). TGF-ß receptor forms ligand-independent hetero-tetramers consisting of $(TßR1)_2/(TßR2)_2$. Activation involves the constitutively active kinase TßR2 that binds the ligand and initiates phosphorylation of TßR1, which cannot bind the ligand in the absence of TßR2. (Massague, 1998; Rahimi and Leof, 2007). FLS2 and BAK1 complex also shares similarities with RTK activation but can also be compared to TLRs in animals, e.g. direct ligand binding was observed in TLR5 and in FLS2 (Smith et al., 2003; Chinchilla et al., 2006). Moreover, FLS2 forms heterodimers with BAK1 upon ligand binding, reminiscent of RTK activation. Heterodimerization is also described for TLR2 recognizing bacterial lipoproteins or lipotechoic acid, which forms receptor complexes with TLR1 or TLR6 depending on the ligand perceived (Triantafilou et al., 2006). Interestingly, TLR2/1 and TLR2/6 complexes pre-exist, while FLS2 heterodimerization is only induced upon ligand binding (Triantafilou et al., 2006; Chinchilla et al., 2007b). Similar to FLS2, ligand-dependent endocytosis was demonstrated for TLR4 (Husebye et al., 2006). A requirement for endosomal localization was observed for RTKs and TGF-ß receptor in mammals (Wunderlich 2001, Panapoulou, E, Gillooly 2002), suggesting signaling of receptors from endosomes. In plants, accumulating evidence also supports signaling from endosomes as shown for BRI and FLS2 (Robatzek et al., 2006; Chinchilla et al., 2007a; Geldner et al., 2007; Serrano et al., 2007). Moreover, LeEIX endocytosis was implicated in xylanase signaling (Ron and Avni, 2004).

Membrane trafficking emerges as a key player contributing to plant immunity. Upon pathogen attack substantial organelles are repositioned and vesicle trafficking pathways are redirected (Schmelzer, 2002; Huckelhoven, 2007). A number of studies reported rapid transport of antimicrobial compounds to the plant pathogen attack site, as well as aggregation of peroxisomes, endoplasmatic reticulum (ER) and Golgi stacks (Takemoto et al., 2003; Koh et al., 2005; Lipka et al., 2005; Eichmann and Huckelhoven, 2008). Endosomal trafficking is part of these pathogen-triggered global rearrangements and is

also linked to the TGN via retrograde trafficking. Moreover, vesicle secretion is paramount for delivering antimicrobial compounds and for reinforcing the cell wall at pathogen attack sites. This is supported by the focal accumulation of PM proteins, e.g. the syntaxin PEN1 (Kwon et al., 2008).

The importance of vesicle trafficking for immunity is underlined by the fact that successful pathogens have evolved specific mechanism to interfere with components of putative endocytic or secretory pathways as a strategy to suppress the extracellular cell-wall associated host defense (Nomura et al., 2006). In humans, interference with membrane traffic is a common feature of virulence as was demonstrated for the human pathogen *Salmonella enterica.* However, in this case interfering with vesicle traffic does not directly suppress host defense responses but fosters the biogenesis and maintenance of a specialized i.e. protected compartment in which *Salmonella* thrive (Cossart and Sansonetti, 2004; Knodler and Steele-Mortimer, 2005). Modulation of host vesicle trafficking in humans and plants appears to be common mechanism to create a favourable environment for bacterial survival and multiplication. Our study further supports a crucial role of endocytosis in plant basal immunity by identifying a set of endocytosis mutants that appear altered in disease resistance. Identifying the responsible genes and the cargoes that are not targeted to the correct compartments in these mutants will shed more light on components involved in PAMP signaling. Further investigations of mutants impaired in late PAMP responses will complement our aim to better understand PAMP signaling in plants.

4.4 PERSPECTIVES

Potentially novel components in PAMP signaling were identified. To further investigate whether FLS2 endocytosis is also impaired in the lines exhibiting defects in late PAMP responses, in particular of *fli1*, they will be transformed with a FLS2-GFP expression construct. Moreover, it will be of interest to study the mutants with uncoupled PAMP responses. This could allow to further dissect the PAMP signaling pathway and to reveal the contribution of individual defense reponses to the overall outcome of disease resistance. To gain knowledge on how the callose response is mediated, genetic identification of the *FLI1* locus will be continued by array genotyping (Borevitz, 2005).

Furthermore, comparative whole genome expression analysis of *fli1* upon pathogen infection at different time points would be informative to better understand how reduced late PAMP responses lead to enhanced susceptibility. Comparing gene expression in *fli1,* which still triggers early flg22 responses, to the *fls2* receptor mutant, which does not trigger any flg22 responses, could reveal which genes mediate rather early vs. late PAMP responses.

Our study of pathogen disease in known membrane trafficking mutants supports a role of endocytosis in PTI. To further corroborate this, the endocytosis mutant collection, especially the *vps* and *gnl1* mutants, should be challenged with a diverse set of pathogens. Moreover, it would be of interest to analyze subcellular markers including FLS2 within these mutants and to study their localization/redistribution upon pathogen infection. This would also allow to potentially implicate yet unknown endocytic regulators in FLS2 endocytosis. However, a role in FLS2 endocytosis is unlikely because of their flg22 sensitivity; this suggests that there must be other roles of endocytic trafficking in immunity than FLS2 endocytosis.

The established automated screening method, which searches for mutants in the endocytic pathway, can also be applied to other lines expressing a fluorescently-tagged protein of interest, e.g. a TGN marker. Depending on the line and the objects/structures to be identified, minor adaptations in the script analyzing the images would be necessary. Nevertheless, these adaptations can be easily done in a short time frame, thus enabling a broad use of this technique. In addition, the images taken can be re-analyzed with a new script detecting e.g. defects in stomata numbers, size of cells, or clustering of endosomes in a "virtual" screen. Once interesting mutants are identified, the respective pool of the mutagenized population can be re-screened to identify this mutant.

Genetic identification of the responsible genes conferring the *fel4* and *fel5* endosomal phenotypes is required and will be performed by traditional map based cloning for *fel4* and whole genome sequencing for *fel5*. Furthermore, electron microscopy should reveal at the ultrastructural level whether membrane compartments such as Golgi, TGN, and ER would be as well altered in *fel4* and *fel5* mutants or appear as in the parental line. Moreover, analysis of other subcellular markers including FLS2, Ara6, Ara7, and a

TGN marker, is needed to address specificity of the trafficking pathways affected in *fel4* and *fel5*, and will also delineate the type of endocytic compartment. Evidently *fel4* and *fel5* will be studied for their responses to various pathogens including virulent and non-pathogenic strains of bacteria, oomycetes and fungi. This should provide more insights into the role of endocytic trafficking in plant immunity.

5 REFERENCES

Alam, S.L., and Sundquist, W.I. (2007). Structural biology - ESCRT service. Nature **447,** 921-922.

Albrecht, C., Russinova, E., Hecht, V., Baaijens, E., and de Vries, S. (2005). The Arabidopsis thaliana SOMATIC EMBRYOGENESIS RECEPTOR-LIKE KINASES1 and 2 control male sporogenesis. Plant Cell **17,** 3337-3349.

Ali, G.S., Prasad, K., Day, I., and Reddy, A.S.N. (2007). Ligand-dependent reduction in the membrane mobility of FLAGELLIN SENSITIVE2, an Arabidopsis receptor-like kinase. Plant and Cell Physiology **48,** 1601-1611.

Aniento, F., and Robinson, D.G. (2005). Testing for endocytosis in plants. Protoplasma **226,** 3-11.

Asai, T., Tena, G., Plotnikova, J., Willmann, M.R., Chiu, W.L., Gomez-Gomez, L., Boller, T., Ausubel, F.M., and Sheen, J. (2002). MAP kinase signalling cascade in Arabidopsis innate immunity. Nature **415,** 977-983.

Avila, E.L., Zouhar, J., Agee, A.E., Carter, D.G., Chary, S.N., and Raikhel, N.V. (2003). Tools to study plant organelle biogenesis. Point mutation lines with disrupted vacuoles and high-speed confocal screening of green fluorescent protein-tagged organelles. Plant Physiol **133,** 1673-1676.

Baluska, F., Hlavacka, A., Samaj, J., Palme, K., Robinson, D.G., Matoh, T., McCurdy, D.W., Menzel, D., and Volkmann, D. (2002). F-actin-dependent endocytosis of cell wall pectins in meristematic root cells. Insights from brefeldin A-induced compartments. Plant Physiology **130,** 422-431.

Barth, M., and Holstein, S.E.H. (2004). Identification and functional characterization of Arabidopsis AP180, a binding partner of plant alpha C-adaptin. Journal of Cell Science **117,** 2051-2062.

Bauer, Z., Gomez-Gomez, L., Boller, T., and Felix, G. (2001). Sensitivity of different ecotypes and mutants of Arabidopsis thaliana toward the bacterial elicitor flagellin correlates with the presence of receptor-binding sites. Journal of Biological Chemistry **276,** 45669-45676.

Bednarek, P., Pislewska-Bednarek, M., Svatos, A., Schneider, B., Doubsky, J., Mansurova, M., Humphry, M., Consonni, C., Panstruga, R., Sanchez-Vallet, A., Molina, A., and Schulze-Lefert, P. (2009). A Glucosinolate Metabolism Pathway in Living Plant Cells Mediates Broad-Spectrum Antifungal Defense. Science **323,** 101-106.

Bloch, D., Lavy, M., Efrat, Y., Efroni, I., Bracha-Drori, K., Abu-Abied, M., Sadot, E., and Yalovsky, S. (2005). Ectopic expression of an activated RAC in Arabidopsis disrupts membrane cycling. Molecular Biology of the Cell **16,** 1913-1927.

Bolte, S., Talbot, C., Boutte, Y., Catrice, O., Read, N.D., and Satiat-Jeunemaitre, B. (2004). FM-dyes as experimental probes for dissecting vesicle trafficking in living plant cells. Journal of Microscopy-Oxford **214,** 159-173.

Borevitz, J. (2005). Array genotyping and mapping. *In* J Salinas, JJ Sanchez-Serrano, eds, Arabidopsis Protocols, Ed. 2. Humana Press, Totowa, NJ.

Boulaflous, A., Faso, C., and Brandizzi, F. (2008). Deciphering the Golgi apparatus: from imaging to genes. Traffic **9,** 1613-1617.

Burgess, A.W., Cho, H.S., Eigenbrot, C., Ferguson, K.M., Garrett, T.P., Leahy, D.J., Lemmon, M.A., Sliwkowski, M.X., Ward, C.W., and Yokoyama, S.

(2003). An open-and-shut case? Recent insights into the activation of EGF/ErbB receptors. Mol Cell **12,** 541-552.

Chen, X.Y., Liu, L., Lee, E., Han, X., Rim, Y., Chu, H., Kim, S.W., Sack, F., and Kim, J.Y. (2009). The Arabidopsis callose synthase gene, GSL8, is required for cytokinesis and cell patterning. Plant Physiol.

Chi, H., and Flavell, R.A. (2008). Innate recognition of non-self nucleic acids. Genome Biol **9,** 211.

Chinchilla, D., Boller, T., and Robatzek, S. (2007a). Flagellin signalling in plant immunity. In Current Topics in Innate Immunity, pp. 358-371.

Chinchilla, D., Bauer, Z., Regenass, M., Boller, T., and Felix, G. (2006). The Arabidopsis receptor kinase FLS2 binds flg22 and determines the specificity of flagellin perception. Plant Cell **18,** 465-476.

Chinchilla, D., Zipfel, C., Robatzek, S., Kemmerling, B., Nurnberger, T., Jones, J.D.G., Felix, G., and Boller, T. (2007b). A flagellin-induced complex of the receptor FLS2 and BAK1 initiates plant defence. Nature **448,** 497-U412.

Chisholm, S.T., Coaker, G., Day, B., and Staskawicz, B.J. (2006). Host-microbe interactions: Shaping the evolution of the plant immune response. Cell **124,** 803-814.

Chou, C.K. (1970). An Electron-Microscope Study of Host Penetration and Early Stages of Haustorium Formation of Peronospora parasitica (Fr.) Tul. on Cabbage Cotyledons. . Ann. Bot. **34,** 189-204.

Clark, S.E., Jacobsen, S.E., Levin, J.Z., and Meyerowitz, E.M. (1996). The CLAVATA and SHOOT MERISTEMLESS loci competitively regulate meristem activity in Arabidopsis. Development **122,** 1567-1575.

Clay, N.K., Adio, A.M., Denoux, C., Jander, G., and Ausubel, F.M. (2009). Glucosinolate metabolites required for an Arabidopsis innate immune response. Science **323,** 95-101.

Colcombet, J., Boisson-Dernier, A., Ros-Palau, R., Vera, C.E., and Schroeder, J.I. (2005). Arabidopsis SOMATIC EMBRYOGENESIS RECEPTOR KINASES1 and 2 are essential for tapetum development and microspore maturation. Plant Cell **17,** 3350-3361.

Collings, D.A., Gebbie, L.K., Howles, P.A., Hurley, U.A., Birch, R.J., Cork, A.H., Hocart, C.H., Arioli, T., and Williamson, R.E. (2008). Arabidopsis dynamin-like protein DRP1A: a null mutant with widespread defects in endocytosis, cellulose synthesis, cytokinesis, and cell expansion. Journal of Experimental Botany **59,** 361-376.

Conner, S.D., and Schmid, S.L. (2003). Regulated portals of entry into the cell. Nature **422,** 37-44.

Cossart, P., and Sansonetti, P.J. (2004). Bacterial invasion: the paradigms of enteroinvasive pathogens. Science **304,** 242-248.

de Torres, M., Mansfield, J.W., Grabov, N., Brown, I.R., Ammouneh, H., Tsiamis, G., Forsyth, A., Robatzek, S., Grant, M., and Boch, J. (2006). Pseudomonas syringae effector AvrPtoB suppresses basal defence in Arabidopsis. Plant Journal **47,** 368-382.

Denoux, C., Galletti, R., Mammarella, N., Gopalan, S., Werck, D., De Lorenzo, G., Ferrari, S., Ausubel, F.M., and Dewdney, J. (2008). Activation of Defense Response Pathways by OGs and Flg22 Elicitors in *Arabidopsis* Seedlings. Molecular Plant **1,** 423-445.

Derksen, J., Rutten, T., Lichtscheidl, I.K., Dewin, A.H.N., Pierson, E.S., and Rongen, G. (1995). Quantitative-Analysis of the Distribution of Organelles in

Tobacco Pollen Tubes - Implications for Exocytosis and Endocytosis. Protoplasma **188,** 267-276.

Dhonukshe, P., Aniento, F., Hwang, I., Robinson, D.G., Mravec, J., Stierhof, Y.D., and Friml, J. (2007). Clathrin-mediated constitutive endocytosis of PIN auxin efflux carriers in Arabidopsis. Current Biology **17,** 520-527.

Ding, Z., Wang, H., Liang, X., Morris, E.R., Gallazzi, F., Pandit, S., Skolnick, J., Walker, J.C., and Van Doren, S.R. (2007). Phosphoprotein and phosphopeptide interactions with the FHA domain from arabidopsis kinase-associated protein phosphatase. Biochemistry **46,** 2684-2696.

Dong, X., Hong, Z., Chatterjee, J., Kim, S., and Verma, D.P. (2008). Expression of callose synthase genes and its connection with Npr1 signaling pathway during pathogen infection. Planta **229,** 87-98.

Dunning, F.M., Sun, W., Jansen, K.L., Helft, L., and Bent, A.F. (2007). Identification and mutational analysis of Arabidopsis FLS2 leucine-rich repeat domain residues that contribute to flagellin perception. Plant Cell **19,** 3297-3313.

Eichmann, R., and Huckelhoven, R. (2008). Accommodation of powdery mildew fungi in intact plant cells. J Plant Physiol **165,** 5-18.

Emons, A.M.C., and Traas, J.A. (1986). Coated Pits and Coated Vesicles on the Plasma-Membrane of Plant-Cells. European Journal of Cell Biology **41,** 57-64.

Enns, L.C., Kanaoka, M.M., Torii, K.U., Comai, L., Okada, K., and Cleland, R.E. (2005). Two callose synthases, GSL1 and GSL5, play an essential and redundant role in plant and pollen development and in fertility. Plant Mol Biol **58,** 333-349.

Felix, G., and Boller, T. (2003). Molecular sensing of bacteria in plants - The highly conserved RNA-binding motif RNP-1 of bacterial cold shock proteins is recognized as an elicitor signal in tobacco. Journal of Biological Chemistry **278,** 6201-6208.

Felix, G., Duran, J.D., Volko, S., and Boller, T. (1999). Plants have a sensitive perception system for the most conserved domain of bacterial flagellin. Plant Journal **18,** 265-276.

Ferrari, S., Galletti, R., Denoux, C., De Lorenzo, G., Ausubel, F.M., and Dewdney, J. (2007). Resistance to Botrytis cinerea induced in Arabidopsis by elicitors is independent of salicylic acid, ethylene, or jasmonate signaling but requires PHYTOALEXIN DEFICIENT3. Plant Physiol **144,** 367-379.

Fliegmann, J., Mithofer, A., Wanner, G., and Ebel, J. (2004). An ancient enzyme domain hidden in the putative beta-glucan elicitor receptor of soybean may play an active part in the perception of pathogen-associated molecular patterns during broad host resistance. J Biol Chem **279,** 1132-1140.

Fowke, L.C., Attree, S., and la Binarova, P. (1999). Light and electron microscopic studies of somatic embryogenesis in spruce. In Morphogenesis in Plant Tissue Cultures, pp. 95-114.

Fradin, E., Zhang, Z., Juarez Ayala, J., Castroverde, C., Nazar, R., Robb, J., Liu, C., and Thomma, B.P. (2009). Genetic dissection of *Verticillium* wilt resistance mediated by tomato Ve1. Plant Physiology**,** DOI:10.1104/pp.1109.136762.

Franchi, L., Amer, A., Body-Malapel, M., Kanneganti, T.D., Ozoren, N., Jagirdar, R., Inohara, N., Vandenabeele, P., Bertin, J., Coyle, A., Grant, E.P., and Nunez, G. (2006). Cytosolic flagellin requires Ipaf for activation of caspase-1 and interleukin 1 beta in salmonella-infected macrophages. Nature Immunology **7,** 576-582.

Friml, J., Wisniewska, J., Benkova, E., Mendgen, K., and Palme, K. (2002). Lateral relocation of auxin efflux regulator PIN3 mediates tropism in Arabidopsis. Nature **415,** 806-809.

Garcia-Brugger, A., Lamotte, O., Vandelle, E., Bourque, S., Lecourieux, D., Poinssot, B., Wendehenne, D., and Pugin, A. (2006). Early signaling events induced by elicitors of plant defenses. Mol Plant Microbe Interact **19,** 711-724.

Gaullier, J.M., Simonsen, A., D'Arrigo, A., Bremnes, B., Stenmark, H., and Aasland, R. (1998). FYVE fingers bind Ptdins(3)P. Nature **394,** 432-433.

Geldner, N., and Robatzek, S. (2008). Plant receptors go endosomal: A moving view on signal transduction. Plant Physiology **147,** 1565-1574.

Geldner, N., Hyman, D.L., Wang, X.L., Schumacher, K., and Chory, J. (2007). Endosomal signaling of plant steroid receptor kinase BRI1. Genes & Development **21,** 1598-1602.

Geldner, N., Anders, N., Wolters, H., Keicher, J., Kornberger, W., Muller, P., Delbarre, A., Ueda, T., Nakano, A., and Jurgens, G. (2003). The Arabidopsis GNOM ARF-GEF mediates endosomal recycling, auxin transport, and auxin-dependent plant growth. Cell **112,** 219-230.

Gifford, M.L., Robertson, F.C., Soares, D.C., and Ingram, G.C. (2005). ARABIDOPSIS CRINKLY4 function, internalization, and turnover are dependent on the extracellular crinkly repeat domain. Plant Cell **17,** 1154-1166.

Gillooly, D.J., Simonsen, A., and Stenmark, H. (2001). Cellular functions of phosphatidylinositol 3-phosphate and FYVE domain proteins. Biochemical Journal **355,** 249-258.

Goh, T., Uchida, W., Arakawa, S., Ito, E., Dainobu, T., Ebine, K., Takeuchi, M., Sato, K., Ueda, T., and Nakano, A. (2007). VPS9a, the common activator for two distinct types of Rab5 GTPases, is essential for the development of Arabidopsis thaliana. Plant Cell **19,** 3504-3515.

Gomez-Gomez, L., and Boller, T. (2000). FLS2: An LRR receptor-like kinase involved in the perception of the bacterial elicitor flagellin in Arabidopsis. Molecular Cell **5,** 1003-1011.

Gomez-Gomez, L., Felix, G., and Boller, T. (1999). A single locus determines sensitivity to bacterial flagellin in Arabidopsis thaliana. Plant Journal **18,** 277-284.

Gomez-Gomez, L., Bauer, Z., and Boller, T. (2001). Both the extracellular leucine-rich repeat domain and the kinase activity of FLS2 are required for flagellin binding and signaling in arabidopsis. Plant Cell **13,** 1155-1163.

Grebe, M., Xu, J., Mobius, W., Ueda, T., Nakano, A., Geuze, H.J., Rook, M.B., and Scheres, B. (2003). Arabidopsis sterol endocytosis involves actin-mediated trafficking via ARA6-positive early endosomes. Current Biology **13,** 1378-1387.

Griffing, L.R. (2008). FRET analysis of transmembrane flipping of FM4-64 in plant cells: is FM4-64 a robust marker for endocytosis? Journal of Microscopy-Oxford **231,** 291-298.

Grunewald, W., Cannoot, B., Friml, J., and Gheysen, G. (2009). Parasitic nematodes modulate PIN-mediated auxin transport to facilitate infection. PLoS Pathog **5,** e1000266.

Gust, A.A., Biswas, R., Lenz, H.D., Rauhut, T., Ranf, S., Kemmerling, B., Gotz, F., Glawischnig, E., Lee, J., Felix, G., and Nurnberger, T. (2007). Bacteria-derived peptidoglycans constitute pathogen-associated molecular patterns triggering innate immunity in Arabidopsis. Journal of Biological Chemistry **282,** 32338-32348.

Haas, T.J., Sliwinski, M.K., Martinez, D.E., Preuss, M., Ebine, K., Ueda, T., Nielsen, E., Odorizzi, G., and Otegui, M.S. (2007). The Arabidopsis AAA ATPase SKD1 is involved in multivesicular endosome function and interacts with its positive regulator LYST-INTERACTING PROTEIN5. Plant Cell **19,** 1295-1312.

Haglund, K., and Dikic, I. (2005). Ubiquitylation and cell signaling. Embo Journal **24,** 3353-3359.

Ham, J.H., Kim, M.G., Lee, S.Y., and Mackey, D. (2007). Layered basal defenses underlie non-host resistance of Arabidopsis to Pseudomonas syringae pv. phaseolicola. Plant J **51,** 604-616.

Hann, D.R., and Rathjen, J.P. (2007). Early events in the pathogenicity of Pseudomonas syringae on Nicotiana benthamiana. Plant J **49,** 607-618.

Hauck, P., Thilmony, R., and He, S.Y. (2003). A Pseudomonas syringae type III effector suppresses cell wall-based extracellular defense in susceptible Arabidopsis plants. Proc Natl Acad Sci U S A **100,** 8577-8582.

Hayashi, F., Smith, K.D., Ozinsky, A., Hawn, T.R., Yi, E.C., Goodlett, D.R., Eng, J.K., Akira, S., Underhill, D.M., and Aderem, A. (2001). The innate immune response to bacterial flagellin is mediated by Toll-like receptor 5. Nature **410,** 1099-1103.

He, K., Gou, X., Yuan, T., Lin, H., Asami, T., Yoshida, S., Russell, S.D., and Li, J. (2007). BAK1 and BKK1 regulate brassinosteroid-dependent growth and brassinosteroid-independent cell-death pathways. Curr Biol **17,** 1109-1115.

Heese, A., Hann, D.R., Gimenez-Ibanez, S., Jones, A.M., He, K., Li, J., Schroeder, J.I., Peck, S.C., and Rathjen, J.P. (2007). The receptor-like kinase SERK3/BAK1 is a central regulator of innate immunity in plants. Proc Natl Acad Sci U S A **104,** 12217-12222.

Holstein, S.E.H. (2002). Clathrin and plant endocytosis. Traffic **3,** 614-620.

Holub, E.B., Beynon, L.J., and Crute, I.R. (1994). Phenotypic and Genotypic Characterization of Interactions between Isolates of Peronospora-Parasitica and Accessions of Arabidopsis-Thaliana. Molecular Plant-Microbe Interactions **7,** 223-239.

Horn, M.A., and Walker, J.C. (1994). Biochemical properties of the autophosphorylation of RLK5, a receptor-like protein kinase from Arabidopsis thaliana. Biochim Biophys Acta **1208,** 65-74.

Huang, L., Chen, X.Y., Rim, Y., Han, X., Cho, W.K., Kim, S.W., and Kim, J.Y. (2009). Arabidopsis glucan synthase-like 10 functions in male gametogenesis. J Plant Physiol **166,** 344-352.

Huckelhoven, R. (2007). Transport and secretion in plant-microbe interactions. Current Opinion in Plant Biology **10,** 573-579.

Hurley, J.H. (2008). ESCRT complexes and the biogenesis of multivesicular bodies. Curr Opin Cell Biol **20,** 4-11.

Hurley, J.H., Im, Y.J., Lee, H.H., Ren, X., Wollert, T., and Yang, D. (2009). Piecing together the ESCRTs. Biochem Soc Trans **37,** 161-166.

Husebye, H., Halaas, O., Stenmark, H., Tunheim, G., Sandanger, O., Bogen, B., Brech, A., Latz, E., and Espevik, T. (2006). Endocytic pathways regulate Toll-like receptor 4 signaling and link innate and adaptive immunity. Embo Journal **25,** 683-692.

Ishida, T., and Hashimoto, T. (2007). An Arabidopsis thaliana tubulin mutant with conditional root-skewing phenotype. J Plant Res **120,** 635-640.

Jacobs, A.K., Lipka, V., Burton, R.A., Panstruga, R., Strizhov, N., Schulze-Lefert, P., and Fincher, G.B. (2003). An Arabidopsis callose synthase, GSL5, is required for wound and papillary callose formation. Plant Cell **15,** 2503-2513.

Jeong, S., Trotochaud, A.E., and Clark, S.E. (1999). The Arabidopsis CLAVATA2 gene encodes a receptor-like protein required for the stability of the CLAVATA1 receptor-like kinase. Plant Cell **11,** 1925-1934.

Johannes, L., and Lamaze, C. (2002). Clathrin-dependent or not: Is it still the question? Traffic **3,** 443-451.

Jones, J.D.G., and Dangl, J.L. (2006). The plant immune system. Nature **444,** 323-329.

Kaku, H., Nishizawa, Y., Ishii-Minami, N., Akimoto-Tomiyama, C., Dohmae, N., Takio, K., Minami, E., and Shibuya, N. (2006). Plant cells recognize chitin fragments for defense signaling through a plasma membrane receptor. Proceedings of the National Academy of Sciences of the United States of America **103,** 11086-11091.

Karlova, R., Boeren, S., Russinova, E., Aker, J., Vervoort, J., and de Vries, S. (2006). The Arabidopsis SOMATIC EMBRYOGENESIS RECEPTOR-LIKE KINASE1 protein complex includes BRASSINOSTEROID-INSENSITIVE1. Plant Cell **18,** 626-638.

Kemmerling, B., Schwedt, A., Rodriguez, P., Mazzotta, S., Frank, M., Qamar, S.A., Mengiste, T., Betsuyaku, S., Parker, J.E., Mussig, C., Thomma, B.P., Albrecht, C., de Vries, S.C., Hirt, H., and Nurnberger, T. (2007). The BRI1-associated kinase 1, BAK1, has a brassinolide-independent role in plant cell-death control. Curr Biol **17,** 1116-1122.

Keppler, L.D., Baker, C.J., and Atkinson, M.M. (1989). Active Oxygen Production During a Bacteria-Induced Hypersensitive Reaction in Tobacco Suspension Cells. Phytopathology **79,** 974-978.

Kim, M.G., da Cunha, L., McFall, A.J., Belkhadir, Y., DebRoy, S., Dangl, J.L., and Mackey, D. (2005). Two Pseudomonas syringae type III effectors inhibit RIN4-regulated basal defense in Arabidopsis. Cell **121,** 749-759.

Kleine-Vehn, J., Dhonukshe, P., Sauer, M., Brewer, P.B., Wisniewska, J., Paciorek, T., Benkova, E., and Friml, J. (2008). ARF GEF-dependent transcytosis and polar delivery of PIN auxin carriers in Arabidopsis. Current Biology **18,** 526-531.

Knodler, L.A., and Steele-Mortimer, O. (2005). The Salmonella effector PipB2 affects late endosome/lysosome distribution to mediate Sif extension. Mol Biol Cell **16,** 4108-4123.

Koh, S., Andre, A., Edwards, H., Ehrhardt, D., and Somerville, S. (2005). Arabidopsis thaliana subcellular responses to compatible Erysiphe cichoracearum infections. Plant J **44,** 516-529.

Konopka, C.A., Backues, S.K., and Bednarek, S.Y. (2008). Dynamics of Arabidopsis dynamin-related protein 1C and a clathrin light chain at the plasma membrane. Plant Cell **20,** 1363-1380.

Kunze, G., Zipfel, C., Robatzek, S., Niehaus, K., Boller, T., and Felix, G. (2004). The N terminus of bacterial elongation factor Tu elicits innate immunity in Arabidopsis plants. Plant Cell **16,** 3496-3507.

Kwon, C., Neu, C., Pajonk, S., Yun, H.S., Lipka, U., Humphry, M., Bau, S., Straus, M., Kwaaitaal, M., Rampelt, H., El Kasmi, F., Jurgens, G., Parker, J., Panstruga, R., Lipka, V., and Schulze-Lefert, P. (2008). Co-option of a default secretory pathway for plant immune responses. Nature **451,** 835-840.

Laemmli, U.K. (1970). Cleavage of Structural Proteins During Assembly of Head of Bacteriophage-T4. Nature **227,** 680-&.

Li, J., and Nam, K.H. (2002). Regulation of brassinosteroid signaling by a GSK3/SHAGGY-like kinase. Science **295,** 1299-1301.

Li, J., Wen, J., Lease, K.A., Doke, J.T., Tax, F.E., and Walker, J.C. (2002). BAK1, an Arabidopsis LRR receptor-like protein kinase, interacts with BRI1 and modulates brassinosteroid signaling. Cell **110,** 213-222.

Lipka, V., Kwon, C., and Panstruga, R. (2007). SNARE-Ware: The role of SNARE-Domain proteins in plant biology. Annual Review of Cell and Developmental Biology **23,** 147-174.

Lipka, V., Dittgen, J., Bednarek, P., Bhat, R., Wiermer, M., Stein, M., Landtag, J., Brandt, W., Rosahl, S., Scheel, D., Llorente, F., Molina, A., Parker, J., Somerville, S., and Schulze-Lefert, P. (2005). Pre- and postinvasion defenses both contribute to nonhost resistance in Arabidopsis. Science **310,** 1180-1183.

Logan, D.C., Scott, I., and Tobin, A.K. (2003). The genetic control of plant mitochondrial morphology and dynamics. Plant J **36,** 500-509.

Logemann, E., and Hahlbrock, K. (2002). Crosstalk among stress responses in plants: Pathogen defense overrides UV protection through an inversely regulated ACE/ACE type of light-responsive gene promoter unit. Proceedings of the National Academy of Sciences of the United States of America **99,** 2428-2432.

Lukowitz, W., Gillmor, C.S., and Scheible, W.R. (2000). Positional cloning in arabidopsis. Why it feels good to have a genome initiative working for you. Plant Physiology **123,** 795-805.

Marc, J., Granger, C.L., Brincat, J., Fisher, D.D., Kao, T.H., McCubbin, A.G., and Cyr, R.J. (1998). A GFP-MAP4 reporter gene for visualizing cortical microtubule rearrangements in living epidermal cells. Plant Cell **10,** 1927-1939.

Martinez-Zapater, J.M., and Salinas, J. (1998). Arabidopsis protocols. Humana Press Inc., Totowa, USA.

Massague, J. (1998). TGF-beta signal transduction. Annu Rev Biochem **67,** 753-791.

Mayer, U., Büttner, G., and Jürgens, G. (1993). Apical-basal pattern formation in the *Arabidopsis* embryo: studies on the role of the *gnom* gene. Development **117,** 149-162.

Meindl, T., Boller, T., and Felix, G. (2000). The bacterial elicitor flagellin activates its receptor in tomato cells according to the address-message concept. Plant Cell **12,** 1783-1794.

Melotto, M., Underwood, W., Koczan, J., Nomura, K., and He, S.Y. (2006). Plant stomata function in innate immunity against bacterial invasion. Cell **126,** 969-980.

Meszaros, T., Helfer, A., Hatzimasoura, E., Magyar, Z., Serazetdinova, L., Rios, G., Bardoczy, V., Teige, M., Koncz, C., Peck, S., and Bogre, L. (2006). The Arabidopsis MAP kinase kinase MKK1 participates in defence responses to the bacterial elicitor flagellin. Plant J **48,** 485-498.

Meyer, D. (2008). Molecular characterization of pathogen-triggered cell-polarity (Universität zu Köln).

Miao, E.A., Alpuche-Aranda, C.M., Dors, M., Clark, A.E., Bader, M.W., Miller, S.I., and Aderem, A. (2006). Cytoplasmic flagellin activates caspase-1 and secretion of interleukin 1 beta via Ipaf. Nature Immunology **7,** 569-575.

Mishina, T.E., and Zeier, J. (2007). Pathogen-associated molecular pattern recognition rather than development of tissue necrosis contributes to bacterial induction of systemic acquired resistance in Arabidopsis. Plant J **50,** 500-513.

Miya, A., Albert, P., Shinya, T., Desaki, Y., Ichimura, K., Shirasu, K., Narusaka, Y., Kawakami, N., Kaku, H., and Shibuya, N. (2007). CERK1, a LysM receptor kinase, is essential for chitin elicitor signaling in Arabidopsis. Proceedings of the National Academy of Sciences of the United States of America **104,** 19613-19618.

Mu, J.H., Lee, H.S., and Kao, T.H. (1994). Characterization of a pollen-expressed receptor-like kinase gene of Petunia inflata and the activity of its encoded kinase. Plant Cell **6,** 709-721.

Navarro, L., Zipfel, C., Rowland, O., Keller, I., Robatzek, S., Boller, T., and Jones, J.D.G. (2004). The transcriptional innate immune response to flg22. interplay and overlap with Avr gene-dependent defense responses and bacterial pathogenesis. Plant Physiology **135,** 1113-1128.

Navarro, L., Bari, R., Achard, P., Lison, P., Nemri, A., Harberd, N.P., and Jones, J.D. (2008). DELLAs control plant immune responses by modulating the balance of jasmonic acid and salicylic acid signaling. Curr Biol **18,** 650-655.

Nielsen, E., Cheung, A.Y., and Ueda, T. (2008). The regulatory RAB and ARF GTPases for vesicular trafficking. Plant Physiol **147,** 1516-1526.

Nishimura, M.T., Stein, M., Hou, B.H., Vogel, J.P., Edwards, H., and Somerville, S.C. (2003). Loss of a callose synthase results in salicylic acid-dependent disease resistance. Science **301,** 969-972.

Nomura, K., Debroy, S., Lee, Y.H., Pumplin, N., Jones, J., and He, S.Y. (2006). A bacterial virulence protein suppresses host innate immunity to cause plant disease. Science **313,** 220-223.

Nühse, T.S., Peck, S.C., Hirt, H., and Boller, T. (2000). Microbial elicitors induce activation and dual phosphorylation of the Arabidopsis thaliana MAPK 6. Journal of Biological Chemistry **275,** 7521-7526.

Nürnberger, T., and Kemmerling, B. (2006). Receptor protein kinases - pattern recognition receptors in plant immunity. Trends in Plant Science **11,** 519-522.

Oh, M.H., Wang, X., Kota, U., Goshe, M.B., Clouse, S.D., and Huber, S.C. (2009). Tyrosine phosphorylation of the BRI1 receptor kinase emerges as a component of brassinosteroid signaling in Arabidopsis. Proc Natl Acad Sci U S A **106,** 658-663.

Paciorek, T., Zazimalova, E., Ruthardt, N., Petrasek, J., Stierhof, Y.D., Kleine-Vehn, J., Morris, D.A., Emans, N., Jurgens, G., Geldner, N., and Friml, J. (2005). Auxin inhibits endocytosis and promotes its own efflux from cells. Nature **435,** 1251-1256.

Pan, J., Fujioka, S., Peng, J., Chen, J., Li, G., and Chen, R. (2009). The E3 Ubiquitin Ligase SCFTIR1/AFB and Membrane Sterols Play Key Roles in Auxin Regulation of Endocytosis, Recycling, and Plasma Membrane Accumulation of the Auxin Efflux Transporter PIN2 in Arabidopsis thaliana. Plant Cell **21,** 568-580.

Pfund, C., Tans-Kersten, J., Dunning, F.M., Alonso, J.M., Ecker, J.R., Allen, C., and Bent, A.F. (2004). Flagellin is not a major defense elicitor in Ralstonia solanacearum cells or extracts applied to Arabidopsis thaliana. Molecular Plant-Microbe Interactions **17,** 696-706.

Philips, J.A., Porto, M.C., Wang, H., Rubin, E.J., and Perrimon, N. (2008). ESCRT factors restrict mycobacterial growth. Proc Natl Acad Sci U S A **105,** 3070-3075.

Rahimi, R.A., and Leof, E.B. (2007). TGF-beta signaling: a tale of two responses. J Cell Biochem **102,** 593-608.

Raiborg, C., and Stenmark, H. (2009). The ESCRT machinery in endosomal sorting of ubiquitylated membrane proteins. Nature **458,** 445-452.

Richter, S., Geldner, N., Schrader, J., Wolters, H., Stierhof, Y.D., Rios, G., Koncz, C., Robinson, D.G., and Jurgens, G. (2007). Functional diversification of closely related ARF-GEFs in protein secretion and recycling. Nature **448,** 488-U410.

Robatzek, S., Chinchilla, D., and Boller, T. (2006). Ligand-induced endocytosis of the pattern recognition receptor FLS2 in Arabidopsis. Genes & Development **20,** 537-542.

Robatzek, S., Bittel, P., Chinchilla, D., Kochner, P., Felix, G., Shiu, S.H., and Boller, T. (2007). Molecular identification and characterization of the tomato flagellin receptor LeFLS2, an orthologue of Arabidopsis FLS2 exhibiting characteristically different perception specificities. Plant Molecular Biology **64,** 539-547.

Robinson, D.G. (1996). Clathrin-mediated trafficking. Trends in Plant Science **1,** 349-355.

Robinson, D.G., Langhans, M., Saint-Jore-Dupas, C., and Hawes, C. (2008). BFA effects are tissue and not just plant specific. Trends in Plant Science **13,** 405-408.

Rojo, E., Zouhar, J., Kovaleva, V., Hong, S., and Raikhel, N.V. (2003). The AtC-VPS protein complex is localized to the tonoplast and the prevacuolar compartment in Arabidopsis. Molecular Biology of the Cell **14,** 361-369.

Ron, M., and Avni, A. (2004). The receptor for the fungal elicitor ethylene-inducing xylanase is a member of a resistance-like gene family in tomato. Plant Cell **16,** 1604-1615.

Rosebrock, T.R., Zeng, L.R., Brady, J.J., Abramovitch, R.B., Xiao, F.M., and Martin, G.B. (2007). A bacterial E3 ubiquitin ligase targets a host protein kinase to disrupt plant immunity. Nature **448,** 370-U313.

Russinova, E., Borst, J.W., Kwaaitaal, M., Cano-Delgado, A., Yin, Y., Chory, J., and de Vries, S.C. (2004). Heterodimerization and endocytosis of Arabidopsis brassinosteroid receptors BRI1 and AtSERK3 (BAK1). Plant Cell **16,** 3216-3229.

Salomon, S., and Robatzek, S. (2006). Induced Receptor Endocytosis of the Receptor Kinase FLS2. Plant Signaling & Behavior **1,** 293-295.

Sambrook, J., and Russel, D. (2001). Molecular Cloning. A Laboratory Manual 3rd ed. Cold Spring Harbor Press, New York.

Schlessinger, J. (2002). Ligand-induced, receptor-mediated dimerization and activation of EGF receptor. Cell **110,** 669-672.

Schmelzer, E. (2002). Cell polarization, a crucial process in fungal defence. Trends Plant Sci **7,** 411-415.

Schulze-Muth, P., Irmler, S., Schroder, G., and Schroder, J. (1996). Novel type of receptor-like protein kinase from a higher plant (Catharanthus roseus). cDNA, gene, intramolecular autophosphorylation, and identification of a threonine important for auto- and substrate phosphorylation. J Biol Chem **271,** 26684-26689.

Schwessinger, B., and Zipfel, C. (2008). News from the frontline: recent insights into PAMP-triggered immunity in plants. Curr Opin Plant Biol **11,** 389-395.

Serrano, M., Robatzek, S., Torres, M., Kombrink, E., Somssich, I.E., Robinson, M., and Schulze-Lefert, P. (2007). Chemical interference of pathogen-associated molecular pattern-triggered immune responses in Arabidopsis reveals

a potential role for fatty-acid synthase type II complex-derived lipid signals. Journal of Biological Chemistry **282,** 6803-6811.

Shah, K., Vervoort, J., and de Vries, S.C. (2001). Role of threonines in the Arabidopsis thaliana somatic embryogenesis receptor kinase 1 activation loop in phosphorylation. J Biol Chem **276,** 41263-41269.

Shah, K., Russinova, E., Gadella, T.W.J., Willemse, J., and de Vries, S.C. (2002). The Arabidopsis kinase-associated protein phosphatase controls internalization of the somatic embryogenesis receptor kinase 1. Genes & Development **16,** 1707-1720.

Shin, H.W., and Nakayama, K. (2004). Guanine nucleotide-exchange factors for arf GTPases: their diverse functions in membrane traffic. J Biochem **136,** 761-767.

Shiu, S.H., and Bleecker, A.B. (2001). Receptor-like kinases from Arabidopsis form a monophyletic gene family related to animal receptor kinases. Proceedings of the National Academy of Sciences of the United States of America **98,** 10763-10768.

Shiu, S.H., Karlowski, W.M., Pan, R.S., Tzeng, Y.H., Mayer, K.F.X., and Li, W.H. (2004). Comparative analysis of the receptor-like kinase family in Arabidopsis and rice. Plant Cell **16,** 1220-1234.

Shpak, E.D., McAbee, J.M., Pillitteri, L.J., and Torii, K.U. (2005). Stomatal patterning and differentiation by synergistic interactions of receptor kinases. Science **309,** 290-293.

Silipo, A., Sturiale, L., Garozzo, D., Erbs, G., Jensen, T.T., Lanzetta, R., Dow, J.M., Parrilli, M., Newman, M.A., and Molinaro, A. (2008). The acylation and phosphorylation pattern of lipid a from Xanthomonas campestris strongly influence its ability to trigger the innate immune response in arabidopsis. Chembiochem **9,** 896-904.

Smith, K.D., Andersen-Nissen, E., Hayashi, F., Strobe, K., Bergman, M.A., Barrett, S.L.R., Cookson, B.T., and Aderem, A. (2003). Toll-like receptor 5 recognizes a conserved site on flagellin required for protofilament formation and bacterial motility. Nature Immunology **4,** 1247-1253.

Sohn, E.J., Kim, E.S., Zhao, M., Kim, S.J., Kim, H., Kim, Y.W., Lee, Y.J., Hillmer, S., Sohn, U., Jiang, L.W., and Hwang, I.W. (2003). Rha1, an Arabidopsis Rab5 homolog, plays a critical role in the vacuolar trafficking of soluble cargo proteins. Plant Cell **15,** 1057-1070.

Sorkin, A., and Goh, L.K. (2009). Endocytosis and intracellular trafficking of ErbBs. Exp Cell Res **315,** 683-696.

Speth, E.B., Imboden, L., Hauck, P., and He, S.Y. (2009). Subcellular Localization and Functional Analysis of the Arabidopsis GTPase RabE. Plant Physiol **149,** 1824-1837.

Spitzer, C., Schellmann, S., Sabovljevic, A., Shahriari, M., Keshavaiah, C., Bechtold, N., Herzog, M., Muller, S., Hanisch, F.G., and Hulskamp, M. (2006). The Arabidopsis elch mutant reveals functions of an ESCRT component in cytokinesis. Development **133,** 4679-4689.

Stenmark, H., Aasland, R., Toh, B.-H., and D'Arrigo, A. (1996). Endosomal localization of the autoantigen EEA1 mediated by a zinc-binding FYVE finger. Journal of Biological Chemistry **271,** 24048-24054.

Stone, B.A., and Stone, A.E.C. (1992). Chemistry and Biology of (1-3)-ß-Glucans. La Trobe Univ. Press, Victoria, Australia.

Sun, W.X., Dunning, F.M., Pfund, C., Weingarten, R., and Bent, A.F. (2006). Within-species flagellin polymorphism in Xanthomonas campestris pv

campestris and its impact on elicitation of Arabidopsis FLAGELLIN SENSING2-dependent defenses. Plant Cell **18,** 764-779.

Takai, R., Isogai, A., Takayama, S., and Che, F.S. (2008). Analysis of Flagellin Perception Mediated by flg22 Receptor OsFLS2 in Rice. Molecular Plant-Microbe Interactions **21,** 1635-1642.

Takemoto, D., Jones, D.A., and Hardham, A.R. (2003). GFP-tagging of cell components reveals the dynamics of subcellular re-organization in response to infection of Arabidopsis by oomycete pathogens. Plant Journal **33,** 775-792.

Tamura, K., Shimada, T., Kondo, M., Nishimura, M., and Hara-Nishimura, I. (2005). KATAMARI1/MURUS3 Is a novel golgi membrane protein that is required for endomembrane organization in Arabidopsis. Plant Cell **17,** 1764-1776.

Tanaka, H., Kitakura, S., De Rycke, R., De Groodt, R., and Friml, J. (2009). Fluorescence imaging-based screen identifies ARF GEF component of early endosomal trafficking. Curr Biol **19,** 391-397.

Teh, O.K., and Moore, I. (2007). An ARF-GEF acting at the Golgi and in selective endocytosis in polarized plant cells. Nature **448,** 493-U411.

Thilmony, R., Underwood, W., and He, S.Y. (2006). Genome-wide transcriptional analysis of the Arabidopsis thaliana interaction with the plant pathogen Pseudomonas syringae pv. tomato DC3000 and the human pathogen Escherichia coli O157:H7. Plant J **46,** 34-53.

Thitamadee, S., Tuchihara, K., and Hashimoto, T. (2002). Microtubule basis for left-handed helical growth in Arabidopsis. Nature **417,** 193-196.

Torres, M.A., Jones, J.D., and Dangl, J.L. (2006). Reactive oxygen species signaling in response to pathogens. Plant Physiol **141,** 373-378.

Triantafilou, M., Gamper, F.G., Haston, R.M., Mouratis, M.A., Morath, S., Hartung, T., and Triantafilou, K. (2006). Membrane sorting of toll-like receptor (TLR)-2/6 and TLR2/1 heterodimers at the cell surface determines heterotypic associations with CD36 and intracellular targeting. J Biol Chem **281,** 31002-31011.

Trotochaud, A.E., Hao, T., Wu, G., Yang, Z.B., and Clark, S.E. (1999). The CLAVATA1 receptor-like kinase requires CLAVATA3 for its assembly into a signaling complex that includes KAPP and a Rho-related protein. Plant Cell **11,** 393-405.

Tse, Y.C., Mo, B.X., Hillmer, S., Zhao, M., Lo, S.W., Robinson, D.G., and Jiang, L.W. (2004). Identification of multivesicular bodies as prevacuolar compartments in Nicotiana tabacum BY-2 cells. Plant Cell **16,** 672-693.

Ueda, K., Matsuyama, T., and Hashimoto, T. (1999). Visualization of microtubules in living cells of transgenic Arabidopsis thaliana. Protoplasma **206,** 201-206.

Ueda, T., Yamaguchi, M., Uchimiya, H., and Nakano, A. (2001). Ara6, a plant-unique novel type Rab GTPase, functions in the endocytic pathway of Arabidopsis thaliana. Embo Journal **20,** 4730-4741.

Ueda, T., Uemura, T., Sato, M.H., and Nakano, A. (2004). Functional differentiation of endosomes in Arabidopsis cells. Plant Journal **40,** 783-789.

Umemoto, N., Kakitani, M., Iwamatsu, A., Yoshikawa, M., Yamaoka, N., and Ishida, I. (1997). The structure and function of a soybean beta-glucan-elicitor-binding protein. Proc Natl Acad Sci U S A **94,** 1029-1034.

Van Der Valk, P., and Fowke, L.C. (1981). Ultrastructural Aspects of Coated Vesicles in Tobacco Nicotiana-Tabacum Protoplasts. Canadian Journal of Botany **59,** 1307-1313.

van Leeuwen, W., Okresz, L., Bogre, L., and Munnik, T. (2004). Learning the lipid language of plant signalling. Trends in Plant Science **9,** 378-384.

Vanhaesebroeck, B., Leevers, S.J., Panayotou, G., and Waterfield, M.D. (1997). Phosphoinositide 3-kinases: A conserved family of signal transducers. Trends in Biochemical Sciences **22,** 267-272.

Vermeer, J.E.M., van Leeuwen, W., Tobena-Santamaria, R., Laxalt, A.M., Jones, D.R., Divecha, N., Gadella, T.W.J., and Munnik, T. (2006). Visualization of PtdIns3P dynamics in living plant cells. Plant Journal **47,** 687-700.

Vogel, J., and Somerville, S. (2000). Isolation and characterization of powdery mildew-resistant Arabidopsis mutants. Proceedings of the National Academy of Sciences of the United States of America **97,** 1897-1902.

Vogel, J.P., Raab, T.K., Somerville, C.R., and Somerville, S.C. (2004). Mutations in PMR5 result in powdery mildew resistance and altered cell wall composition. Plant Journal **40,** 968-978.

Voigt, B., Timmers, A.C.J., Samaj, J., Hlavacka, A., Ueda, T., Preuss, M., Nielsen, E., Mathur, J., Emans, N., Stenmark, H., Nakano, A., Baluska, F., and Menzel, D. (2005). Actin-based motility of endosomes is linked to the polar tip growth of root hairs. European Journal of Cell Biology **84,** 609-621.

von Zastrow, M., and Sorkin, A. (2007). Signaling on the endocytic pathway. Curr Opin Cell Biol **19,** 436-445.

Vreugdenhil, D., Aarts, M.G.M., Koornneef, M., Nelissen, H., and Ernst, W.H.O. (2004). Natural variation and QTL analysis for cationic mineral content in seeds of Arabidopsis thaliana. Plant Cell and Environment **27,** 828-839.

Wang, X., Li, X., Meisenhelder, J., Hunter, T., Yoshida, S., Asami, T., and Chory, J. (2005). Autoregulation and homodimerization are involved in the activation of the plant steroid receptor BRI1. Dev Cell **8,** 855-865.

Wang, X., Kota, U., He, K., Blackburn, K., Li, J., Goshe, M.B., Huber, S.C., and Clouse, S.D. (2008). Sequential transphosphorylation of the BRI1/BAK1 receptor kinase complex impacts early events in brassinosteroid signaling. Dev Cell **15,** 220-235.

Wang, Y.S., Pi, L.Y., Chen, X., Chakrabarty, P.K., Jiang, J., De Leon, A.L., Liu, G.Z., Li, L., Benny, U., Oard, J., Ronald, P.C., and Song, W.Y. (2006). Rice XA21 binding protein 3 is a ubiquitin ligase required for full Xa21-mediated disease resistance. Plant Cell **18,** 3635-3646.

Winter, V., and Hauser, M.T. (2006). Exploring the ESCRTing machinery in eukaryotes. Trends in Plant Science **11,** 115-123.

Woollard, A.A., and Moore, I. (2008). The functions of Rab GTPases in plant membrane traffic. Curr Opin Plant Biol **11,** 610-619.

Yun, H.S., Bae, Y.H., Lee, Y.J., Chang, S.C., Kim, S.K., Li, J., and Nam, K.H. (2009). Analysis of phosphorylation of the BRI1/BAK1 complex in arabidopsis reveals amino acid residues critical for receptor formation and activation of BR signaling. Mol Cells **27,** 183-190.

Zerial, M., and McBride, H. (2001). Rab proteins as membrane organizers. Nat Rev Mol Cell Biol **2,** 107-117.

Zipfel, C. (2008). Pattern-recognition receptors in plant innate immunity. Current Opinion in Immunology **20,** 10-16.

Zipfel, C., Robatzek, S., Navarro, L., Oakeley, E.J., Jones, J.D.G., Felix, G., and Boller, T. (2004). Bacterial disease resistance in Arabidopsis through flagellin perception. Nature **428,** 764-767.

Zipfel, C., Kunze, G., Chinchilla, D., Caniard, A., Jones, J.D.G., Boller, T., and Felix, G. (2006). Perception of the bacterial PAMP EF-Tu by the receptor EFR restricts Agrobacterium-mediated transformation. Cell **125,** 749-760.

APPENDIX A: LIST OF FIGURES

APPENDIX B: LIST OF SUPPLEMENTARY FIGURES

APPENDIX C: LIST OF TABLES

ACKNOWLEDGEMENTS

Diese Arbeit wurde am Max-Planck-Institut für Züchtungsforschung in der Abteilung von Prof. Dr. Paul Schulze-Lefert angefertigt. Ich möchte mich bei allen bedanken, die mich während der Anfertigung dieser Doktorarbeit unterstützt haben, insbesondere bei:

Silke Robatzek nicht nur für ihre exzellente Betreuung sondern auch für die Möglichkeit meine Arbeit in ihrer Gruppe durchzuführen. Vielen Dank für dieses spannende Thema!

Prof. Dr. Paul Schulze-Lefert für die stete Unterstützung und für das automatische konfokale Mikroskop (Opera) ohne das ein Teil dieser Arbeit nicht möglich gewesen wäre.

Prof. Dr. Ulf-Ingo Flügge als “second supervisor” und die Übernahme des Koreferats.

Prof. Dr. Sacco de Vries for participating as external examiner. Thank you!

Prof. Dr. Martin Hülskamp für die Übernahme des Prüfungsvorsitzes.

Der International Max Planck Research School (IMPRS) insbesondere den Koordinatoren Ralf Petri und Olof Persson für die Förderung und der Möglichkeit an Praktika und Soft Skill Kursen teilzunehmen.

Der AG Robatzek für die tägliche Unterstützung. Petra für die große Hilfe bei den zahlreichen genetischen Screens und PCRs, Denise für die Hilfe beim Start der Arbeit und der Übernachtungsmöglichkeit in Köln, Heidrun für die Hilfe bei den Pseudomonaden Infektionen, Sophia für die Ethlyenmessungen, Madlen für die Iodbindestudien und die Statistikeinführung, und Nico, Vera, and Thomas for thoughtful discussions.

Prof. Dr. Josef Samaj für die La/FYVE-GFP Linie sowie Prof. Dr. Teun Munnik für die Col/FYVE-GFP Linie.

Sandra und Jagreet für die Hilfe beim Mapping und viele aufmunternde Gespräche.

Dem Opera Team. Vor allem Dorit Meyer, Kurt Stüber, Sebastian Schaaf, Serkan Boztepe und der Firma Perkin Elmer (ehemals Evotec; insbesonder bei Olavi Ollikainen, Kurt Herrenknecht und Norbert Garbow). Elmon Schmelzer für die tollen Mikroskopie Einführungen und Hilfe bei technischen Problemen.

Everybody from the PSL group for the nice working atmosphere. Marco and Ana for the help with the Peronospora infections.

Meinen Freunden und meiner Familie insbesondere meinem Mann für die grenzenlose Hilfe, Unterstützung und Geduld während dieser Zeit.

VIELEN DANK!

ERKLÄRUNG

„Ich versichere, dass ich die von mir vorgelegte Dissertation selbstständig angefertigt, die benutzten Quellen und Hilfsmittel vollständig angegeben und die Stellen der Arbeit – einschließlich Tabellen, Karten und Abbildungen –, die anderen Werken im Wortlaut oder dem Sinn nach entnommen sind, in jedem Einzelfall als Entlehnung kenntlich gemacht habe; dass diese Dissertation noch keiner anderen Fakultät oder Universität zur Prüfung vorgelegen hat; dass sie – abgesehen von den auf Seite XIII angegebenen Teilpublikationen – noch nicht veröffentlicht worden ist sowie, dass ich eine solche Veröffentlichung vor Abschluss des Promotionsverfahrens nicht vornehmen werde. Die Bestimmungen dieser Promotionsordnung sind mir bekannt. Die von mir vorgelegte Dissertation ist von Prof. Dr. Paul Schulze-Lefert betreut worden."

Köln, im April 2009 _____

Susanne Salomon